

Modeling of Proton Exchange Membrane Fuel Cell Performance Degradation and Operation Life

By

Vahid Ahmadi Sarbast

B.Sc., Persian Gulf University, Iran, 2009

M.Sc., Polytechnic University of Tehran, Iran, 2012

A Thesis Submitted in Partial Fulfillment of the Requirements for the Degree of

Master of Applied Science

in the Department of Mechanical Engineering

©Vahid Ahmadi Sarbast, 2021

University of Victoria

All rights reserved. This thesis may not be reproduced in whole or in part, by photocopy or other means, without the permission of the author.

Modeling of Proton Exchange Membrane Fuel Cell Performance Degradation and Operation Life

By

Vahid Ahmadi Sarbast

B.Sc., Persian Gulf University, Iran, 2009

M.Sc., Polytechnic University of Tehran, Iran, 2012

Supervisory Committee

Dr. Zuomin Dong (Department of Mechanical Engineering)

Co-Supervisor

Dr. Andrew Rowe (Department of Mechanical Engineering)

Co-Supervisor

Abstract

Supervisory Committee

Dr. Zuomin Dong (Department of Mechanical Engineering)

Co-Supervisor

Dr. Andrew Rowe (Department of Mechanical Engineering)

Co-Supervisor

Proton Exchange Membrane Fuel Cell (PEMFC) is the most commonly used type of hydrogen fuel cell and a promising solution for vehicular and stationary power applications. This research starts with an extensive review of the PEMFC research, including experimental testing, and performance modeling and performance degradation modeling using relatively accurate and easy-to-use mechanistic models. Next, a new PEMFC performance degradation model is introduced by amending the semi-empirical, mechanistic performance model to support the design and control of PEMFC systems and fuel cell electric vehicles (FCEVs).

The new model takes into account critical factors impacting PEMFC performance. The performance degradation due to the oxidation of catalyst platinum (Pt) and loss of active surface area is captured by fitting the degradation model parameters using experimental data to capture the observed PEMFC performance fading. The new performance degradation model is then tested and further improved under the four typical load modes that a PEMFC system experiences in a vehicular application under regular driving cycles. The model is also fitted with PEMFC experimental degradation data under different load modes to improve modeling accuracy.

The new model is applied and tested using simulations of a representative FCEV. The actual power load on an 80 kW PEMFC system in the modelled FCEV was obtained using the Advanced Vehicle Simulator (ADVISOR) under the US EPA Urban Dynamometer Driving Schedule (UDDS). With the ability to predict the operation life of the PEMFC, the appropriate sizes of the PEMFC system and the energy storage system (ESS) can be determined. Improved power control and energy management can be developed to extend the operation life of the PEMFC and lower the lifecycle cost of the FCEV.

Table of Contents

SUPERVISORY COMMITTEE	II
ABSTRACT	III
TABLE OF CONTENTS	IV
LIST OF TABLES	VII
LIST OF FIGURES	VIII
NOMENCLATURE	XI
ACKNOWLEDGMENTS	XIV
CHAPTER 1. INTRODUCTION	1
1.1. GENERAL BACKGROUND.....	1
1.2. FUEL CELL ELECTRIC VEHICLE	2
1.3. PEMFC PERFORMANCE DEGRADATION	4
1.3.1. Degradation with time	4
1.3.2. Degradation associated with a different type of operations	5
1.3.3. Reversible and irreversible degradation.....	7
1.4. MODELING.....	7
1.5. OUTLINE OF THE THESIS	8
CHAPTER 2. OVERVIEW OF RELATED WORK	10
2.1. EXISTING PEMFC PERFORMANCE MODELS	10
2.2. EXISTING PEMFC PERFORMANCE DEGRADATION MODELS	11
2.3. PEMFC DEGRADATION UNDER DIFFERENT VEHICULAR LOAD MODES	13
2.3.1. Startup/shutdown	13
2.3.2. Idling.....	15
2.3.3. Dynamic load.....	16
2.3.4. High power	17
2.4. SUMMARY.....	18
CHAPTER 3. NEW PEMFC MODEL	19
3.1. NEW PEMFC PERFORMANCE MODEL	19
3.1.1. Form of the PEMFC Performance Model.....	19
3.1.2. Determination of Model Parameters	23
3.2. NEW PEMFC PERFORMANCE DEGRADATION MODEL	24
3.2.1. Form of the New Model	24
3.2.2. Parameter Determination of the Semi-Empirical Model	30

3.2.3. New Unified Semi-empirical PEMFC Performance Degradation Model	31
3.3. SUMMARY	32
CHAPTER 4. VALIDATION OF THE NEW MODEL	33
4.1. PEMFC TEST DATA FOR MODEL VALIDATION	33
4.2. IMPROVED MODELING ACCURACY	36
4.3. IMPROVED CAPABILITY	38
4.4. SUMMARY	42
CHAPTER 5. RESULTS AND DISCUSSION	43
5.1. PEMFC PERFORMANCE DEGRADATION DATA FOR TESTING	43
5.2. SIMULATION PROCEDURE	44
5.3. PERFORMANCE AND PERFORMANCE DEGRADATION MODEL TERMS AND PARAMETERS	49
5.4. VOLTAGE DEGRADATION AND PEMFC LIFE	55
5.5. SUMMARY	57
CHAPTER 6. CONCLUSION AND RESEARCH CONTRIBUTIONS	58
6.1. SUMMARY	58
6.2. RECOMMENDATIONS	59
6.3. RESEARCH CONTRIBUTIONS	59
REFERENCES	61
APPENDIX A. RELATED VEHICLE TECHNICAL SPECIFICATIONS	68
TOYOTA PRIUS TECHNICAL SPECIFICATION	69
NISSAN LEAF TECHNICAL SPECIFICATION	70
TOYOTA MIRAI TECHNICAL SPECIFICATION	71
APPENDIX B. PEMFC PERFORMANCE DEGRADATION DUE TO DEGRADING COMPONENTS	72
PROTON EXCHANGE MEMBRANE (PEM)	72
ELECTRODES (ANODE AND CATHODE CATALYSTS)	74
BIPOLAR	75
GDL	75
SEALING GASKET	77
PEMFC COMPONENTS DEGRADATION IN LITERATURE	77
APPENDIX C. SOURCES PEMFC PERFORMANCE DEGRADATION DATA	81
IEEE PHM 2014 DATA	81
EXPERIMENTAL DATA FROM LIN ET AL. [101]	84
APPENDIX D. ADDITIONAL RESULTS OF FCEV SIMULATION	86

MODEL FITTING RESULTS.....	86
ADVISOR SIMULATION RESULTS.....	87
MODEL SIMULATION RESULTS	90
APPENDIX E. MATLAB CODES OF PERFORMANCE DEGRADATION SIMULATIONS	95
EXAMPLE MATLAB CODE FOR FINDING RUL USING PEMFC PERFORMANCE DEGRADATION MODEL.....	95

List of Tables

Table 1-1. Recent commercialized PEMFC Vehicles	3
Table 2-1. Different models used in this thesis.....	11
Table 2-2. Semi-Empirical performance degradation models in the literature.	13
Table 3-1. Polarization curve equation parameters.....	19
Table 3-2. New performance model’s terms.....	23
Table 3-3. New performance model’s parameters	24
Table 3-4. Effect of different voltage loss terms in four loading modes	26
Table 3-5. Degradation effects of each vehicular load mode.....	26
Table 3-6. Effect of PEMFC degradation on different parameters in four loading modes	27
Table 3-7. Parameters in new performance degradation model in OCV & startup/shutdown	27
Table 3-8. Parameters in new performance degradation model in the idling loading mode.....	28
Table 3-9. Parameters in new performance degradation model in the dynamic loading mode	29
Table 3-10. Parameters in new performance degradation model in high power loading mode.....	30
Table 3-11. Aging parameters are related to four loading modes.....	30
Table 3-12. Constant/operating and initial parameters of new performance degradation model.....	31
Table 3-13. Degrading parameters of new performance degradation model	31
Table 4-1. Performance model accuracy comparison using experiments with constant current	37
Table 4-2. Performance model accuracy comparison using experiments with rippled currents	37
Table 4-3. Performance degradation model accuracy comparison using experiments with constant current	37
Table 4-4. Performance degradation model accuracy comparison using experiments with rippled currents	38
Table 4-5. polarization curve parameters using fitting methods in zero time	39
Table 5-1. Constant/operating and initial parameters of new performance degradation model with 95% confidence bounds	45
Table 5-2. Degrading parameters of new performance degradation model with 95% confidence bounds.....	45
Table 5-3. Three powertrains used in simulations	46
Table B-1. PEMFC electrode degradation caused by different load cycling	74
Table B-2. Electrode degradation phenomenon and consequences	75
Table C-1. Results excel sheet No. 1 description	82
Table C-2. Results excel sheet No. 2 descriptions.....	82

List of Figures

Figure 1-1. Prognostic methods classifications	2
Figure 1-2. four load modes in a PEMFC.....	3
Figure 1-3. PEMFC degradation that caused by different load mode [8]	5
Figure 1-4. Air/Hydrogen interface formation during startup/shutdown [10]	5
Figure 1-5. Flowchart of the core idea of this thesis.....	9
Figure 3-1. Activation loss vs. current density over exchange current density plotted using a different formula	22
Figure 4-1. voltage and power vs. current density of a PEMFC	33
Figure 4-2. Polarization curve test data with a constant current for the different times during degradation	34
Figure 4-3. Polarization curve test data with a rippled current for the different times during degradation	34
Figure 4-4. PEMFC stack voltage degradation data for both tests with rippled current and the test with a constant current.....	35
Figure 4-5. Polarization curves after different operation time [101]	35
Figure 4-6. voltage degradation at different current densities [101].....	36
Figure 4-7. Polarization curve prediction derived from the performance degradation model compared with polarization curve from experimental data at three different times	38
Figure 4-8. polarization curve at zero time [101]	39
Figure 4-9. Voltage degradation data in OCV [101] and the fitted curve.....	39
Figure 4-10. Voltage degradation data in idling [101] and the fitted curve	40
Figure 4-11. Voltage degradation data in 500 mA/cm ² [101] and the fitted curve	40
Figure 4-12. Voltage degradation data in 500 mA/cm ² [101] and the fitted curve	41
Figure 4-13. Current load mode used in the simulation from ref [101]	41
Figure 4-14. Voltage degradation results of simulation compared with the experimental data	42
Figure 5-1. Performance degradation model fitting result	43
Figure 5-2. Simulation procedure flowchart.....	44
Figure 5-3. UDDS cycle speed per time in second	46
Figure 5-4. ADVISOR simulation power results for the FCHEV with a small ESS closer look	47
Figure 5-5. ADVISOR simulation power results for the FCHEV with a large ESS closer look	48
Figure 5-6. PEMFC's output load power comparison in three powertrains closer look	49
Figure 5-7. Voltage and Current of FCHEV in one cycle for simulation with small ESS.....	49
Figure 5-8. PtO potential increases with time.....	50
Figure 5-9. Crossover current density degradation with time.....	51
Figure 5-10. Crossover current density degradation with time closer look.	51
Figure 5-11. Ohmic resistance increase with time	52
Figure 5-12. Active surface area degradation with time	53
Figure 5-13. Activation loss term degradation with time	53

Figure 5-14. Ohmic loss term degradation with time	54
Figure 5-15. Concentration loss term degradation with time.....	54
Figure 5-16. Voltage degradation with time in four different currents: 10A, 35A, 70A, and 90 A for powertrain with small ESS.....	55
Figure 5-17. PEMFC voltage degradation in one load mode and at four different times: 0h, 1,000h, 4,000h, and 10,000h for the powertrain with small ESS	56
Figure 5-18. PEMFC voltage difference in one load mode and three different times: 1,000h, 4,000h, and 10,000h with time 0h for the powertrain with small ESS	56
Figure 5-19. Comparison of voltage degradation in three powertrains and four different currents: 10A, 35A, 70A, and 90A	57
Figure A-1. FCHEV architecture (Toyoya Mirai) [104].....	68
Figure A-2. Toyota Prius technical specification	69
Figure A-3. Nissan Leaf technical specification.....	70
Figure A-4. Toyota Mirai technical specification.....	71
Figure B-1. Membrane degradation processes.....	73
Figure B-2. Degradation in bipolar plates of PEMFC	75
Figure B-3. Bipolar plate SEM images: a) starting time, b) and c) after 300 h degradation test [20]	76
Figure C-1. 1 KW fuel cell test bench [86].....	81
Figure C-2. Two tests have been done for the experiment[86].....	82
Figure C-3. Polarization curve test data with a constant current for the different times during degradation.....	83
Figure C-4. Polarization curve test data with a rippled current for the different times during degradation.....	83
Figure C-5. PEMFC stack voltage degradation data for both tests with rippled current and the test with a constant current.....	84
Figure C-6. load mode used in the experiment	84
Figure C-7. Experimental data [101]	85
Figure D-1. Performance degradation model prediction expanded at the time for the model fitted with test2	86
Figure D-2. Performance degradation model plot fitted with polarization curves at different times and voltage degradation at $I = 0.7 \text{ A/cm}^2$ for test2.....	87
Figure D-3. ADVISOR simulation power results for the FCHEV with small ESS	87
Figure D-4. ADVISOR simulation power results for the FCHEV with large ESS.....	88
Figure D-5. PEMFC's output load power comparison between three powertrains	88
Figure D-6. The power difference between the powertrain with no ESS and two others	89
Figure D-7. Propulsion power of an FCEV with no ESS and a large ESS	89
Figure D-8. Voltage and Current density of PEMFC in one cycle for simulation with no ESS	90
Figure D-9. Voltage and Current of PEMFC in one cycle for simulation with large ESS	90
Figure D-10. Concentration loss parameter (m) changing with time.....	91
Figure D-11. Concentration loss parameter (n) changing with time	91

Figure D-12. Voltage degradation with time in four different currents: 10A, 35A, 70A, and 90 A for powertrain with no ESS	92
Figure D-13. PEMFC voltage degradation in one load mode and four different times: 0h, 1,000h, 4,000h, and 10,000h for the powertrain with no ESS	92
Figure D-14. PEMFC voltage difference in one load mode and three different times: 1,000h, 4,000h, and 10,000h with time 0h for powertrain with no ESS	93
Figure D-15. Voltage degradation with time in four different currents: 10A, 35A, 70A, and 90 A for powertrain with large ESS	93
Figure D-16. PEMFC voltage degradation in one load mode and four different times: 0h, 1,000h, 4,000h, and 10,000h for the powertrain with large ESS	94
Figure D-17. PEMFC voltage difference in one load mode and three different times: 1,000h, 4,000h, and 10,000h with time 0h for powertrain with large ESS	94

Nomenclature

ADVISOR	Advanced Vehicle Simulator	
AFC	Alkaline Fuel Cell	
ARSM	Adaptive Response Surface Method	
AST	Accelerated Stress Test	
CFD	Computational Fluid Dynamic	
CHP	Combined Heat and Power	
DMFC	Direct Methanol Fuel Cell	
DST	Dynamic Stress Test	
ECSA	Electro Chemical Surface Area	
ESS	Energy Storage System	
FCEV	Fuel Cell Electric Vehicle	
FCHEV	Fuel Cell Hybrid Electric Vehicle	
FCLAB	Fuel Cell Laboratory	
FCV	Fuel Cell Vehicle	
GA	Genetic Algorithms	
GDL	Gas Diffusion Layer	
GM	General Motors	
ICE	Internal Combustion Engine	
LSFCHEV	Low-Speed Fuel Cell Hybrid Electric Vehicle	
MCFC	Molten Carbonate Fuel Cell	
NEDC	New European Driving Cycle	
OCV	Open Cell (Circuit) Voltage	
PAFC	Phosphoric Acid Fuel Cell	
PEM	Proton Exchange (Polymer Electrolyte) Membrane	
PEMFC	Proton Exchange (Polymer Electrolyte) Membrane Fuel Cell	
PFSA	Polymers of PerFluoroSulfonic Acid	
Pt	Platinum	
PtO	Platinum Oxide	
RH	Relative Humidity	
RMSE	Root Mean Square Error	
RUL	Remaining Useful Life	
SA	Simulated Annealing	
SSE	Sum of Square Error	
SOFC	Solid Oxide Fuel Cell	
SQP	Sequential Quadratic Programming	
UDDS	Urban Dynamometer <i>Driving</i> Schedule	
USABC	United States Advanced Battery Consortium	
UTC	United Technologies Corporation	
A_{active}	Active Surface Area	cm^2
$A_{\text{active},0}$	Active Surface Area at time = 0	cm^2
A_1	Active Surface Area degradation parameter	cm^2
A_2	Active Surface Area degradation parameter	s^{-1}

B	Mass-transfer overvoltage parameter	V
B _c	Cathode Mass-transfer overvoltage parameter	V
B _a	Anode Mass-transfer overvoltage parameter	V
E _{rev}	Reversible open-circuit voltage	V
E _c	Activation energy	J/mol
F	Faraday constant	C/mol
i	Current density	A/ cm ²
I	Current	A
i _o	Exchange-current density	A/ cm ²
i _{o,c}	Cathode exchange-current density	A/ cm ²
i _{o,a}	Anode exchange-current density	A/ cm ²
i _L	Limiting current density	A/ cm ²
i _{L,a}	Anode limiting current density	A/ cm ²
i _{L,c}	Cathode limiting current density	A/ cm ²
i _{loss}	Loss current density	A/ cm ²
i _{loss} ^I	Loss current density degradation parameter	s ⁻¹
i _{loss,0}	Loss current density at time = 0	A/ cm ²
i _{loss} ^I	Loss current density degradation parameter at idling load mode	s ⁻¹
i _{loss} ^D	Loss current density degradation parameter at dynamic load mode	s ⁻¹
m	The parameter in the concentration loss experimental equation	V
m ₀	Parameter in concentration loss experimental equation at time = 0	V
m ₁	The parameter in concentration loss experimental equation degradation parameter	s ⁻¹
m ^H	The parameter in concentration loss experimental equation degradation parameter at high power load mode	s ⁻¹
n	The parameter in the concentration loss experimental equation	cm ² /A
n ₀	Concentration loss experimental equation parameter at time = 0	cm ² /A
n ₁	Concentration loss experimental equation degradation parameter at low power load mode	s ⁻¹
n ^H	Concentration loss experimental equation degradation parameter at high power load mode	s ⁻¹
n ^s	Number of startup/shutdown mode	
R	Ohmic resistance	Ωcm ²
R _{cr}	Contact resistance	Ωcm ²
R _{ele}	Electronic resistance	Ωcm ²
R _{memb}	Ionic (membrane) resistance	Ωcm ²
R ₀	Ohmic resistance at time = 0	Ωcm ²
R ₁	Ohmic resistance degradation parameter	s ⁻¹
R ^D	Ohmic resistance degradation parameter at dynamic load mode	s ⁻¹
R ^H	Ohmic resistance degradation parameter at high power load mode	s ⁻¹
T	Temperature	K
t	Time	s
t ^D	Time of dynamic load mode	s
t ^H	Time of high power load mode	s
t ^I	Time of idling load mode	s
t ^{OCV}	Time of OCV load mode or startup/shutdown cycle number	s

V	Cell voltage	V
V_S	Cell voltage during startup/shutdown cycling	V
V_D	Cell voltage during the dynamic load mode	V
V_H	Cell voltage during the high power load mode	V
V_I	Cell voltage during the idling load mode	V
V_{OCV}	Cell voltage during OCV load mode	V
V_{PtO}	Potential due to the formation of platinum oxide	V
$V_{PtO,0}$	PtO potential degradation parameter	V
V_{PtO}^I	PtO potential degradation parameter	Vs^{-1}
V_{PtO}^S	PtO potential degradation parameter at OCV load mode or startup/shutdown cycling	s^{-1}
V_{PtO}^I	PtO potential degradation parameter at idling load mode	Vs^{-1}
α	Charge transfer	-----
α_a	Charge transfer in the anode	-----
α_c	Charge transfer in the cathode	-----
η_{act}	Activation losses	V
η_{Ohm}	Ohmic loss	V
η_{con}	Mass-transfer losses	V

Acknowledgments

I want to thank my supervisors Dr. Zuomin Dong and Dr. Andrew Rowe, for first affording me the opportunity to be part of their research and then for all their professional support and guidance through this thesis.

I give my special thanks to my wife, Mina, for her encouragement and emotional support in the past two years.

Chapter 1. Introduction

This chapter presents the background of the research and the research problem. First, a brief overview of Proton Exchange Membrane Fuel Cells (PEMFCs), the research on PEMFC performance modeling, and vehicular applications of PEMFC are given. Then PEMFC performance degradation research is reviewed, and at the end, the outline of this thesis is provided.

1.1. General background

PEMFCs are electrochemical devices that convert the chemical energy of the external sources of hydrogen fuel and oxidants to electricity without combustion occurring. These external fuel sources differentiate a PEMFC from a battery, as it can run in a steady state as long as the reactants feed the system. At present, one significant obstacle to the broad commercialization of PEMFC is its high lifecycle cost, heavily associated with limited life due to performance degradation over time [1]. Researchers have paid much attention to this critical issue over the past decade, and as vehicular applications of PEMFCs expand, more complex performance degradation processes have been observed. Therefore, understanding the performance degradation of PEMFC and using appropriate and optimized system design and operation controls to reduce degradation are essential.

Monitoring degradation and predicting failure, or remaining useful life (RUL), using an economically acceptable method of scheduling maintenance to prevent the failure is called prognostic. Prognostic can be classified into three approaches [1, 2], as summarized in Figure 1-1. A Model-Free method refers to methods that typically use machine learning algorithms, neural networks, or signal processing algorithms to predict performance degradation of PEMFC. These methods do not need any model; thus, they do not need to understand the degradation mechanism or physics of a PEMFC. On the other hand, Model-Based approaches use a multiphysics, empirical, or semi-empirical model to investigate the degradation phenomenon. Hybrid methods combine the two previous strategies, leading to a more complicated approach.

Each of the mentioned methods has advantages and disadvantages for PEMFC degradation prediction. Most important for the PEMFC is to have a mechanism that can predict critical parameters and RUL by carrying out less complicated experimental tests. Semi-empirical model-based methods, or hybrid methods, are the answer. More precise information can be found in [2]. This study uses a semi-empirical model-based approach due to its simplicity compared to the hybrid method, also, to reduce the cost of experiments.

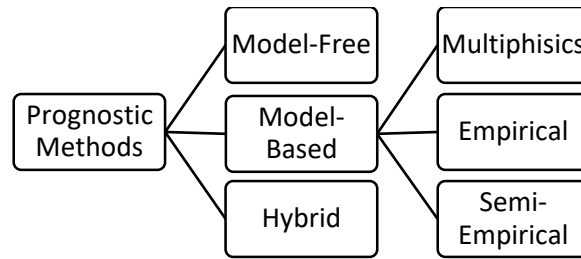


Figure 1-1. Prognostic methods classifications

1.2. Fuel cell electric vehicle

Fuel Cell Electric Vehicle (FCEV) or Fuel Cell Hybrid Electric Vehicle (FCHEV) uses a fuel cell system (usually a PEMFC) as the vehicle’s propulsion power source and an onboard battery or ultra-capacitor energy storage system (ESS) to serve as the energy buffer. PEMFC is an excellent alternative to converter energy for electric motors and to replace internal combustion engines (ICEs), reducing vehicle emissions from fossil fuels; however, there are two essential obstacles to this conversion. First, ICEs are cheaper mainly because of mass production and material used, and more importantly, the performance of PEMFCs degrade in use, reducing their operation life. More frequent replacement increases the vehicle’s overall cost. Second, the degradation rate of a PEMFC differs based on the amount of its output power and power variation patterns. *Startup/shutdown*, *idling*, *dynamic load* (load changing), and *high power* are four different load modes affecting PEMFC performance degradation [3-7].

Figure 1-2 demonstrates the four load modes in a PEMFC stack of 114 kW maximum power. The first mode is *startup/shutdown* and occurs when reactants are introduced into the fuel cell, and it starts to have output and from the time that fuel cell is turned off until the fuel is exhausted completely. The *idling* mode is when PEMFC works at a very low, less than ten percent of the full output power; for example, when the vehicle is stopped at a stop light. The PEMFC thus only produces the power needed for the auxiliary devices to allow the pumps, compressors, and the heater or the cooler of the PEMFC system to operate. The *dynamic* mode is the varying load at midrange power occurring during the normal operation of the PEMFC while the vehicle is running with frequent changes of the speed (acceleration, deceleration, and brakes). The *high power* mode is defined as the loads above 90 percent of the maximum power, for instance, when the vehicle goes up the hill with a full load.

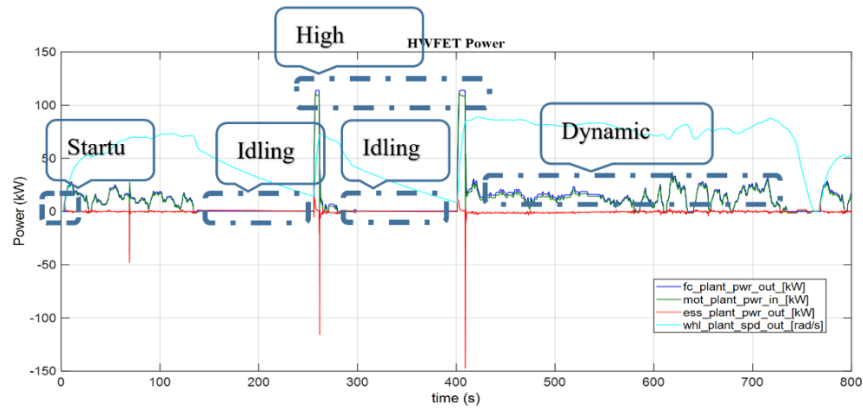


Figure 1-2. four load modes in a PEMFC

Because of slower response compared to ICEs, an energy storage system, or battery, is used besides the PEMFC. The battery pack also covers peak loads to reduce the PEMFC’s degradation and size. Finding the optimum design and control strategy for a PEMFC hybrid electric vehicle (FCHEV) is vital to handle those obstacles. The best operating conditions for the PEMFC are to work on constant output power and use a battery for peak loads. Figure A-1 in Appendix A. showing an FCHEV (Toyota Mirai) architecture as an example; the main components are the PEMFC, battery pack, high-pressure H₂ tank, and electric motor. In recent years, efforts to commercialize FCHEV have increased. Three of the latest versions of FCHEVs are Mercedes-Benz GLC, Toyota Mirai, and Hyundai Nexo, summarized in Table 1-1, showing the power and/or energy of the PEMFC, motor, and battery ESS.

Table 1-1. Recent commercialized PEMFC Vehicles

	GLC	Mirai	Nexo
PEMFC	147 kW	114 kW	95 kW
Motor	147 kW	113 kW	120 kW
Battery	13.8 kWh	1.6 kWh	1.56kWh / 40kW

There are two measures on the capability of a battery Energy Storage System (ESS), the energy capacity indicating the amount of energy it can store, and the power capability showing the maximum energy releasing and absorbing ability over a given time. The power capability helps the PEMFC system when extra power is needed for vehicle propulsion. The energy capability determines how long the battery ESS can help the PEMFC system with the supplement power. When an FCEV is optimized, the capacity of the battery ESS needs to be determined. Table 1-1 is explained here in detail to illustrate how a better design can help reduce the degradation. As shown in Table 1-1, the ESS of the Nexo can add 40 kW more power to the 95 kW PEMFC system in case the 120 kW motor needs to operate close to max capacity, reducing the size of the PEMFC by using the power from the battery ESS.

On the other hand, the GLC has a larger battery ESS, allowing the vehicle to operate longer when the PEMFC cannot operate, for instance, when running out of fuel. Different powertrain designs affect the sizes of the ESS and the PEMFC system. The degradation of the PEMFC will lead to reduced system capability from the original design. In Mirai, a 114 kW PEMFC system and a 113 kW motor are used. As a result, the compact sedan needs only around 80 kW maximum power, thus allowing the fuel cell to work at its lower midrange powers and reducing the rate of fuel cell degradation.

Optimizing the vehicle power control can force the PEMFC to operate in its mid-power range. The battery ESS can absorb and release excess energy during the idling and high power modes. When working with very low or very high power output, the PEMFC suffers more performance degradation than midrange output power in the idling and high power modes. The size of the battery ESS, the size of the PEMFC system, and the degradation and cost of both need to be studied under different power load modes.

1.3. PEMFC Performance Degradation

PEMFCs are complicated electrochemical devices having several components with different materials and properties. PEMFCs undergo a complex process in the presence of two-phase fluid flow with a range of humidity, pressure, and temperature. Therefore, they are subject to several degradation phenomena which reduce the useful life of a PEMFC.

1.3.1. Degradation with time

PEMFC encounters two main types of degradation: a) chemical degradations (as an electrochemical device, chemical reactions in the PEMFC cause these degradations), and b) mechanical degradation (although a PEMFC does not have any moving parts, some operating conditions like thermal cycling cause performance loss with time).

Gas crossover is one primary degradation process as it is an internal process of PEMFC that happens while PEMFC is working or even when there is no load on it. Flooding is another cause of performance degradation, especially during load up at high current densities, which can be resolved after decreasing load or working in dynamic load. Flooding causes a reduction in oxygen conductivity at the cathode. Although there may be good filtering and purifications in preparing and producing air and fuel, some impurities still exist in the inlet gasses that cause degradation in PEMFC regardless of operating conditions. Startup/shutdown is one important load mode that causes degradation in PEMFC, which cannot be ignored. Although scientists have proposed several methods of preventing degradation during startup/shutdown, none of them can eliminate the degradation effects of startup/shutdown. The degradation of PEMFC will be explained in detail later in this chapter and in Appendix A.

1.3.2. Degradation associated with a different type of operations

All four mentioned load modes cause significant degradation. The dynamic load (load changing) and then the startup/shutdown load modes are the most crucial cause of PEMFC degradation, respectively [8] (Figure 1-3), as they are the most common load modes in a fuel cell used at vehicular applications. In this section, the degradation processes caused by these different load modes are discussed.

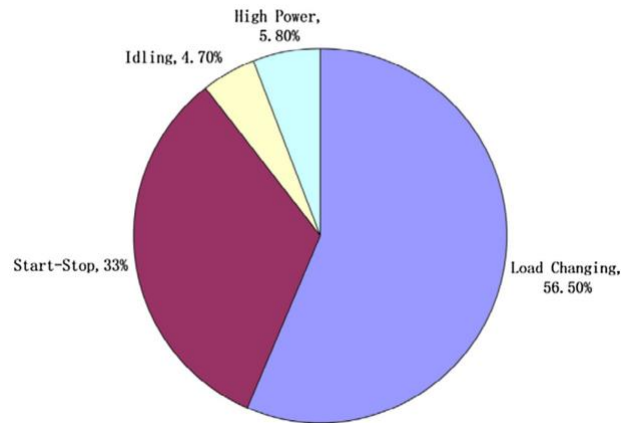


Figure 1-3. PEMFC degradation that caused by different load mode [8]

Startup and shutdown

According to [7], startup/shutdown would be as frequent as 38,500 cycles equal to 107h [9]. Hydrogen/Air interface forms first, at startup due to the existence of air at the anode and cathode before starting up, and second at shut down because of oxygen penetration from cathode to the anode side and through the membrane and incoming air from exhaust system. Figure 1-4 shows a schematic of these processes [8].

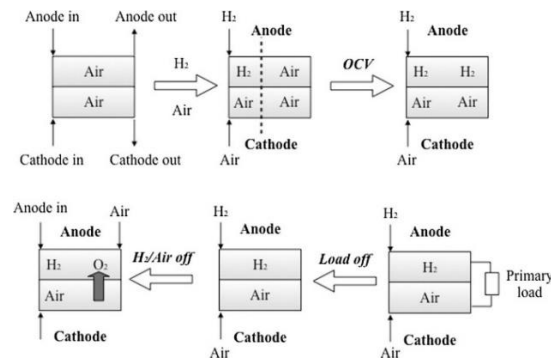


Figure 1-4. Air/Hydrogen interface formation during startup/shutdown [10]

Hydrogen/Air boundary at the anode is the leading cause of degradation in startup/shutdown [11, 12], leading to a reverse current [12, 13] and excessive-high potential [13, 14], which show as an acceleration of corrosion and oxidation of carbon support and migration of catalyst particles [7, 15, 16]. According to [8], accelerated aging experiments are the most common method to study degradation in startup/shutdown loading mode due to their collaboration. Suggested solutions to mitigate startup/shutdown degradation are mainly classified into two groups [8]: a) Key materials for the catalyst layer, and b) Using more stable materials (instead of carbon) that will prevent catalyst carrier corrosion as a result of startup/shutdown cycling [8]. Many automotive companies have studied developing appropriate startup/shutdown strategies to prevent PEMFC degradation, including UTC, General Motors (GM), Honda, Ford, Toyota, Nissan, and Daimler. These control schemes seem to be a good way at the time that alternative materials would uneconomically increase PEMFC costs [8].

Idling

Idling is a typical loading condition on urban roads. In this situation, the cell voltage is 0.85-1.0 V (i.e., at high potential) and a very low current density (on the order of $10 \text{ mA}\cdot\text{cm}^{-2}$ [17-19] [20]). Idling results in an acceleration in the catalyst dissolution and corrosion of the carbon support [7]. Another problem is the drying of the membrane due to insufficient water production [17].

Dynamic load

Dynamic or changing load is the most common mode in vehicular usage. In this case, the PEMFC needs to change its output power rapidly to meet electric motor power demand. More complicated water management is required in this situation, and gas starvation in the PEMFC may exist. Gas starvation mainly occurs when the PEMFC shifts to a higher output power level. In this situation, gas suppliers may not be able to provide the oxygen or hydrogen needed. Forming pinholes, anode and cathode carbon corrosion that finally lead to the decay in active surface area are gas starvation results in the dynamic load mode [21-23].

PEMFC produces more water at higher currents due to a higher reaction rate and less water at lower currents, and there are rapid water content fluctuations in PEMFC operating at dynamic load [24, 25]. This phenomenon causes some mechanical degradation in the membrane, catalyst, and other parts of PEMFC. Also, it causes a change in the contact area between components, leading to an increase in loss current and an increase in ohmic resistance. Thermal cycling due to the dynamic reaction rate combined with potential cycling causes Pt dissolution, Pt particle growth, and ionomer redistribution conductivity, affecting the active surface area at the end [21, 25-31].

High power

During operation, occasionally, PEMFCs have to produce more than mid-power. Working under this overload condition will accelerate the degradation process in two ways, and both lead to the decrease in catalyst active surface area [7]:

- a) Membrane: chemical corrosion [7].
- b) Catalyst: Dissolution and agglomeration of platinum and carbon support corrosion [7].

1.3.3. Reversible and irreversible degradation

Degradation in a PEMFC is not always a constant phenomenon, and sometimes it is recoverable, which is called reversible degradation in the literature. This type of degradation usually occurs during durability tests where the state of PEMFC is constant, so inserting some disturbance to the system's operating conditions removes it. Most common reversible degradations are due to the mass transfer problems coming from water stock at pores of the gas diffusion layer and the catalyst due to the hydrophilicity of materials, which has been reported in the literature as flooding [32-35]. Another main reason could be platinum catalyst oxidation or dissolution [32, 36-38].

This type of degradation could be a rare phenomenon in a PEMFC working at a vehicular load mode because the load frequently changes. If the experimental data from the Accelerated Stress Test (AST) are used, these degradation effects should be removed to have an accurate prediction. Researchers use potential cycling, characterization, and gas purging methods to recover PEMFC performance during durability tests [17, 18, 32, 33, 35, 39, 40].

1.4. Modeling

Knowing and being able to extend the useful life is of primary importance for applying PEMFCs in transportation. A performance model provides a way to estimate how each parameter or operating condition affects PEMFC performance. This understanding helps to find optimum operating conditions, parameter values, and component size. The degradation of a PEMFC system under different operating conditions can be predicted if the PEMFC performance model can be amended, and the parameters of the amended performance degradation portion can be determined using PEMFC test data.

Present models in the literature have some drawbacks. First, the only model considering all the PEMFC vehicular power modes is an empirical equation that does not give any information on the degradation of performance model parameters and does not work with all types of experimental data. Second, other models do not consider the effects of vehicular load modes, and they are only generic degradation models. Third,

a comprehensive model, which covers the impact of all four load modes and gives information on the variations of the model parameters and works well with all PEMFC degradation data, does not yet exist.

This study develops an improved PEMFC performance degradation model related to the different load modes (startup/shutdown, idling, dynamic load, and high power) found in vehicular applications. This model will then be used for the simulation of a PEMFC powered FCEV under a typical driving cycle.

1.5. Outline of the thesis

The structure of the remaining parts of the thesis is as follows. Chapter 2 provides a literature review of performance and degradation models. In Chapter 3, a new semi-empirical performance model and degradation models are introduced and explained. Chapter 4 focuses on the validation of the new performance and performance degradation models using experimental data.

Chapter 5 uses the proposed performance degradation models with an actual load profile of an FCEV to illustrate the degradation of the PEMFC over a long period that cannot be observed in an experimental setup due to the limitation in time and cost. Finally, the research contributions are summarized in Chapter 6. Figure 1-5 shows a flowchart summarizing the process of introducing the new semi-empirical performance degradation models related to vehicular PEMFC load profiles.

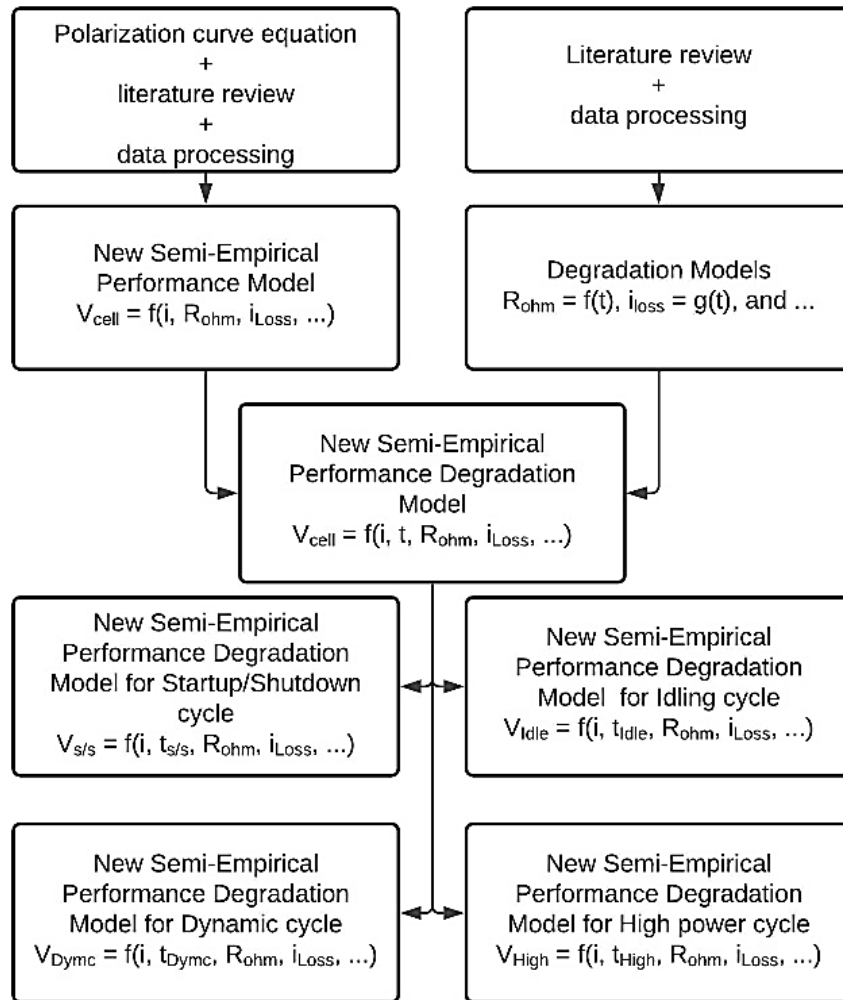


Figure 1-5. Flowchart of the core idea of this thesis

Chapter 2. Overview of Related Work

This chapter outlines the PEMFC performance and performance degradation-related research and lists the best PEMFC performance degradation models found in this study. First, a quick review of PEMFC performance and performance degradation modeling research is carried out. Then, the PEMFC performance degradation phenomena of different vehicle operation modes are discussed. The PEMFC performance and performance degradation models can be classified into three primary categories: theoretical, empirical, and semi-empirical models.

2.1. Existing PEMFC Performance Models

To identify the optimal design and develop the optimal control strategies of a PEMFC system, understanding the performance of the PEMFC is essential. The output voltage usually measures the performance of the PEMFC under a given current and inlet fuel rate. The performance of a PEMFC can be estimated using a model that solves mass transfer PDE of reactants through the PEMFC components. The typical theoretical models are based on the Navier-Stokes equations of fluid flow. This type of modeling is a theoretical model. These models cover all phenomenon that happens while the PEMFC is working and can give a good understanding of the effect of different operating conditions and different material types on PEMFC's performance. The solutions of these complex equations are usually time-consuming and challenging, prohibiting their direct use in FCEV system design and operation control.

Rowe and Li [41] developed a one-dimensional and non-isothermal mathematical model of PEMFC and studied operating parameters on PEMFC performance and membrane water management. They concluded that sufficient anode humidification is needed to maintain membrane hydrated sufficiently, except for reformed fuels and high operating pressures. The reduced cathode humidification will affect the cathode temperature profile as well. According to their study, optimizing operating temperature and pressure for a different cell operating conditions and performance is attainable. Flow field modeling using PEMFC is a typical method to optimize cell size, material, and performance. Water distribution is an essential issue while PEMFC is working primarily in idling and dynamic power load modes.

A semi-empirical model combines the formula explaining the physics of the problem, usually derived from theoretical models, and the formula derived using empirical data. The polarization curve equation is the most frequently used semi-empirical performance model that covers whole PEMFC performance. The polarization curve is a voltage-current line from which the efficiency and power of PEMFC can be derived. The related equation is derived by subtracting different energy losses in the PEMFC in the form of voltage losses. Various equations for representing the polarization curve have been used in the literature as a

PEMFC performance model. Table 2-1 summarises four different PEMFC performance models reported in the literature.

Table 2-1. Different models used in this thesis

No.	Leading Author	Year	Model
Model 1	Bressel, Liu	2016, 2017	$V = E_{rev} - \frac{RT}{2\alpha_c F} \ln\left(\frac{i}{i_{o,c}}\right) - iR + B_c \ln\left(1 - \frac{i}{i_{L,c}}\right)$
Model 2	Mao	2017	$V = E_{rev} - \frac{RT}{2\alpha_c F} \ln\left(\frac{i}{i_{o,c}}\right) - \frac{RT}{2\alpha_c F} \ln\left(\frac{i_{loss}}{i_{o,c}}\right) - iR - me^{ni}$
Model 3	Hu	2018	$V = E_{rev} - \frac{RT}{2\alpha_c F} \ln\left(\frac{i + i_{loss}}{i_{o,c}}\right) - iR - me^{ni}$
Model 4	Jouin	2016	$V = E_{rev} - \frac{RT}{2\alpha_c F} \ln\left(\frac{i + i_{loss}}{i_{o,c}}\right) - \frac{RT}{4\alpha_a F} \ln\left(\frac{i + i_{loss}}{i_{o,a}}\right) - i(R_{ion} + R_{ele} + R_{cr}) + B_c \ln\left(1 - \frac{i}{i_{L,c}}\right)$

Each model has advantages and limitations. Model 1 [42, 43] considered all significant losses, but it did not cover crossover loss thus giving no physical value for the model parameters, especially at lower current densities. Model 2 [44] improved the previous one in two ways. The first term includes crossover loss, and the second term uses an empirical formula for concentration loss but still has a significant drawback. At very low current densities, the second term gives a negative value for the voltage loss; the crossover current is missing and should be deducted from the current. Model 3 [45] solved the second problem of Model 2 by combining the second and third terms in the former model. Model 4 [39] is more comprehensive and considers activation loss in the anode side of PEMFC. It still has the first problem of Model 2. These models have more drawbacks, which will be discussed in detail in the following chapter.

2.2.Existing PEMFC Performance Degradation Models

A performance degradation model predicts how the performance of the PEMFC decays over time during operation. It also can show how the key parameters of the PEMFC performance model change with time. Modeling performance degradation of PEMFC is essential to predict the state of health of the PEMFC stack and its RUL and study the different degradation causes and find mitigation solutions. Two different approaches are found for performance degradation modeling of PEMFC in literature: empirical and semi-empirical methods. Empirical modeling is the way of representing the data without an understanding of the physics of the problem. There is usually a regression model based on experimental data, using curve fitting to determine model parameters without reflecting the physics of the problem. Pei, Chang [17] proposed a quick and straightforward PEMFC's RUL model. The model was based on several AST tests that showed

close to linear voltage degradation with time for PEMFC in different load modes. The model equation is as follow:

$$RUL = \frac{\Delta V}{K(V'_1 n_1 + V'_2 n_2 + V'_3 t_1 + V'_4 t_2)} \quad (2-1)$$

Where, ΔV is the allowable voltage difference, V'_1 to V'_4 are the voltage degradation rate in the four different load modes startup/shutdown, dynamic, idling, and high power, respectively. n_1 and n_2 are the number of cycles in the startup/shutdown and the dynamic modes; t_1 , and t_2 are the time of working in idling and high power modes; K is the adjusting factor, and RUL is the remaining useful life of the PEMFC. They used the proposed model to study the effect of each loading mode in a bus fuel cell system's RUL and found out that dynamic load, startup/shutdown, high power, and idling load modes contributed 56.5, 33, 5.8, and 4.7 percent respectively in PEMFC degradation and performance loss. This result shows that for that specific bus load profile with its PEMFC, dynamic load and startup/shutdown possess a significant portion in performance losses. Chen, Pei [3] benefited from the model indicated in [17] as a quick method for estimating RUL in a vehicular PEMFC. First, they found the model parameters using the results of their test. Then, they used those parameters to estimate PEMFC RUL under two different load modes. A semi-empirical PEMFC performance degradation model is formed using a performance model based on the physics of PEMFCs combined with degradation formula for different terms derived mainly using curve fitting technics with experimental data. Wishart, Dong [46] used a semi-empirical model from Royal Military College researchers and a PC6-1200 stack from Palcan Power Systems, installed to a low-speed fuel cell hybrid electric vehicle (LSFCHEV). They used a local optimization method called sequential quadratic programming (SQP) and two global methods named simulated annealing (SA) and genetic algorithms (GA). They focused on the optimal operating condition leading to peak performance and not optimizing electrochemical parameters used in the design phase. The final aim was to reach maximum net power and maximum energetic efficiency for both stationary and vehicular applications separately.

Jouin, Gouriveau [39] used a general polarization curve equation proposed in [47] as a degradation model with only neglecting concentration and cross-over losses at the anode. They used a published experimental degradation formula for each parameter to form their model as a function of time. Initial parameters were derived by applying the least square method to fit a model to experimental polarization curve data at $t = 0$. Time-varying parameters estimated using power degradation test data. They used four different data sets with constant current and current ripples [48] and Micro-CHP mission profile [49]. Their model showed a good prediction of the RUL of PEMFC. Mao, Jackson [44] investigated the RUL of PEMFC by estimating key parameter variation during the degradation process. They used a different polarization curve equation with neglecting activation loss at the anode and an experimental formula for concentration loss at the

cathode. They succeeded in gaining parameter value by fitting their model with polarization curves data at different time steps and finally proposed various models for the degradation of each parameter. According to them, the proposed model can predict RUL at dynamic conditions as well as steady conditions. Hu, Xu [45] utilized an equation proposed in [17] for a PEMFC working under different load modes to simplify their model. They divided PEMFC working time into two distinct periods based on the nature of the polarization curve and the point that each loss intensifies for their specified load mode test; one for $V > 0.7 V$ and the other for $I < 0.4 A/cm^2$ to simplify the fitting procedure.

A simpler model was used by different researchers considering ohmic resistance and limiting current density as the only two degrading parameters. These researches used extended Kalman filter (EKF) algorithm, particle filter (PF) algorithm [50], adaptive unscented Kalman filter (AUKF) algorithm [43], Gaussian process state-space algorithm [51], long short-term memory recurrent neural networks (LSTM-RNNs) [52] and unscented particle filter algorithm[53] to determine the model parameters and predict the RUL of a PEMFC. **Error! Reference source not found.** summarizes three semi-empirical performance degradation models in the literature.

Table 2-2. Semi-Empirical performance degradation models in the literature.

Performance Degradation Model	
1 Degradation-Model2, Mao2017	$V(I, t) = E_{rev} - \frac{RT}{2\alpha F} \ln\left(\frac{I}{A_{active}}\right) - \frac{RT}{2\alpha F} \ln\left(\frac{b_1 - b_2 t}{a_1 - a_2 t}\right) - d_1 e^{d_2 t} \text{Exp}\left(\frac{I}{A_{active}} e_1 e^{e_2 t}\right) - \frac{I}{A_{active}} (c_1 - c_2 t)$
2 Degradation-Model3, Hu, 2018	$V(I, t) = [U_{eq,0} - IR_0 - A \ln(I)] - Ak_c t_2 - Ik_R t_1$
3 Degradation-Model4, Jouin, 2017	$V(I, t) = E_{rev} - \frac{RT}{2\alpha_c F} \ln\left(\frac{I(t)}{A_0 e^{b_{A1} t + A_1 e^{b_{A2} t}} + i_{loss,0} e^{b_{loss} t}}\right) - \frac{RT}{4\alpha_a F} \ln\left(\frac{I(t)}{A_0 e^{b_{A1} t + A_1 e^{b_{A2} t}} + i_{loss,0} e^{b_{loss} t}}\right) - \frac{I(t)}{A_0 e^{b_{A1} t + A_1 e^{b_{A2} t}}} (R_{ion,0} e^{b_{ion} t} + R_0 + b_R t) + (B_{c,j} + b_D t) \ln\left(1 - \frac{I(t)}{\frac{4F}{RT} \left(\frac{D_{O_2,j} + b_D t}{L_{GDL}}\right) P_{O_2}}\right)$

2.3. PEMFC Degradation under Different Vehicular Load Modes

Different vehicle load modes have distinct degradation effects. Modeling and degradation in the literature for various load conditions are thus discussed separately.

2.3.1. Startup/shutdown

Reiser, Bregoli [54] used a one-dimensional model and reverse current mechanism to study the startup/shutdown process of PEMFC. They showed that cathode interfacial potential difference could be as

high as 1.44 V. While carbon corrosion, cathode electrode thinning, and decrease in Electro Chemical Surface Area (ECSA), or active surface area, were results of this phenomenon to the performance degradation of PEMFC. Tang, Qi [12] determined that degradation during startup/shutdown due to the high potential shows up as corrosion of carbon supports, decrease in cathode catalyst layer thickness, ECSA, and thus its performance loss. During their experiments, a noticeable degradation is observed in the first thirty cycles. They showed that after fifty cycles, ECSA remained about 30 percent of its initial value and cathode catalyst layer thickness reduced to about 1/3 of initial after eighty cycles. Eom, Kim [55] carried out an experiment using a PEMFC exposed to reverse current to simulate startup/shutdown conditions in vehicular usage. They investigated how platinum loading amount at anode catalyst affects the cathode catalyst degradation during the startup/shutdown process. It was revealed that reducing platinum loading from 0.4 to 0.1 mg cm², which does not significantly affect PEMFC performance, decreases the reverse current considerably due to less oxygen reduction in the anode. Furthermore, platinum loading loss causes performance and ECSA decrease, increasing charge transfer resistance because of carbon support corrosion and Pt agglomeration.

Shen, Hou [56] conducted different experiments to study the effects of startup/shutdown on PEMFC performance degradation and found solutions to reduce the effect of startup/shutdown. They used thin copper wire between two membranes in a three-electrode PEMFC. The potential difference of membrane inlet and outlet was 0.8 V, making the potential difference between cathode and membrane outlet as 1.6 V, a high potential, thus causes carbon support corrosion. They also found that an increase in hydrogen or air flow rate diminishes hydrogen/air boundary lasting time. They concluded that purging with nitrogen during the shutdown is not always a good solution, but doing it at startup and applying a dummy load at shutdown is the right solution to diminish the effects of startup/shutdown at performance degradation PEMFC. Kim, Lee [14] used air/hydrogen alternatively as anode gas supply to simulate fuel starvation during the startup/shutdown of a PEMFC. Cathode electrode potential was as high as 1.4 V during the formation of air/hydrogen boundary. They measured CO₂ amount and showed that carbon corrosion directly has a potential higher than 1.0 V. They also found a generation of CO and SO₂ at potentials higher than 1.2 V. The rate of CO formation was more than the SO₂. Although lower temperatures decrease carbon support corrosion, it does not have any effect on cathode potential. Katayanagi, Shimizu [57] inserted two different load mode startup/shutdown and dynamic loads to PEMFC to study the performance degradation of PEMFC. The square-wave potential between 0.6–1.0 V was applied in dynamic load, and the results showed Pt particle agglomeration, thus decreasing ECSA after 1000 cycles test. In the startup/shutdown simulation, saw-wave potential between 1.0 and 1.5 V was applied for 1000 cycles, and corrosion of carbon supports was a significant cause of performance degradation observed in this process.

Dhanushkodi, Kundu [58] carried out experiments by inserting square-wave potential with different upper limits with the same lower limit of 1.0 V to a PEMFC and observing CO₂ emission. Results showed that carbon corrosion increase with higher potential at the upper bound and became almost double when upper potential changed from 1.42 to 1.5 V. It was also concluded that platinum particles in catalyst increase the rate of carbon corrosion. Using online mass spectroscopy during cyclic voltammetry Roen, Paik [59] concluded that carbon supports corrosion increase by increasing platinum loading in the catalyst. Ishigami, Takada [60] simulated the startup/shutdown by inserting hydrogen/air alternatively to the anode side. Carbon support corrosion was a significant result, and they concluded that the shutdown process has a more severe effect on the performance degradation of PEMFC than the startup process. Lin, Cui [61] carried out 1800 startup/shutdown experiments with a PEMFC. The results showed that cathode catalyst degradation at the hydrogen side outlet was more intensive because the cell reversal happened almost in that area. The same result was reported by Lamibrac, Maranzana [62], Durst, Lamibrac [63], and Kreitmeier, Wokaun [64].

2.3.2. Idling

Franck-Lacaze, Bonnet [65] studied the effect of idling by comparing PEMFC degradation under three different current densities 20, 120, and 540 mA cm⁻². Degradation in 120 mA cm⁻² was less than 540 mA cm⁻² while working under very low current densities, saying 20 mA cm⁻² showed a more severe increase in the equivalent cell circuit resistance. The loss of fluorine from the membrane was reported four times greater in 540 mA cm⁻². Han, Shul [66] performed AST tests at OCV using three different membrane types, Nafion NRE212, HP, and SPES50, for 800 hours, and the results showed an increase in hydrogen crossover ohmic resistance also ECSA loss. They concluded that the membrane with lower permeability would last longer. Gaumont, Maranzana [67] carried out three different AST tests. First, constant current test using H₂/N₂ leads to increased membrane resistance and membrane thinning close to the cathode catalyst layer. The second test formed at 1.2 V potential and resulted in carbon support corrosion. The third experiment was the repetition of startup and caused degradation in the cathode catalyst layer close to the anode outlet and carbon support corrosion. Gummalla, Atrazhev [68] used a theoretical model and studied the effect of RH on membrane chemical degradation and concluded that lowering the RH, increasing temperature and decreasing membrane thickness cause more fluoride to be released in membrane structure.

Kundu, Fowler [69] tested four different RH, 100, 75, 50, and 20 percent RH, at OCV potential and monitored fluoride release. A decrease in the RH, increase gas crossover, and degradation in the ionomer layer close to the cathode catalyst was also observed. They also used a semi-mechanism model to study the fluoride release results, which fit their experimental data well. Ghassemzadeh, Kreuer [70] showed that under OCV, oxygen migrates to the anode without the help of electro-osmotic drag. Ferreira, Shao-Horn

[71] found that degradation effects show up as ECSA decreases are more severe at 0.95 V, saying OCV or idling conditions compare to 0.75 V potential. Similar degradation results are reported by Akita, Taniguchi [72] using 1.0 and 0.8 V potential tests. Large Pt particles were found in the membrane, and they concluded that the amount of Pt particles in the membrane is relative to the gas concentration. Zhang, Yuan [35] carried out an OCV test for 256 hours. The results showed that membrane thinning and catalyst agglomeration are the main degradation effects of working at OCV, which indicates that ECSA and OCV decrease. ECSA loss was 51.9 percent during this 256 hours' test at OCV potential.

Guilminot, Corcella [73], Wang, Kumar [74], and Guilminot, Corcella [75] showed that Pt dissolution in membrane ionomer occurs when operating close to OCV potentials. According to test results by Zhang, Litter [76], after 2000 hours of OCV test, 55 percent of cathode Pt catalysts were distributed into the membrane. A 9-cell Mk1100 Ballard stack was tested by Narimani et al. [77, 78] to evaluate hydrogen emission at idling and low current densities. The results showed that hydrogen emissions are highly related to the current demand and cathode oxygen concentration. They also provided a model to estimate the hydrogen amount in the cathode outlet and showed that the model worked correctly.

2.3.3. Dynamic load

Liu, Wang [26] conducted a PEMFC degradation acceleration test for 1000 hours using the Chinese NERC Fuel Cell and Hydrogen Technology Drive Cycle Test Protocol. As a result, $70 \mu\text{V h}^{-1}$ voltage degradation rate at 500 mA/cm^2 was reported on average. Furthermore, a 55 percent reduction in the active surface area occurred, and hydrogen cross-over increased from 2 mA cm^{-2} at 300 h to 17 mA cm^{-2} at 900 h. The hydrogen crossover is the primary cause of membrane failure during dynamic load [26]. Yu, Li [10] carried out AST dynamic load mode test for 300 hours using NEDC driving cycle for 55°C and 75°C with 50 percent RH. Although they used a low current density (0.52 A/cm^2) for a full load at their dynamic load test, they still observed a high degradation rate. Both degradation rate and recovery were higher as temperature increases. The degradation rate increased with time, but the recovery rate decreased with time passing. It was also showed that recovery is lower at high current densities.

Weng, Hsu [24] used current cycling of 70 to 700 mA/cm^2 for 450 cycles and 150 hours. The cell was divided into eight segments and close to downstream at segments 6 to 8 where the humidity cycling is more, degradation was more severe, and that is due to the increase in hydrogen crossover. However, they did not notice a significant degradation during their experiment. Mukundan, Baker [27] conducted an accelerated stress test (AST) using RH cycling at OCV to investigate membrane degradation. Membrane thinning and forming cracks in the membrane were the degradation results of their tests. Alavijeh, Khorasany [28] used an accelerated mechanical stress test and showed that creating cracks is an obvious result of humidity

cycling in both membrane and catalyst layers. Chang, Liu [25] studied the effect of thermal and humidity cycling using three experiments, each for 500 cycles. Results showed that thermal cycling does not significantly degrade while humidity cycling degrades membrane and CL distinctively, and combining both increases degradation much more. Catalyst agglomeration and decrease in active surface area, crack growth, increase in ohmic resistance, and charge transfer resistance was observed during the experiment using thermal and humidity cycling. Crack length growth was 13-30 percent in the humidity cycling test and 2-6 times in the humidity/thermal cycling experiment simultaneously. The active surface area changed from $64.1 \text{ m}^2 \text{ g}^{-1}$ to $49.1 \text{ m}^2 \text{ g}^{-1}$ after 500 thermal/humidity cycles [25]. Venkatesan, Dutta [29] conducted square-wave potential cycling for voltages between 0.6 and 1.3 V, resulting in Pt/C and CL structure change and ionomer redistribution that leads to active surface area decrease. Dou, Hou [21] explored the effect of oxidant starvation in a single cell. They found out that at a current density of $600 \text{ mA} \cdot \text{cm}^{-2}$, the cell voltage decrease from -0.08 to -0.2 if the cathode stoichiometric ratio decrease from 0.9 to 0.2. At low stoichiometric ratios, oxygen and hydrogen reduction reactions can occur at the cathode simultaneously, leading to the formation of pinholes and membrane and catalyst degradation. Carbon corrosion is more common in fuel starvation than oxygen starvation. Taniguchi, Akita [22] performed a single-cell test to study the effect of air starvation on PEMFC degradation. Air starvation leads to cell reversal, and after 120 min they observed a 46 percent reduction in active surface area. Zhao, Shahgaldi [79] conducted a wet-dry cycle test of PEMFC and concluded that humidity cycling due to dynamic load modes leads to catalyst particle agglomeration, pinholes formation, and growth of cracks that cause degradation of active surface area and catalyst activity. Patterson and Darling [23] showed that fuel starvation causes cathode catalyst degradation after 100 hours of PEMFC testing. Wang, Huang [30] examined PEMFC vehicular dynamic load mode using a cycling current density between $25 \text{ mA} \cdot \text{cm}^{-2}$ and $600 \text{ mA} \cdot \text{cm}^{-2}$ for 100 cycles, similar to idling to rated current dynamic load. A voltage decrease rate of $1.0 \text{ } \mu\text{V} \cdot \text{cycle}^{-1}$ at $25 \text{ mA} \cdot \text{cm}^{-2}$ at idling and $2.0 \text{ } \mu\text{V} \cdot \text{cycle}^{-1}$ at mid-power was observed. The decrease in cathode catalyst thickness was resulted in their test because of dynamic load cycling and carbon corrosion was because of working at high current densities. Guétaz, Escribano [31] found out that degradation is non-uniform in load cycling but more uniform at constant load. After their dynamic load test cathode catalyst particles agglomeration was more intensive at cathode inlet than other areas. Hydrogen starvation and oxygen crossover are two main factors increasing degradation effects in dynamic load cycling.

2.3.4. High power

The amount of researches on the degradation of PEMFC working at high power loads is not significant. Zhang, Yang [80] reported cathode flooding, hot spots formation, and gas starvation, respectively leading

to water management difficulty, polymer degradation, and chemical degradation of membrane and carbon corrosion as degradation effects of working in the high power mode.

2.4. Summary

The PEMFC performance and performance degradation modeling efforts reported in recent literature have been overviewed in this chapter. Three different types of performance and performance degradation models are discussed. The semi-empirical models present an accuracy level close to the theoretical models and simplicity of an empirical model. Although the researchers have worked extensively on PEMFC performance degradation modeling in recent years, there is still a lack of a suitable model for FCEV design and control optimizations. First, the empirical model introduced by Pei, Chang [17] presented a major step forward in capturing the performance degradation behaviors of a PEMFC. However, the model still has two drawbacks: a) the lack of information on how the physical properties of PEMFC change with time, and b) the linear model is less capable of reflecting the nonlinear PEMFC degradation trend shown by the data collected over its whole life. Several other researchers have introduced and used semi-empirical performance degradation models based on the polarization curve equation, as shown in Table 2.2. These models were introduced using lab experiment data under various ideal operation conditions, different from the actual power load patterns of an FCEV. These models are unable to capture the observed effects of different vehicular load modes on PEMFC degradation. Dealing with the power variation under these operation modes is vital in designing and controlling an FCEV to reduce the degradation of the PEMFC. This study will introduce new semi-empirical performance and performance degradation models to address these issues.

Chapter 3. New PEMFC Model

In this chapter, using the literature review in Chapter 2 and studying the experimental data, a new semi-empirical PEMFC performance model with adopted terms will be introduced. This new performance model will then be used to form a new semi-empirical performance degradation model, which will then be related to the PEMFC vehicular load modes. Finally, later in Chapter 5, these new models will be used to study the degradation and PEMFC remaining useful life.

3.1. New PEMFC Performance Model

In this section, a new semi-empirical performance model based on polarization curve equation will be improved.

3.1.1. Form of the PEMFC Performance Model

In a general polarization curve equation, shown in Equation (3-1) [47], several voltage loss terms contribute to a decrease of the reversible voltage to the operating output voltage of the fuel cell under a specific current.

$$\begin{aligned}
 V = E_{rev} - \frac{RT}{2\alpha_c F} \ln\left(\frac{i + i_{loss}}{i_{o,c}}\right) - \frac{RT}{4\alpha_a F} \ln\left(\frac{i + i_{loss}}{i_{o,a}}\right) - i(R_{memb} + R_{ele} + R_{cr}) \\
 + B_c \ln\left(1 - \frac{i}{i_{L,c}}\right) + B_a \ln\left(1 - \frac{i}{i_{L,a}}\right)
 \end{aligned} \tag{3-1}$$

This equation m contains 15 parameters, as listed in Table 3-1. E_{rev} is the reversible voltage which is sometimes known as an OCV, which is not correct.

Table 3-1. Polarization curve equation parameters

Parameter	Description
V	The output voltage of the cell
i	Current density in cell area (A/cm ²)
E_{rev}	The reversible voltage or Nernst voltage (V)
T	Temperature of cell
α_c & α_a	Charge transfer at anode and cathode
i_{loss}	Loss current density due to the crossover
$i_{o,c}$ & $i_{o,a}$	Exchange current density at anode and cathode
R_{memb}	Resistance to ion transfer in membrane and catalyst
R_{elec}	Resistance to electron transfer
R_{cr}	Resistance due to the contact of GDL-CL-Membrane
B_c & B_a	Concentration loss term parameters
$i_{L,c}$ & $i_{L,a}$	Limiting current density at anode and cathode

Reversible voltage is the amount of potential expected to get base on the chemical reaction in PEMFC and is estimated using Equation 3-2 [81]:

$$E_{rev} = 1.229 - 0.85 \times 10^{-3}(T - 298.15) + 4.309 \times 10^{-3}T \times \left[\ln(P_{H_2,interface}) + \frac{1}{2} \ln(P_{O_2,interface}) \right] \quad (3-2)$$

Where $P_{H_2,interface}$ and $P_{O_2,interface}$ are the pressure and the temperature at the catalyst and the GDL interface.

In a PEMFC connected to reactant reservoirs but not to load, the reversible voltage decreases mainly due to the two different PEMFC related voltage losses [37]. Crossover, which is the crossing of H₂ and O₂ molecules and electrons through the membrane, has two effects: i) the Crossing reduce the potential of electric current production, and ii) H₂ or O₂ molecule that crosses will react directly with O₂ at cathode or H₂ at the anode, respectively, causing a reverse potential not considered in the above equation [103]. This reduction in voltage (performance) is mainly because of the reaction between Pt and oxygen resulting in Platinum Oxide (PtO), which happens mainly when the cell voltage is greater than 0.8V [37]. Neglecting this mechanism affects the value of other parameters. It results in an incorrect value, especially for the activation-loss term's parameters. Still, considering a discreet model to be able to affect it at higher voltages (greater than 0.8 V) will increase the complexity of the performance degradation models to be introduced later in this chapter, which means there would be two models for each loading mode, or the initial value of the parameters of each model will be different. To simplify the model, it is considered as a constant parameter at all ranges of cell operating voltage which reduce the reversible cell voltage in the polarization curve equation.

The second and third terms in Equation 3-1 are activation losses (potential). Activation potential values are different in anode and cathode. The results of fitting with experimental data show equal exchange current densities for anode and cathode, which is incorrect and does not give any physical meaning [82]. To overcome this problem, a combined equation is proposed in [82].

$$\frac{RT}{\alpha F} \ln \left(\frac{i + i_{loss}}{i_o} \right) \quad (3-3)$$

$$\frac{1}{\alpha} = \frac{1}{2\alpha_c} + \frac{1}{4\alpha_a} \quad (3-4)$$

$$i_o = i_{o,c} \frac{\alpha}{2\alpha_c} \cdot i_{o,a} \frac{\alpha}{4\alpha_a} \quad (3-5)$$

Charge transfer parameters in anode and cathode are two other parameters that significantly impact PEMFC performance. All electrochemical reactions have transition states. Charge transfer shows how much this transition state is intended to lead to products or reactants. The charge transfer parameter is

between 0 and 1, and the higher parameter shows more reaction and less activation loss. For one-step transition states, symmetry parameter is used, but both PEMFC reactions are multi transition states, and summation of α_c and α_a is not always equal to unity, and according to Frano [82] $\alpha_a = 0.5$ and $\alpha_c = 0.1-0.5$. However, there is no information on determining them or changing with current or their degradation process. Considering these parameters as degrading parameters depends on the PEMFC as they depend on electrode material and structure, which degrade during PEMFC working. Eqn. (3-6) shows exchange current density relationship with operating parameters (regardless of electrode type) [82]:

$$i_o = i_o^{ref} a_c L_c \left(\frac{p_r}{p_r^{ref}} \right)^\gamma \text{Exp} \left[\frac{-E_c}{RT} \left(1 - \frac{T}{T_{ref}} \right) \right] \quad (3-6)$$

When it is written in the form of Ampere per square centimeter of Pt:

$$i_o = i_o^{ref} \left(\frac{p_r}{p_r^{ref}} \right)^\gamma \text{Exp} \left[\frac{-E_c}{RT} \left(1 - \frac{T}{T_{ref}} \right) \right] \quad (3-7)$$

Exchange current density also depends on the temperature and pressure/concentration of reactants. The temperature may change due to the degradation of the cooling system. The concentration of gases may vary due to the degradation of the gas diffusion layer, so there is the possibility of degradation in exchange current density. According to Frano [82], the anode's exchange current density is much higher than the cathode ($\sim 10^{-3}$ versus $\sim 10^{-9}$ A cm⁻² Pt, at 25 °C and 1 atm for acid electrolyte). However, the overpotential of the anode is always negligible, but the degradation of anode exchange current density is more important; thus, both should be considered in the performance degradation model. Overall, using a unified formula for both not only considers the effect of all the parameters also simplifies the model.

The logarithmic formula for activation loss does not provide a reasonable estimate at a very low current. The reason is that the activation loss term gives a negative value at the points where the exchange current density is higher than the current density, and the value of this term adds potential to the reversible voltage instead of deducting a value. The activation loss changes linearly with current at very low current densities, so Eqn. (3-8) fits well for the low current densities. The logarithmic equation (Eqn. (3-9)) fits with the experimental data at higher current densities.

$$\eta_{act} = \frac{RT}{2\alpha F} \frac{i}{i_o} \quad (3-8)$$

$$\eta_{act} = \frac{RT}{\alpha F} \ln \left[\frac{i}{i_o} \right] \quad (3-9)$$

Eqn. (3-9) comes from the Butler-Volmer equation when the assumption is that the second term is negligible compared to the first term, which is correct only at higher current densities. To resolve this

problem, an inverse hyperbolic sin is suggested [83], which comes from the Butler-Volmer equation when considering equal charge transfers.

$$i = i_0 \left\{ \exp\left(\frac{\alpha_a F \eta_{act}}{RT}\right) - \exp\left(-\frac{\alpha_c F \eta_{act}}{RT}\right) \right\} \quad (3-10)$$

$$\frac{i}{i_0} = \exp\left[\frac{\alpha_a F \eta_{act}}{RT}\right] - \exp\left[-\frac{\alpha_c F \eta_{act}}{RT}\right] = 2 \sinh\left[\frac{\alpha F \eta_{act}}{RT}\right] \quad \text{if } \alpha_a = \alpha_c = \alpha \quad (3-11)$$

Solving for the activation loss will give:

$$\eta_{act} = \frac{RT}{\alpha F} \sinh^{-1}\left[\frac{i}{2i_0}\right] \quad (3-12)$$

The hyperbolic inverse sin equation plot in Figure 3-1 fit well at lower currents with the linear formula and higher currents with the logarithmic formula, showing this is a good formula to model activation loss.

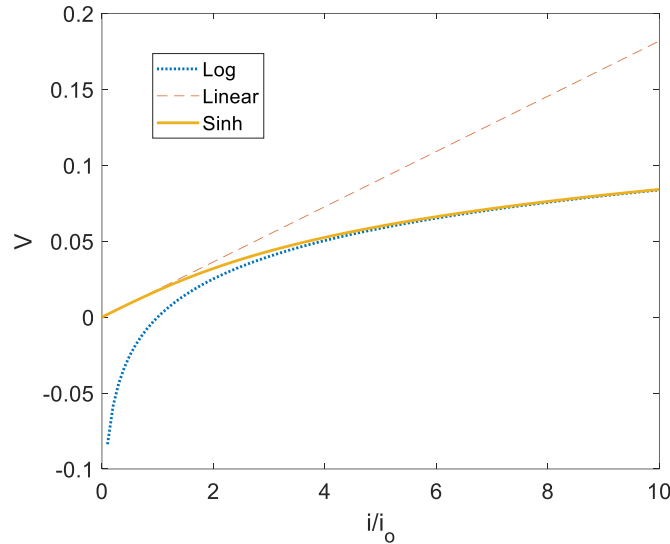


Figure 3-1. Activation loss vs. current density over exchange current density plotted using a different formula

Ohmic resistance combines three different resistances, contact resistance, electron resistance, and proton resistance.

$$\eta_{ohm} = iR = iR_{elec} + iR_{cr} + iR_{memb} \quad (3-13)$$

According to Frano [82] and Owejan [84], electronic resistance is not as significant as contact resistance, and contact resistance has the same order of magnitude as membrane resistance. Contact resistance changes because of degradation in GDL layers, and ionic resistance varies due to membrane degradation. Also, the degradation rate might be different between contact and membrane resistance. Still, because their initial value is in the same order of magnitude, and to decrease the complexity of the model, one parameter is assumed to capture both mechanisms. Concentration loss becomes prominent when the reactant is consumed faster than it can reach the surfaces of the catalyst; also, the higher rate of water production

causes more water in the GDL pores, which decreases the gas transfer paths. Concentration loss is less critical at the anode than the cathode because there is pure hydrogen and no water production. In addition, there are non-uniform current distribution areas above the ribs of bipolar plates that have lower limiting current density. Therefore, the logarithmic term with a limiting current parameter does not fit well with experimental data. Instead, an exponential relationship for the concentration loss is used, as shown in Eqn. 3-14, and found to have a better fit with the experimental data.

$$\eta_{con} = me^{ni} \quad (3-14)$$

Where m and n are empirical parameters, this equation has a drawback in zero current density where effects of concentration loss are not expected. Still, this equation has a value equal to parameter m at zero current density. Estimations show that the magnitude of m is less than 0.1 percent of OCV voltage, but an improvement is proposed in the form of Eqn. (3-15) [85]:

$$m(e^{ni} - 1) \quad (3-15)$$

Substituting all the mentioned formula for each term in Eqn. (3-1), the new semi-empirical performance model would be:

$$V = E_{rev} - V_{PtO} - \frac{RT}{\alpha F} \sinh^{-1} \left(\frac{i + i_{loss}}{2i_o} \right) - iR - m(e^{ni} - 1) \quad (3-16)$$

This is the new semi-empirical performance model introduced in this study. The model will be used later in Section 3.2 to form the new semi-empirical performance degradation model. Table 3-2 summarizes the terms of the new performance model and their definitions.

Table 3-2. New performance model's terms

Term	Definition
E_{rev}	Reversible Voltage
V_{PtO}	Pt Oxidation Potential
$\frac{RT}{\alpha F} \sinh^{-1} \left(\frac{i + i_{loss}}{2i_o} \right)$	Activation Loss(+ Crossover)
iR	Ohmic Loss
$m(e^{ni} - 1)$	Concentration Loss

3.1.2. Determination of Model Parameters

Equation (3-16) has two constant parameters (F , R), two operating parameters (T , E_{rev}) and eight performance parameters: A_{active} , V_{PtO} , α , i_{loss} , i_o , R , m , n which change with time as the PEMFC degrades. **Error! Reference source not found.** summarizes all the parameters of the model. V_{PtO} is the voltage loss d

ue to the potential between PtO and Pt at the catalyst, α is the charge transfer parameter related to anode and cathode side's charge transfer parameter, i_{loss} is the loss current density (mainly due to the hydrogen crossover), and i_o is the exchange current density.

Table 3-3. New performance model's parameters

Parameter	Value	Source
F	96485C mol ⁻¹	Faraday's constant
R	8.314J·K ⁻¹ ·mol ⁻¹	Gas constant
E _{rev}	≅1.187 V	[86]
T	≅55°C	Datasheet
A _{active}	≅100 cm ²	Datasheet
V _{PtO}	Curve Fitting	Data
α	Curve Fitting	Data
i_{loss}	Curve Fitting	Data
i_o	Curve Fitting	Data
R	Curve Fitting	Data
m	Curve Fitting	Data
n	Curve Fitting	Data

R is the Ohmic resistance (a combination of protonic (Ionic), electronic, and contact resistance due to electron and proton transfer in PEMFC). m and n parameters are experimental parameters relating to concentration loss. m is a parameter relating to water management, gasses permeability, and cell geometry resulting in non-uniform distribution of reactants in catalyst, and n is a parameter relating to limiting current density.

3.2. New PEMFC Performance Degradation Model

The new performance model includes the best approach for each loss term and consists of a missing term from all previous models (PtO potential). This performance model is combined with a degradation measuring portion, resulting in a new semi-empirical performance degradation model covering all the benefits of previously introduced models.

3.2.1. Form of the New Model

Substituting degradation formula for parameters in Eqn. (3-16) results in a semi-empirical performance degradation model. The last step is to relate this new model with different loading modes. First, because

current density is not accessible, it is replaced with total current and active surface area (or ECSA) in Eqn. (3-16) according to:

$$i(t) = \frac{I(t)}{A_{active}} \quad (3-17)$$

Base on the literature review and using the fitting, degradation formulas for the parameters are as follows. Eqn. (3-18) derived using the fitting tools in MATLAB with the experimental data in [71, 87-92], and it is a new formula for active surface area degradation introduced in this study.

$$A_{active} = A_{active,0} - A_1 \ln(A_2 t + 1) \quad (3-18)$$

Eqns. (3-19) and (3-20) are both for the PtO potential degradation. The first one is derived from fitting with the OCV experimental data and is used to model the startup/shutdown, and the second for all the other experimental data. Both equations will be used in the performance degradation modeling.

$$V_{PtO} = V_{PtO,0} \exp(V_{PtO}^1 t) \quad (3-19)$$

$$V_{PtO} = V_{PtO,0} + V_{PtO}^1 t \quad (3-20)$$

Equation (3-21) is for the ohmic loss. Also, the linear formula has been used for the contact and electronic resistances. Still, the exponential formula gives the best fit when using one ohmic resistance parameter instead of the three parameters [93].

$$R = R_0 \exp(R_1 t) \quad (3-21)$$

$$i_{loss} = i_{loss,0} \exp(i_{loss}^1 t), \quad (3-22)$$

Equation (3-22) gives the degradation formula for the crossover current density used in several pieces of literature [27, 94-99].

$$m = m_0 \exp(m_1 t) \quad , \quad n = n_0 \exp(n_1 t), \quad (3-23)$$

These two equations relate the parameters in the empirical formula for the concentration loss with time. The exponential formula is reported in [44]. By replacing the parameters with their degradation formula in the performance model, the new PEMFC semi-empirical performance degradation model becomes:

$$\begin{aligned} V = E_{rev} - (V_{PtO,0} + V_{PtO} t) - \frac{RT}{\alpha F} \sinh^{-1} \left(\frac{\frac{I(t)}{A_{active}} + i_{loss,0} \cdot \exp(i_{loss}^1 t)}{2i_o} \right) \\ - \frac{I(t)}{A_{active}} \cdot (R_0 \exp(R_1 t)) \\ - m_0 \exp(m_1 t) \left[\exp\left(\frac{I(t)}{A_{active}} \cdot n_0 \exp(n_1 t)\right) - 1 \right] \end{aligned} \quad (3-24)$$

This model still has the drawback of not relating to the four load modes of an FCEV. A PEMFC works in a range of current densities. Each voltage loss term of the polarization curve equation may have a different value under any current density. At very low current density, the concentration loss term is negligible by its nature. Also, the ohmic loss term can be ignored, comparing to the two remaining terms with some error. During startup/shutdown and the idling load modes, where the current density is very low or zero, these two terms are dropped in the model. The PEMFC is still working in a range that concentration loss is negligible for the dynamic load mode so that this term is eliminated in the model for this mode. Table 3-4 summarizes which term (Voltage losses) of the performance model participates in voltage degradation for a specific load mode.

Table 3-4. Effect of different voltage loss terms in four loading modes

	Activation	Ohmic	Concentration
Startup/Shutdown	Yes	No	No
Idle/OCV	Yes	No	No
Dynamic load	Yes	Yes	No
High power	Yes	Yes	Yes

As discussed in Chapter 2, different loading modes have distinct degradation effects on the PEMFC. This means some parameters may not cause degradation under some load modes. Table 3-5 summarizes the learning from the literature in Chapter 2 and Section 1.3.2. Table 3-6 summarizes which parameters are affected by a specific load mode, and “No” means it does not degrade under that particular operating mode. This table uses the results in and references [80, 91, 100].

Table 3-5. Degradation effects of each vehicular load mode

Load Mode	Degradation effects
Startup/shutdown	1- Active surface area decreases due to carbon corrosion [11-14, 55-57, 59-65, 68] 2- Active surface area decreases due to the cathode catalyst layer thinning [7, 15, 16]
Idling load	1- Active surface area decrease[7] 2- Hydrogen crossover increase [67-70] 3- Ohmic resistance increase [67-68]
Dynamic load	1- Active surface area decreases due to the pinholes formation and cathode catalyst particles agglomeration [80] [21-23] 2- Hydrogen crossover increase [24, 26] 3- Ohmic resistance increases due to the decrease in contact area[24, 25]
High power load	1- Ohmic resistance increases due to the Membrane chemical corrosion [7] 2- Active surface area decreases due to the Dissolution and agglomeration of Platinum and carbon support corrosion [7].

Table 3-6. Effect of PEMFC degradation on different parameters in four loading modes

Load	i_{loss}	V_{PtO}	A_{active}	R	m & n
Startup/Shutdown	No	Yes	Yes	No	No
Idle	Yes	Yes	Yes	No	No
Dynamic load	Yes	No	Yes	Yes	Yes
High power	No	No	Yes	Yes	Yes

Here A_{active} and R are active surface area and ohmic resistance, respectively. During startup/shutdown and while PEMFC is working at high power, the crossover current density does not change significantly. Thus we can say this parameter does not degrade with these two load modes. Based on the literature review, the PtO potential decreases primarily during startup/shutdown and idling load. Its degradation is negligible while PEMFC is working at dynamic and high power load. Considering exceptions in Table 3-4 and Table 3-6, the final semi-empirical performance degradation models for each four load modes will be:

1) Open circuit voltage or startup/shutdown mode

For the PEMFC working at the OCV, since there is no current, the ohmic and concentration loss cancel out. The same assumptions will be made for the startup/shutdown mode, as the current density will be very low if it exists. The only difference is that working on OCV, which is odd in a PEMFC stack as there are always auxiliary components like pumps and compressors that connect to the PEMFC. However, the time of working at OCV is the parameter affecting the degradation in this load mode and, for the startup/shutdown mode, the number of cycles affects the degradation. So the degradation model for startup/shutdown would be:

$$V_S(n^S) = E_{rev} - (V_{PtO,0} \exp(V_{PtO}^S n^S)) - \frac{RT}{\alpha F} \sinh^{-1} \left(\frac{i_{loss,0}}{2i_o} \right) \quad (3-25)$$

The exponential formula has been used for the PtO potential degradation as this formula gives a better fit with the experimental data than the linear equation. The explanation for each parameter is summarized in Table 3-7.

Table 3-7. Parameters in new performance degradation model in OCV & startup/shutdown

parameter	description
V_S	Voltage value during startup/shutdown cycling
n^S	Number of startup/shutdown cycle
$V_{PtO,0}$	Voltage loss due to the PtO potential at the beginning of startup/shutdown cycling
V_{PtO}^S	Voltage degradation rate due to the PtO potential change
$i_{loss,0}$	Loss current density value at the beginning of startup/shutdown cycling.

2) Idling mode

Ohmic and concentration loss terms are negligible in the idling load. So, the semi-empirical performance degradation model for the idling load mode will be:

$$V_I(I, t^I) = E_{rev} - (V_{PtO,0} + V_{PtO}^I t^I) - \frac{RT}{\alpha F} \sinh^{-1} \left(\frac{\frac{I(t^I)}{A_{active}(t^I)} + i_{loss,0} \cdot \exp(i_{loss}^I \cdot t^I)}{2i_o} \right) \quad (3-26)$$

Table 3-8. Parameters in new performance degradation model in the idling loading mode

Parameter	Description
V_I	Voltage value during idling load
t^I	Time while PEMFC works at idling
I	Cell or stack current varying with time
$V_{PtO,0}$	Voltage loss due to the PtO potential at the beginning of the idling load
V_{PtO}^I	Voltage degradation rate due to the PtO potential change
$i_{loss,0}$	Loss current density value at the beginning of idling load
i_{loss}^I	Voltage degradation rate due to the change in loss current density
A_{active}	Active surface area during idling load

3) Dynamic mode

During the dynamic mode, the effect of PtO potential is more negligible because of higher currents; thus, its degradation is negligible. Although the current density is higher than the idling load, it is still low enough to neglect the concentration loss. Thus the semi-empirical performance degradation loss in this loading mode is defined as:

$$V_D(I, t^D) = E_{rev} - (V_{PtO,0}) - \frac{RT}{\alpha F} \sinh^{-1} \left(\frac{\frac{I(t^D)}{A_{active}(t^D)} + i_{loss,0} \cdot \exp(i_{loss}^D \cdot t^D)}{2i_o} \right) - \frac{I(t^D)}{A_{active}(t^D)} (R_o \exp(R^D t^D)) \quad (3-27)$$

The parameters of this equation are summarized in Table 3-9.

Table 3-9. Parameters in new performance degradation model in the dynamic loading mode

Parameter	Description
V_D	Voltage value during dynamic load
t^D	Time while PEMFC works at dynamic load
I	Cell or stack current varying with time
$V_{PtO,0}$	Voltage loss due to the PtO potential at the beginning of the dynamic load
$i_{loss,0}$	Loss current density value at the beginning of the dynamic load
i_{loss}^D	Voltage degradation rate due to the change in loss current density
R_0	Ohmic resistance value at the beginning of the dynamic load
R^D	Ohmic resistance rate due to the change in loss current density
A_{active}	Active surface area during dynamic load

4) High power mode

A high power mode is not a typical load mode, and PEMFC usually faces it during going up the hills at high speed. This power range means the fuel cell is working close to the limiting current density. The effect of concentration loss is starting to decrease PEMFC power at a more rapid rate, so the degradation in concentration loss should be taken into account. The loss current density becomes negligible in this loading mode because higher current densities increase the reaction rate. This degradation effect can be removed from the new performance degradation model. In conclusion, the PEMFC semi-empirical performance degradation model at a high power mode will become:

$$V_H(I, t^H) = E_{rev} - (V_{PtO,0}) - \frac{RT}{\alpha F} \sinh^{-1} \left(\frac{\frac{I(t^H)}{A_{active}(t^H)} + i_{loss,0}}{2i_o} \right) - \frac{I(t^H)}{A_{active}(t^H)} (R_0 \exp(R^H t^H)) - m_0 \exp(m^H t^H) [\exp(\frac{I(t^H)}{A_{active}(t^H)} n_0 \exp(n^H t^H)) - 1] \quad (3-28)$$

Table 3-10 summarizes the parameters of this equation.

Table 3-10. Parameters in new performance degradation model in high power loading mode

Parameter	Description
V_H	Voltage value during high power load
t^H	Time while PEMFC works at high power
I	Cell or stack current varying with time
$V_{PtO,0}$	Voltage loss due to the PtO potential at the beginning of the high power load
$i_{loss,0}$	Loss current density value at the beginning of high power load
R_0	Ohmic resistance value at the beginning of high power load
R^H	Ohmic resistance rate due to the change in loss current density
m_0	Concentration loss first parameter value at the beginning of high power load
m^H	Concentration loss first parameter rate due
n_0	Concentration loss second parameter value at the beginning of high power load
n^H	Concentration loss second parameter rate
A_{active}	Active surface area during high power load

In summary, seven initial parameters and ten degradation parameters need to be determined in the new model. Table 3-11 summarizes the degradation parameters under the four different operation modes.

Table 3-11. Aging parameters are related to four loading modes

load mode	Parameter1	Parameter2	Parameter3	Parameter4	Parameter5
S/S	A_1	A_2	V_{PtO}^S	-----	-----
Idle/OCV	A_1	A_2	V_{PtO}^I	i_{loss}^I	-----
Dynamic load	A_1	A_2	i_{loss}^D	R^D	-----
High power	A_1	A_2	R^H	m^H	n^H

3.2.2. Parameter Determination of the Semi-Empirical Model

In the new PEMFC performance degradation models, there are 22 constants, operating, initial and degrading parameters. Table 3-12 summarizes constant/operating and initial parameters. The first group is measured from curves and data sheets in the literature. The second group is obtained by fitting the performance model with the polarization curve data at the beginning. Table 3-13 summarizes the degrading parameters estimated using the performance degradation model and voltage degradation data of PEMFC and the curve fitting methods.

Table 3-12. Constant/operating and initial parameters of new performance degradation model

Parameter	Value	Source
E_{rev}	Based on data	[86]
F	96485C mol ⁻¹	Faraday's constant
R	8.314J·K ⁻¹ ·mol ⁻¹	Gas constant
T	Based on data	Datasheet
$A_{active,0}$	Based on data	Datasheet
$V_{PtO,0}$	Based on data	Fitting
α	Based on data	Fitting
$i_{loss,0}$	Based on data	Fitting
i_o	Based on data	Fitting
R_0	Based on data	Fitting
m_0	Based on data	Fitting
n_0	Based on data	Fitting

Table 3-13. Degrading parameters of new performance degradation model

Parameter	Value	Source
V_{PtO}^S	Based on data	Fitting
V_{PtO}^I	Based on data	Fitting
i_{loss}^S	Based on data	Fitting
i_{loss}^I	Based on data	Fitting
R^D	Based on data	Fitting
R^H	Based on data	Fitting
m^H	Based on data	Fitting
n^H	Based on data	Fitting
A_1	Based on data	Fitting
A_2	Based on data	Fitting

3.2.3. New Unified Semi-empirical PEMFC Performance Degradation Model

These four new models associated with different FCEV operation/loading modes can be combined to form a unified model. This unified model is useful when there are no test data for these loading modes separately, and the experiment has been done using a combined load pattern with startup/shutdown, idling, dynamic, and high power load modes.

$$\begin{aligned}
V = E_{rev} - (V_{Pt0,0} + V_{Pt0}^I t^I) \exp(V_{Pt0}^S n^S) \\
- \frac{RT}{\alpha F} \sinh^{-1} \left(\frac{\frac{I(t)}{A_{active}} + i_{loss,0} \cdot \exp(i_{loss}^I \cdot t^I + i_{loss}^D \cdot t^D)}{2i_0} \right) \\
- \frac{I(t)}{A_{active}} \cdot (R_0 \text{Exp}(R^D t^D + R^H t^H)) \\
- m_0 \exp(m^H t^H) \left[\exp\left(\frac{I(t^H)}{A_{active}(t^H)} n_0 \exp(n^H t^H)\right) - 1 \right]
\end{aligned} \tag{3-29}$$

S, *I*, *D*, and *H* are indexes for startup/shutdown, idling, dynamic, and high power load modes. Active surface area (A_{active}) changes due to the degradation under these four load modes. Assuming the degradation rate in this parameter changes differently under each loading mode, eight parameters exist for the new model, increasing the complexity of the model. On the other hand, the model fitting results for this model showed a similar value for each of them because of the nature of the numerical solution. For these reasons, assuming Eqn. (3-18) for all four load modes with the same degradation parameter (A_1, A_2) is an acceptable assumption, and

$$t = t^I + t^D + t^H \tag{3-30}$$

3.3. Summary

This chapter introduced a new, generic semi-empirical performance model capturing the main mechanisms of PEMFC performance. By including performance degradation capturing terms and parameters, a new PEMFC performance degradation model is created. This new performance degradation model is related to the four FCEV operation/loading modes, removing insignificant terms, forming four new semi-empirical performance degradation sub-models, one for each operation mode. Model degradation parameters are then determined by fitting experimental data specific to each mode of operation. In Chapter 4, the newly introduced models will be validated using experimental data and compared with models introduced previously in the literature. In Chapter 5, these new models will be used to simulate the PEMFC performance in FCEV operations and predict the PEMFC performance degradation.

Chapter 4. Validation of the New Model

This chapter examines the accuracy and capability improvement of the new semi-empirical performance and performance degradation models introduced in Chapter 3. First, experimental data used in this study are explained, and then the accuracy of the newly introduced model is discussed and compared to other models in the literature. In the end, the benefit of the new performance degradation model is shown for each PEMFC load mode.

4.1. PEMFC Test Data for Model Validation

The most common experimental PEMFC performance data is voltage as a function of current - a so-called polarization curve. Power is simply the voltage multiplied by current, so polarization curve data represent the PEMFC's power at different currents or current densities. Figure 4-1 shows the polarization and power curves of a PEMFC using experimental data [86] for current densities from 0.0 to 1.0 A/cm².

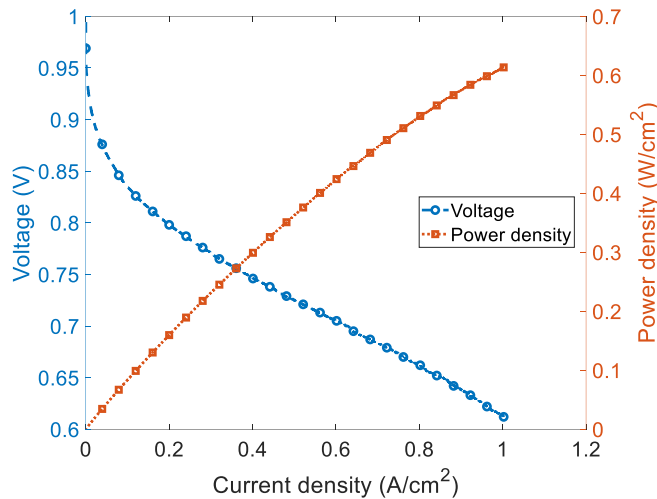


Figure 4-1. voltage and power vs. current density of a PEMFC

Three sets of experimental data are used to show the accuracy and capability improvement of the proposed models. The first two sets of data are from a five-cell stack with an active surface area of 100 cm² assembled at FCLAB [86] with a maximum current density of 1.0 A/cm². Two sets of data are derived using a 1kW test bench. The first PEMFC was degraded at constant current 70 A, and in the second test, another PEMFC with the exact specification was tested at the same current with rippled currents and a frequency of 5 HZ, with more details in [86]. Polarization curve data at the starting time and after each week of

operation was measured. Figure 4-2 and Figure 4-3 show polarization curves plotted for the first and second data sets, respectively, and Figure 4-4 demonstrates the voltage degradation with time for both experimental data.

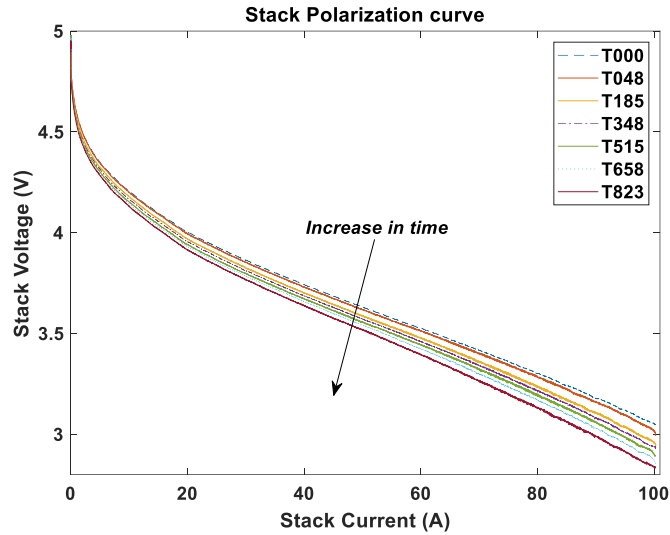


Figure 4-2. Polarization curve test data with a constant current for the different times during degradation

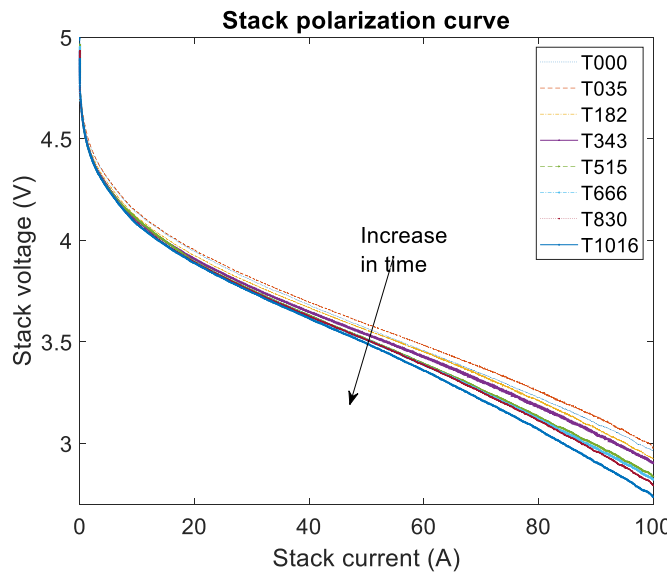


Figure 4-3. Polarization curve test data with a rippled current for the different times during degradation

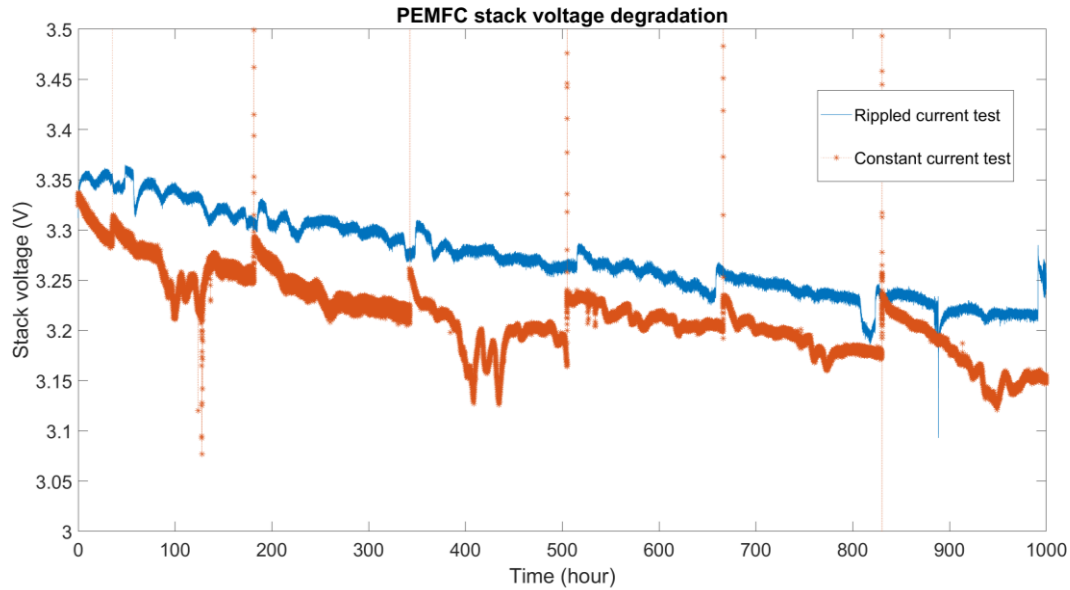


Figure 4-4. PEMFC stack voltage degradation data for both tests with rippled current and the test with a constant current

The second data sets used for the validation are data from Lin, Li [101]. The test simulates a driving load containing: startup/shutdown, idling, mid-power ranges, and high power loads. Figure 4-5 shows polarization curves at the beginning and four different times during operation. The test duration was 370 hours, and voltage degradation data was recorded in OCV, 200, 500, and 700 mA/cm² current densities. Figure 4-6 shows the voltage degradation at OCV, or zero current, and three other current densities as a function of time.

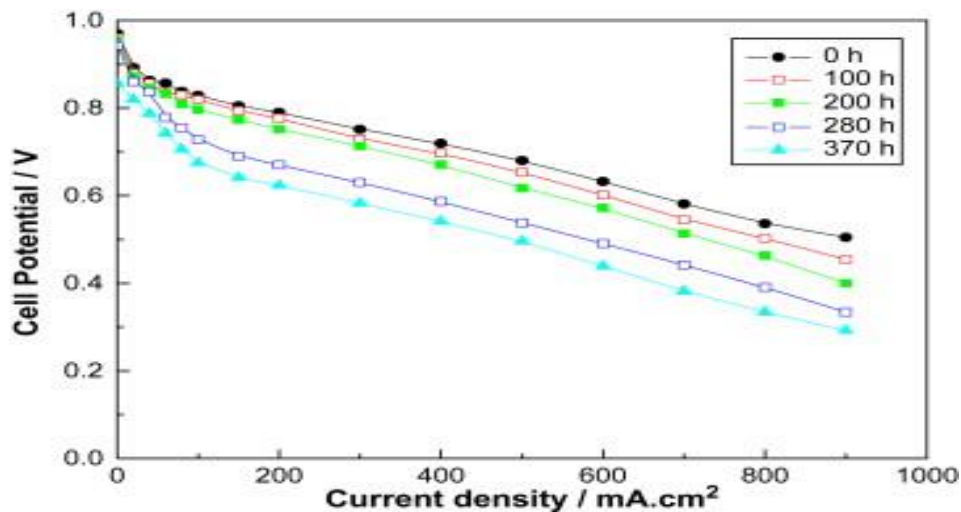


Figure 4-5. Polarization curves after different operation time [101]

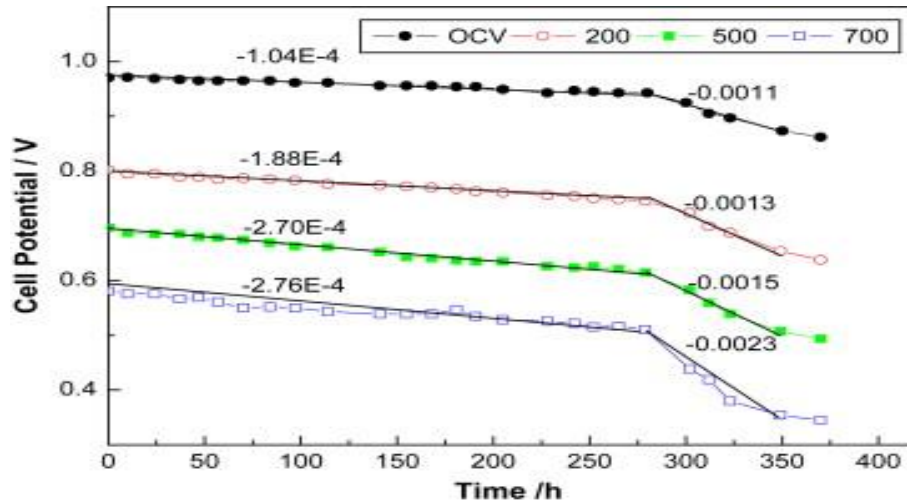


Figure 4-6. voltage degradation at different current densities [101]

4.2. Improved Modeling Accuracy

The newly introduced models are compared with three other recent semi-empirical performance and performance degradation models from literature to discuss the accuracy of the new models and validate them. The selected models from literature that are used for validation are all three models from Table 2-2 for the performance degradation and the following models for the performance model validation:

- 1) Jouin, Gouriveau [39],2016 (and Data): Model 4 in Table 2-1
- 2) Mao, Jackson [44],2017 (and Data): Model 2 in Table 2-1
- 3) Hu, Xu [45], 2018: Model 3 in Table 2-1

Table 4-1 and Table 4-2 summarize each performance model's accuracy. The least absolute residuals method is used for the fitting (refer to MATLAB Curve Fitting Toolbox User Guide for more explanation). The RMSE, R-Square, and SSE values are three different general terms to show the error a model has when fitting with experimental data. The results indicate that the new performance model has lower error than the other models, both in the test with constant current and the test with rippled currents. (The R-square values equal to 1 is due to the fitting accuracy of $1e-04$ and rounding. By looking at RMSE and SSE, it is clear that the new model is an improvement.)

This improvement is related to the additional and modified terms adopted in the new model:

- a) Adding PtO potential to the polarization curve equation helps estimate the value of other parameters like loss current density, exchange current density, and charge transfer is much more realistic,

- b) Using a different formula for the activation loss improves parameter values at very low current density, and
- c) Using the empirical formula for the concentration loss so as to obtain zero at OCV.

Table 4-1. Performance model accuracy comparison using experiments with constant current

Error type	New model	Jouin's model	Mao's Model	Hu's Model
RMSE	2 e-04	3 e-04	7 e-04	3 e-04
R-square	1.000	1.000	0.9999	1.000
SSE	4 e-05	7 e-05	44 e-05	8 e-05

Table 4-2. Performance model accuracy comparison using experiments with rippled currents

Error type	New model	Jouin's model	Mao's Model	Hu's Model
RMSE	1.5 -04	2 e-04	4e-04	7 e-04
R-square	1.000	1.000	1.000	0.9999
SSE	3 e-05	4 e-05	13 e-05	6 e-05

Each performance degradation model has been fitted with the PEMFC performance degradation data in ref [86]. The error results are in Table 4-3 and Table 4-4. The new performance degradation model has less error compared to previous models from the literature. Two reasons for improvement are:

- a) A better performance model is used to derive the PEMFC performance parameters as the basis of the new performance degradation model; and,
- b) The degradation formula was properly chosen from literature or formed using curve fitting like the formula for the active surface area, unlike all other formulae in the literature.

Table 4-3. Performance degradation model accuracy comparison using experiments with constant current

Error type	New model	Jouin's model	Mao's Model	Hu's Model
RMSE	3 e-04	5 e-04	4 e-04	64e-04
R-square	0.9985	0.9951	0.9971	0.3111
SSE	1 e-04	3 e-04	2 e-04	475 e-04

Table 4-4. Performance degradation model accuracy comparison using experiments with rippled currents

Error type	New model	Jouin's model	Mao's Model	Hu's Model
RMSE	5 e-04	11 e-04	6 e-04	100 e-04
R-square	0.9957	0.9817	0.9939	-0.6366
SSE	3 e-04	11 e-04	4 e-04	1016 e-04

Figure 4-7 shows the ability of the new performance degradation model to predict the PEMFC performance (polarization curve) at different times based on degradation data at a constant midrange current. The small differences between experiment and model predictions may be attributed to reversible voltage degradation in the collected data. The polarization curves data contain only irreversible data, but the model is fitted with the voltage degradation data; thus, the model results predict more degradation.

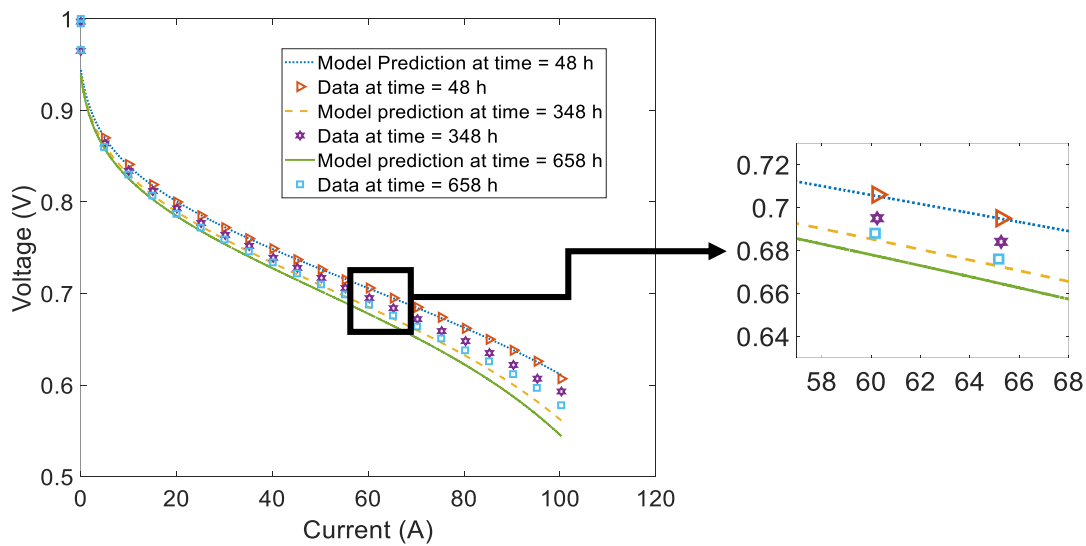


Figure 4-7. Polarization curve prediction derived from the performance degradation model compared with polarization curve from experimental data at three different times

4.3.Improved Capability

It has been reported that the voltage degradation (as a function of time) in a PEMFC is not always linear [101-103]. This behaviour is shown below as well as the ability of the PEMFC performance degradation model. Data used to show this capability are from [101]. The voltage degradation rate reported is based on constant current density. Using the polarization curve recorded before the experiment, shown in Figure 4-8, the model parameters at time = 0 are estimated and reported in Table 4-5.

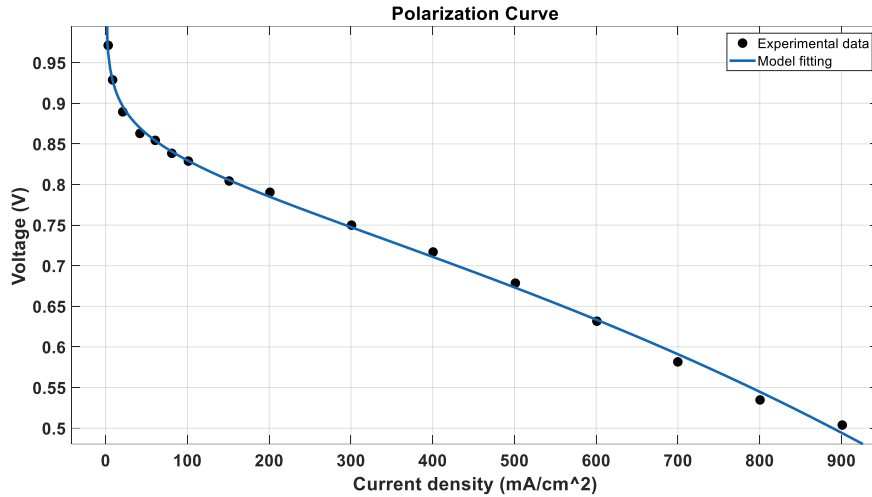


Figure 4-8. polarization curve at zero time [101]

Table 4-5. polarization curve parameters using fitting methods in zero time

parameters	$V_{Pt0}(V)$	α	$i_{loss}(A/cm^2)$	$i_o(A/cm^2)$	$R(\Omega cm^2)$	$m(V)$	$n(cm^2/A)$
Value	0.1339	0.67	6.009e-06	0.09999	1.005e-06	0.1734	0.001075

The degradation data reported for this experiment are voltage degradation under different currents (OCV, 200 mA/cm², 500 mA/cm², and 700 mA/cm²) without any clear information on the time portion of each load in one cycle and the degradation effects of startup/shutdown cycle. To be able to profit the data, OCV degradation data is applied to the model for startup/shutdown load model, and the degradation data for 200 mA/cm², 500 mA/cm², and 700 mA/cm² are considered as degradation data to be applied to the idling, dynamic, and high power load models, respectively.

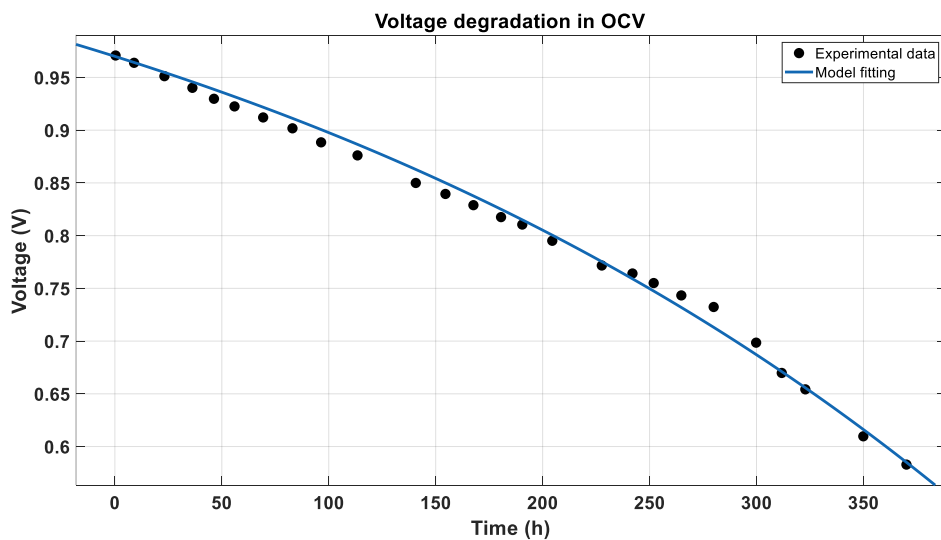


Figure 4-9. Voltage degradation data in OCV [101] and the fitted curve

Figure 4-9 shows experimental data for OCV and the fitted model. At OCV, the current density is zero, so there are only two affecting terms, and the performance degradation model for this operating mode is Eqn. (3-25).

The performance degradation model for idling mode is Eqn. (3-26) and degradation results are simulated using a current density of 200 mA/cm² (which is considered idling). As seen in Figure 4-10, the model fitted well with the data from the experiment. At a higher current density of 500 mA/cm², the PEMFC is considered to be in a dynamic load mode and the model is Eqn. (3-27). With $i = 500$ 500 mA/cm², model results are shown in Figure 4-11.

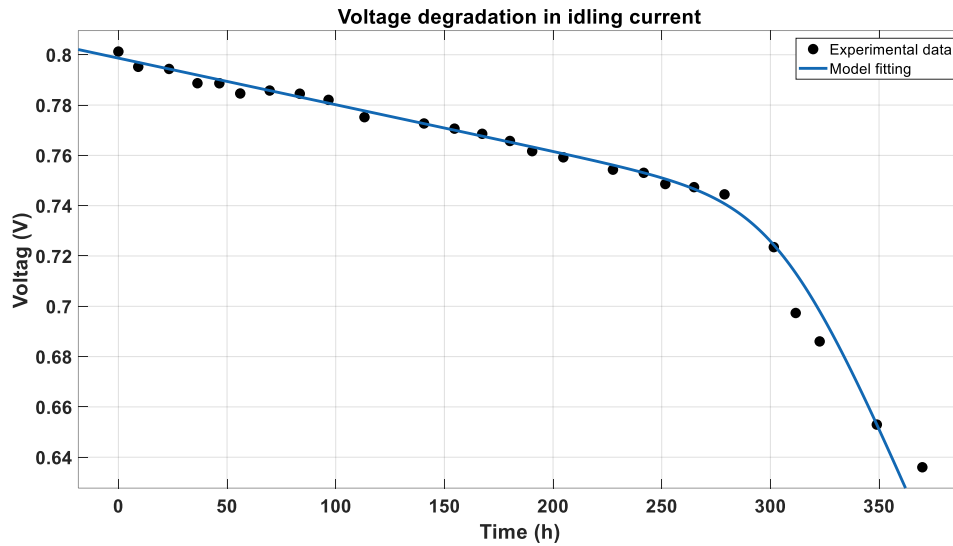


Figure 4-10. Voltage degradation data in idling [101] and the fitted curve

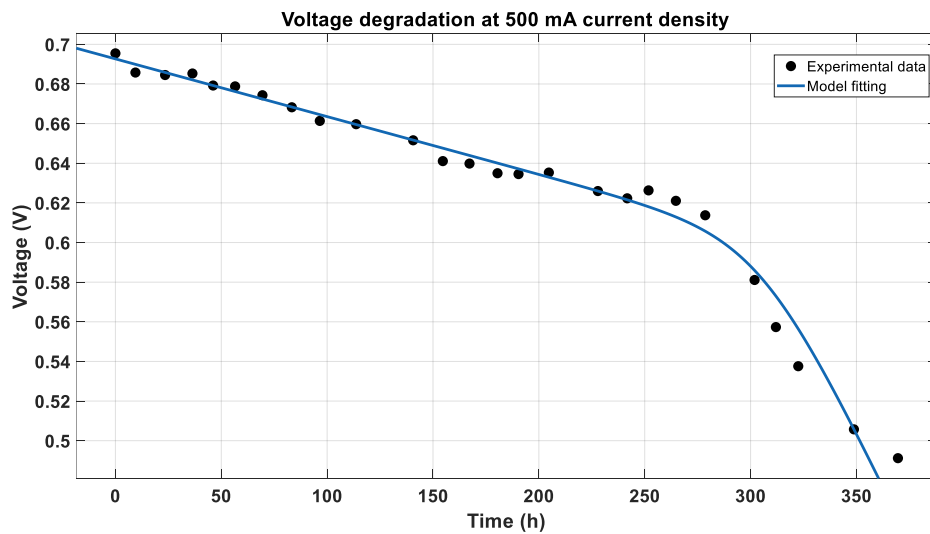


Figure 4-11. Voltage degradation data in 500 mA/cm² [101] and the fitted curve

For the last load mode, i.e., working at high power, 700 mA/cm^2 current density is chosen and the Equation (3-28) is used as the model. Figure 4-12 shows that the proposed model can predict the performance of the PEMFC under the high-power mode. It was showed that the newly proposed performance degradation model could simulate voltage degradation in different load modes; however, the data used were not from separate degradation data for each of the four load modes. So for example, if the voltage degradation at low current densities was considered as degradation data under idling mode, because the PEMFC has worked under higher currents (higher power) during the test, operating under those higher currents affect the parameters degradation (for example, crossover current density degrades both at idling and dynamic load mode) which are considered at idling mode model. Thus, the performance degradation model would not be accurate. To have better models and remove the errors, separate tests for each loading mode are essential.

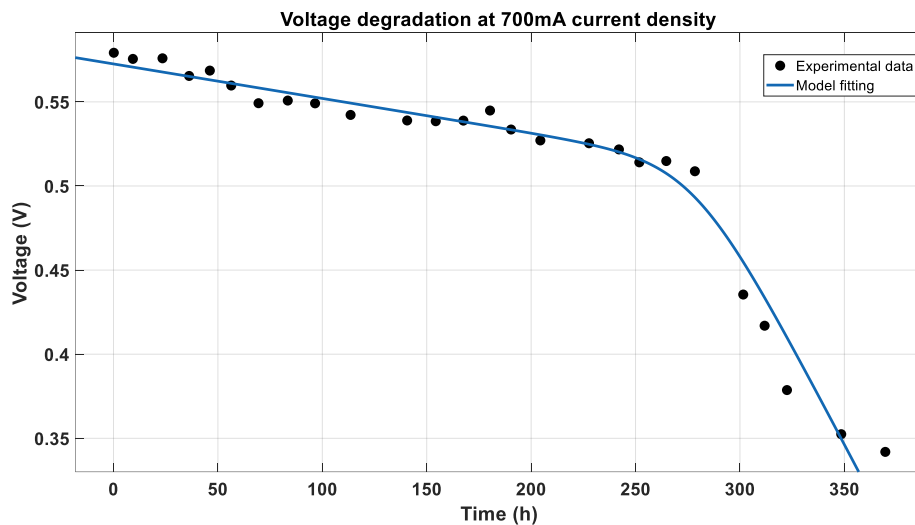


Figure 4-12. Voltage degradation data in 500 mA/cm^2 [101] and the fitted curve

A PEMFC is simulated using data in [101] and load profile shown in Figure 4-13 which is similar to load profile used in [101]. The voltage degradations are reported as the simulation results.

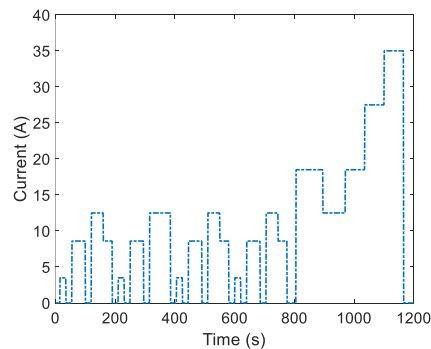


Figure 4-13. Current load mode used in the simulation from ref [101]

The simulation results are plotted in Figure 4-14 with experimental voltage degradation data. At OCV, the simulated and experimental curves match together very well. Still, there seems to be a difference as the current increase because of what is explained before. However, the overall curves show the accuracy of the new performance degradation model.

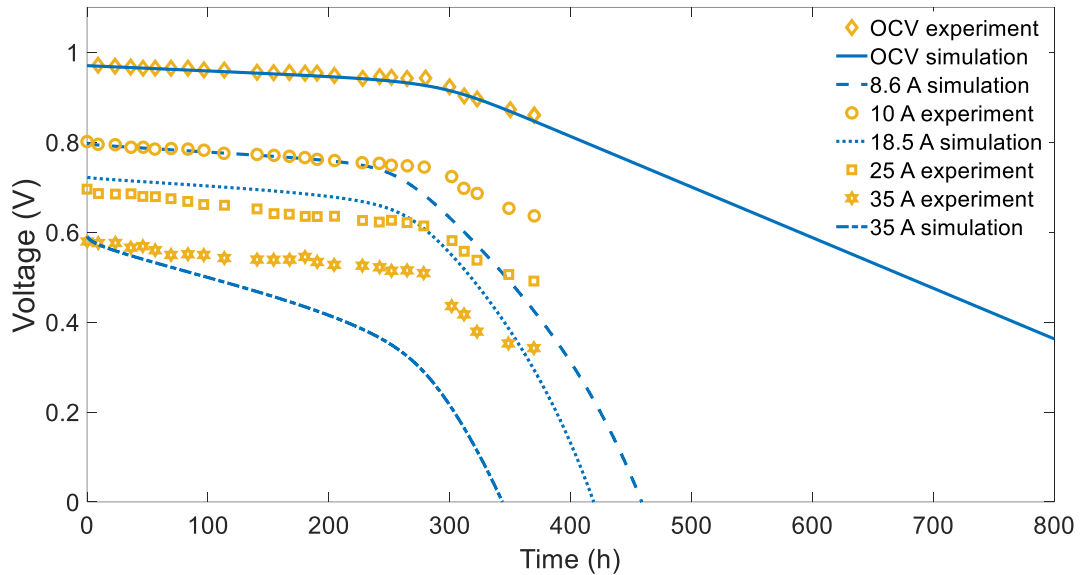


Figure 4-14. Voltage degradation results of simulation compared with the experimental data

4.4. Summary

This chapter first showed that the newly introduced PEMFC performance model had better accuracy than the previous models from the literature. Next, the new semi-empirical performance degradation models related to various FCEV operation/load modes showed an improved capability to predict the non-linearity behaviour of PEMFC performance degradation with time. In contrast, the previous empirical model can only predict the linear portion of the performance degradation due to the linear equation used in the model. Last, the new performance degradation models were validated using data from dynamic load experiments, and the prediction results fitted well with the experimental data.

In the next chapter, to see the full benefit of the new models, these models will be used in actual vehicle operation simulations of real FCEV powertrain components (motor, PEMFC, ESS).

Chapter 5. Results and Discussion

The newly introduced PEMFC performance degradation model is used to simulate the deprivation of the PEMFC system in an FCEV driven in an actual vehicle driving cycle in this chapter. The model parameters, listed in Table 3-12 and Table 3-13, are first determined using curve-fitting on experimental data. The drop of the output voltage of the PEMFC system after years of continued use of the FCEV is then estimated, determining the end-life of the vehicle's PEMFC system.

5.1. PEMFC Performance Degradation Data for Testing

The experimental test data in [86] is chosen to determine the performance and degradation of the PEMFC stack. Two sets of PEMFC performance degradation experiments have been conducted in this reported work [86], constant load current with and without ripples. The experimental data from the condition of a constant load current with minor ripples are used in this work, assuming that the large propulsion power variations are smoothed out by the energy management of the battery ESS. The PEMFC operating at the voltage of 0.7 V and degrading with time are considered. Although the PEMFC voltage degradation test data at 0.7 A/cm² contain both inseparable reversible and irreversible degradations, the experiment-obtained PEMFC polarization curve data showed performance deprivation of the PEMFC after its recovery [86]. The PEMFC degradation model is thus fitted using the polarization curve data of the PEMFC at different times. The fitted plot and the polarization curves data are shown in Figure 5-1.

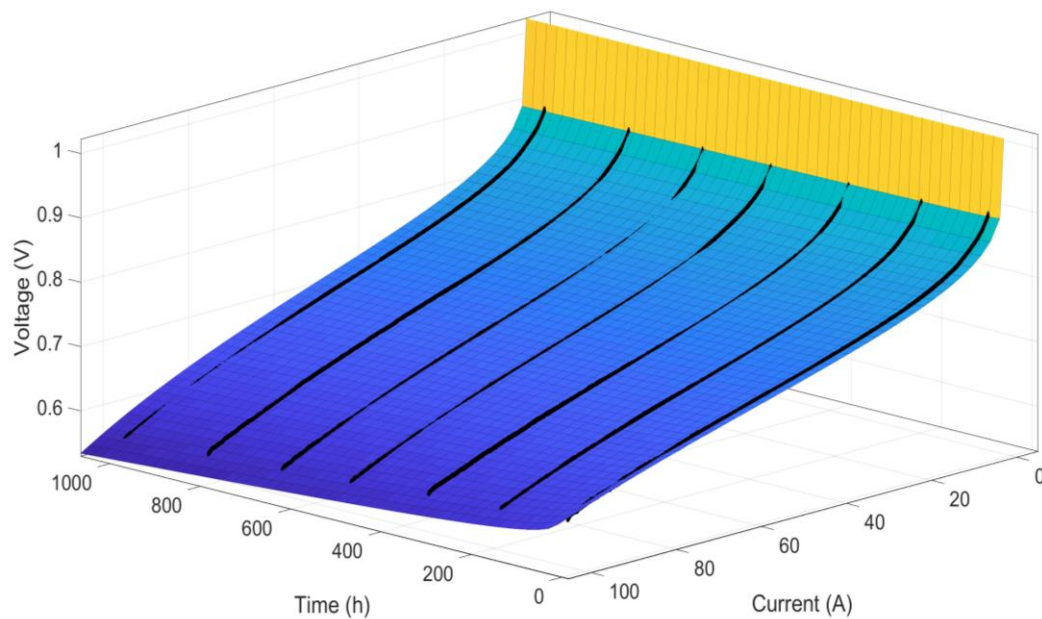


Figure 5-1. Performance degradation model fitting result

5.2.Simulation Procedure

The flowchart, shown in Figure 5-2, illustrates the use of the newly introduced PEMFC performance degradation model in predicting the performance variation of a given FCEV operating under a specific driving cycle continuously.

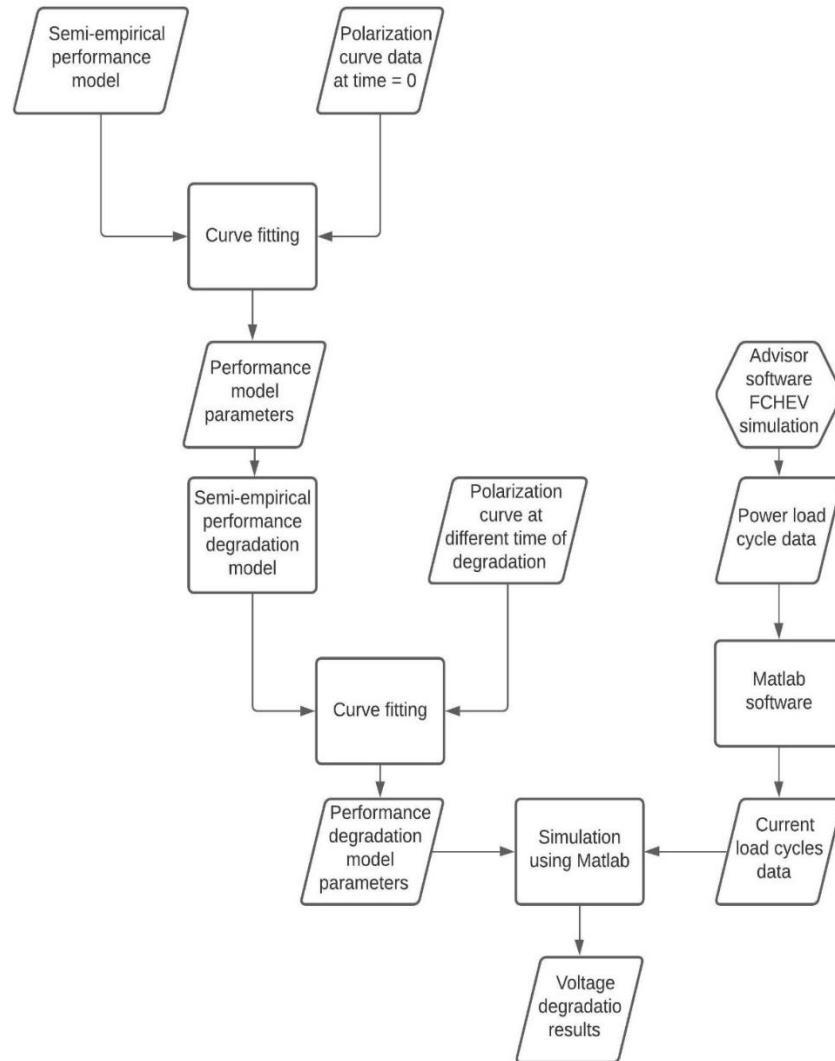


Figure 5-2. Simulation procedure flowchart

The new semi-empirical performance model (Equation (3-16)) is first fitted with the original polarization curve data at time zero. The model parameters of a fresh PEMFC system with no degradation are estimated. The obtained performance model parameters are then used as the initial parameters of the performance degradation model. In this work, the unified performance degradation model, Eqn. (3-29), has been used

due to the lack of PEMFC test data under different FCEV operation modes. With the model parameters determined, the model equations under each PEMFC loading mode, Equations (3-26) to (3-28), are used in the simulations with different load conditions. Since the data of PEMFC performance degradation during the startup/shutdown was not available in [86], the degrading parameter (V_{PtO}^S) relating to this load mode was set to zero, thus, this operation mode was not considered in the simulation. Table 5-1 and Table 5-2 summarize the parameters of the PEMFC performance model at the initial state and after some time of operation with 95 percent confidence bounds. With the model parameters determined, FCEV simulations are conducted to obtain the different load modes of the PEMFC system during vehicle operations.

Table 5-1. Constant/operating and initial parameters of new performance degradation model with 95% confidence bounds

Parameter	Value	Source	95% confidence bounds
$A_{active,0}$	99.42 cm^2	Curve Fitting	-2.562e+04, 2.582e+04
V_{PtO}^0	0.1597 V	Curve Fitting	0.1555, 0.1638
α	0.813	Curve Fitting	0.812, 0.814
i_{loss}^0	0.0003151 A/cm^2	Curve Fitting	-0.08119, 0.08182
i_o	0.0002829 A/cm^2	Curve Fitting	-0.07288, 0.07345
R^0	0.08389 Ωcm^2	Curve Fitting	-21.61, 21.78
m^0	0.003549 V	Curve Fitting	0.003503, 0.003595
n^0	2.29 cm^2/A	Curve Fitting	-590.1, 594.7

Table 5-2. Degrading parameters of new performance degradation model with 95% confidence bounds

Parameter	Value	Source	95% confidence bounds
V_{PtO}^S	0	Curve Fitting	NA
V_{PtO}^I	2.779e - 06 V/h	Curve Fitting	2.749e-06, 2.81e-06
i_{loss}^I	0.001934 h^{-1}	Curve Fitting	0.001921, 0.001947
i_{loss}^D	0.001934 h^{-1}	Curve Fitting	0.001921, 0.001947
R^D	9.141e - 05 h^{-1}	Curve Fitting	9.046e-05, 9.235e-05
R^H	9.141e - 05 h^{-1}	Curve Fitting	9.046e-05, 9.235e-05
m^H	0.0001618 h^{-1}	Curve Fitting	0.0001596, 0.000164
n^H	0 h^{-1}	Curve Fitting	Fixed at bound
A_1	2.524 cm^2	Curve Fitting	-650.4, 655.5
A_2	4.864 h^{-1}	Curve Fitting	-6.677, 16.41

The vehicle operation simulation tool, ADVISOR, is used to obtain the needed propulsion power from the PEMFC system in the FCEV. To use ADVISOR, one needs to define the vehicle specification, choose the powertrain of the FCEV, determine the sizes of the critical powertrain components (e.g. PEMFC system, motor/generator and battery ESS), and specify the driving cycle of the vehicle. The software then simulates the operation, performance, energy use, and emissions of the vehicle. Three different powertrains are considered: a) an FCEV with no energy storage system, b) an FCHEV with a small battery ESS to cover

the peak load, and c) an FCHEV with a large battery ESS. The chassis of the Toyota Prius was chosen in the simulations. The motor and PEMFC power is set to 80 kW based on the needed propulsion power of the 73 kW Toyota Prius or 80 kW Nissan Leaf motor, as detailed in Appendix A. The size of the battery ESS is chosen based on the battery ESS of the Toyota Mirai FCHEV, a small ESS of 1.65 kWh (also the same as the Toyota Prius HEV). For the FCHEV with a large battery ESS, a 6.6 kWh battery pack is chosen, four times the previous one. It is worth mentioning that Nissan Leaf has a 24 kWh ESS as a pure electric vehicle with an 80 kW electric motor. Specifications of the three selected powertrains are given in Table 5-3.

Table 5-3. Three powertrains used in simulations

	NO ESS	SMALL ESS	LARGE ESS	DETAILS
ESS (kWh)	0	1.65	6.6	Li-Ion
MOTOR (kW)	80	80	80	MC-AC75
FC (kW)	80	80	80	-----
TOTAL MASS (kg)	1463	1463	1626	-----

Operations of the three different FCEV/FCHEVs have been simulated using ADVISOR and ten UDDS driving cycles. The FCEV's PEMFC output power is used as the load to determine the performance degradation of the PEMFC. Figure 5-3 represents the vehicle's speed variations under one UDDS operation cycle. In this combined highway-urban driving cycle, the maximum speed is approximately 91 kilometres per hour. There exist several accelerations, decelerations, and start/stops. However, the vehicle's PEMFC system still works at the start/stops of the vehicle.

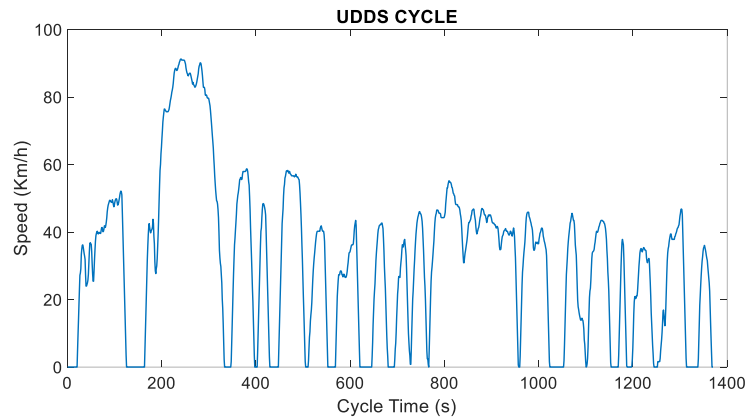


Figure 5-3. UDDS cycle speed per time in second

The operation current and load modes of the PEMFC system are obtained from the needed PEMFC power output from the simulation of vehicle operation and the PEMFC performance model. A program in MATLAB is developed to use the results from ADVISOR and the new performance degradation model to

count the PEMFC degradation over time. The detailed PEMFC voltage degradation is estimated in each time step during the FCEV operation with an accuracy of one second, reflecting the continuous load change of the PEMFC. One cycle of UDDS is 1,369-second long. Ten thousand hours of operation is found to be a good period to show the degradation of the vehicle's PEMFC system. This time is approximately equal to a car running for five hours a day and five days a week for eight years, representing the use pattern of a taxi or a public city bus. On the other hand, this time also represents a personal vehicle operating about two hours a day and five days a week for around twenty years. When estimating the mileage, the UDDS cycle covers 12 km, and 10,000 hours of the UDDS cycle translates to about 315 km or 195 kilo-miles, comparable to the maximum working mileage for an ICE.

Figure 5-4 and Figure 5-5 show the needed propulsion power from ADVISOR with the small and large ESS, respectively. The output power of the PEMFC and ESS, and the input power of the propulsion motor are shown. The vehicle with the larger ESS consumed more power than the one with the small ESS due to the heavier powertrain with a larger battery pack. The battery ESS is mainly used to provide cover peak power and overcome the slower response of the PEMFC. Because ADVISOR does not have a no ESS PEMFC system powertrain, an FCEV simulation model with a very small ESS was used. In all ADVISOR simulations, the PEMFC system output power has not surpassed more than 40 kW or 50 percent of the PEMFC system's max power. Therefore, the PEMFC system has never worked in the high power load mode, and the vehicle does not need excessive propulsion power under the UDDS driving cycle.

The effect of startup/shutdown is ignored in this simulation, as previously mentioned. Only the idling and dynamic load modes are thus considered in the simulations.

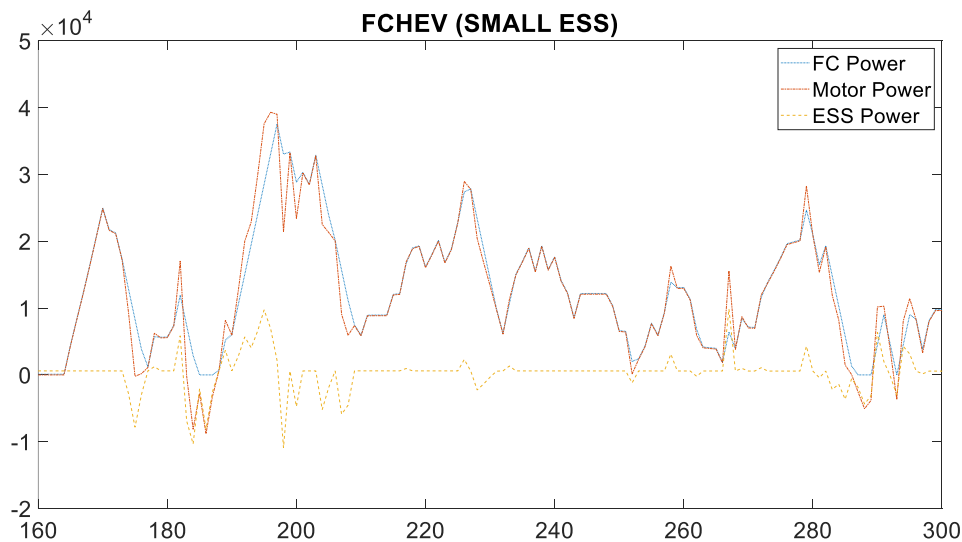


Figure 5-4. ADVISOR simulation power results for the FCHEV with a small ESS closer look

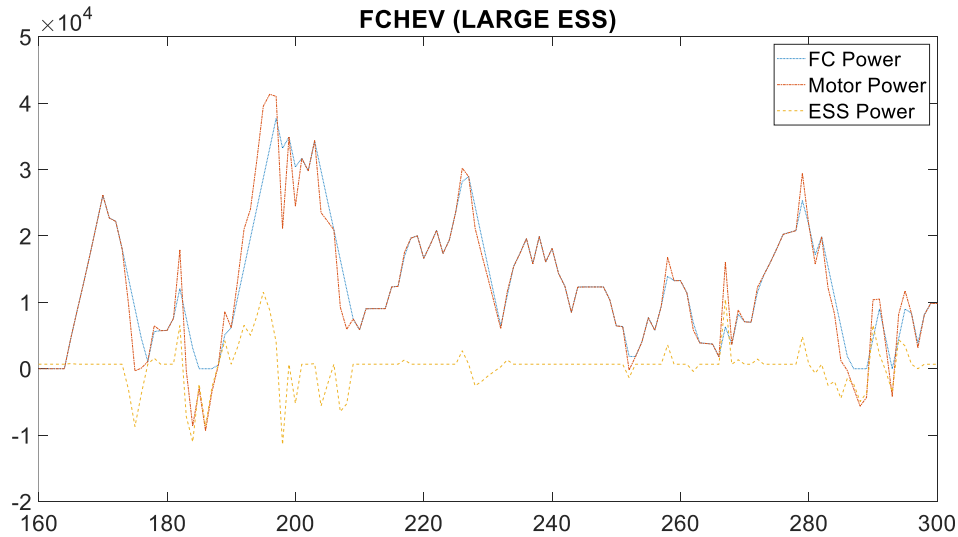


Figure 5-5. ADVISOR simulation power results for the FCHEV with a large ESS closer look

Figure 5-6 shows the actual power load of the vehicle’s PEMFC system in the three different powertrains. There are two noticeable points in this plot. First, the PEMFC in a pure FCEV without any ESS has worked at higher output power at peak loads because there is no ESS to cover load surge. Secondly, the PEMFC system in the powertrain with a large battery ESS produced more power as the vehicle is heavier with the large ESS pack, and more power was needed to drive the vehicle.

The current density and voltage relations of the PEMFC system in the FCEV with a small battery ESS are shown in Figure 5-7 (additionally, Figure D-8 and Figure D-9 in Appendix D.). Parameters of the PEMFC performance model are given in Table 5-1. During the PEMFC performance degradation simulation, the output current of the PEMFC is considered to be constant to determine the voltage degradation of the PEMFC. The power load on the PEMFC system is used to identify the different load modes during vehicle operation. Specifically, the operation condition with the output power less than ten percent of the maximum power of the PEMFC is considered in the idling mode, changing between ten and ninety percent of the maximum power as in the *dynamic mode* and more than ninety percent as in the *high power mode*. The voltage load, shown in Figure 5-7 (as well as Figure D-8 and Figure D-9 in Appendix D.), is used as the reference voltage of the fresh PEMFC with no degradation. The current density varies between zero to slightly higher than 0.4 A/cm². When comparing to the maximum cell current density of 1.0 A/cm², less than fifty percent of the PEMFC power capacity is used by the modelled vehicles.

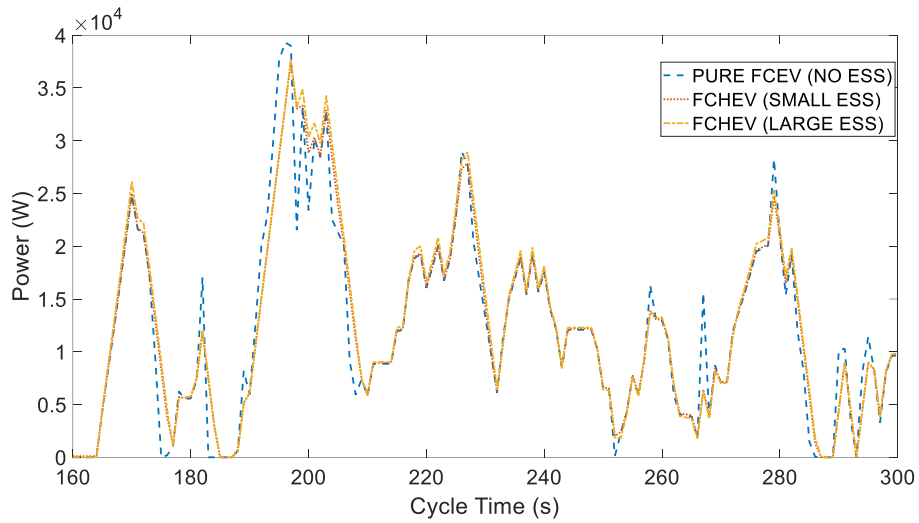


Figure 5-6. PEMFC's output load power comparison in three powertrains closer look

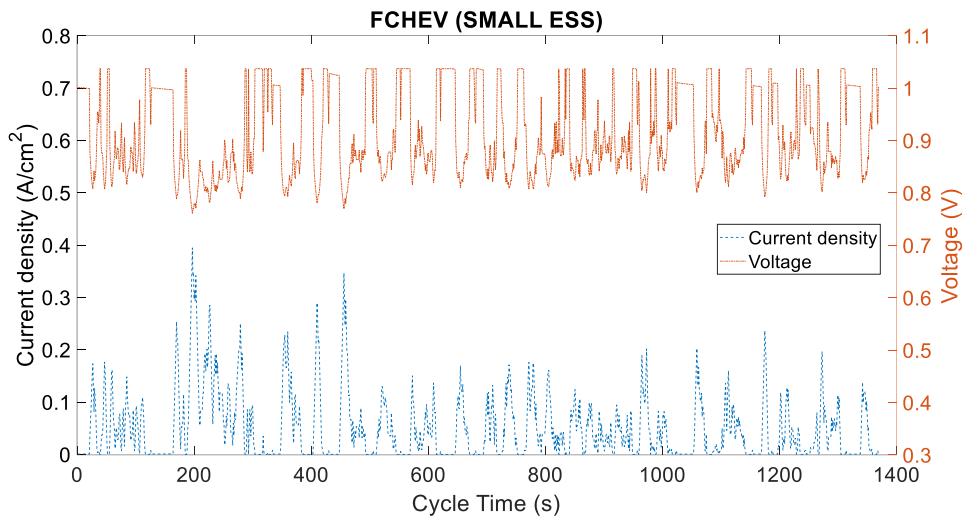


Figure 5-7. Voltage and Current of FCHEV in one cycle for simulation with small ESS

5.3. Performance and Performance Degradation Model Terms and Parameters

Figure 5-8 to Figure 5-12 show the performance degradations of the three different powertrains. Figure 5-8 represents the Pt oxidation potential degradation increase with time, reaching about 0.02 V, which equals 12.5 percent of the initial value (0.1597 V) and 1.63 percentage of reversible voltage. Powertrain with the large ESS shows less degradation than the others since the PEMFC system has worked less in the idling conditions to charge the battery for maintaining the ESS state of charge over the minimum value.

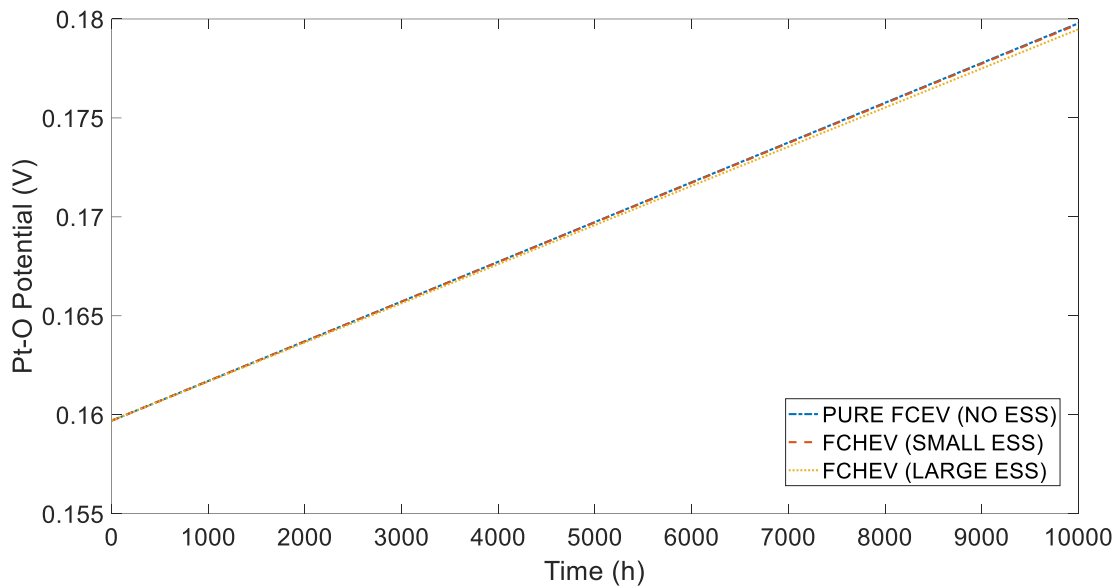


Figure 5-8. PtO potential increases with time

In Figure 5-9, crossover current density (primarily due to the hydrogen crossover through the membrane) is plotted. The initial amount is 0.0003151 A/cm^2 , but the final value is a lot higher. The crossover current degradation is a significant obstacle to PEMFC life. Figure 5-10 shows a closer view at the first five thousand hours, which clarifies that the crossover current density exceeds the PEMFC current density after around four thousand hours, indicating the end of life of the PEMFC. The activation loss term formula has three different parameters: charge transfer, exchange current density, and crossover current density. All three may change due to performance degradation during the PEMFC operation. Still, only the crossover current density is considered to degrade in the model, so the variation estimated for this term may not be accurate. Thus this plot may have the effects of variation of the two other terms, and the actual value of the crossover current density would be less than the shown value. This might not be the true physical value of the crossover current density. The increase in this value after 4,000 hours of operation does not mean the end of life of the PEMFC. Normally 4,000 hours is a reasonable life for the PEMFC system in an FCEV, and the overall PEMFC power should be considered to determine the state of health of PEMFC.

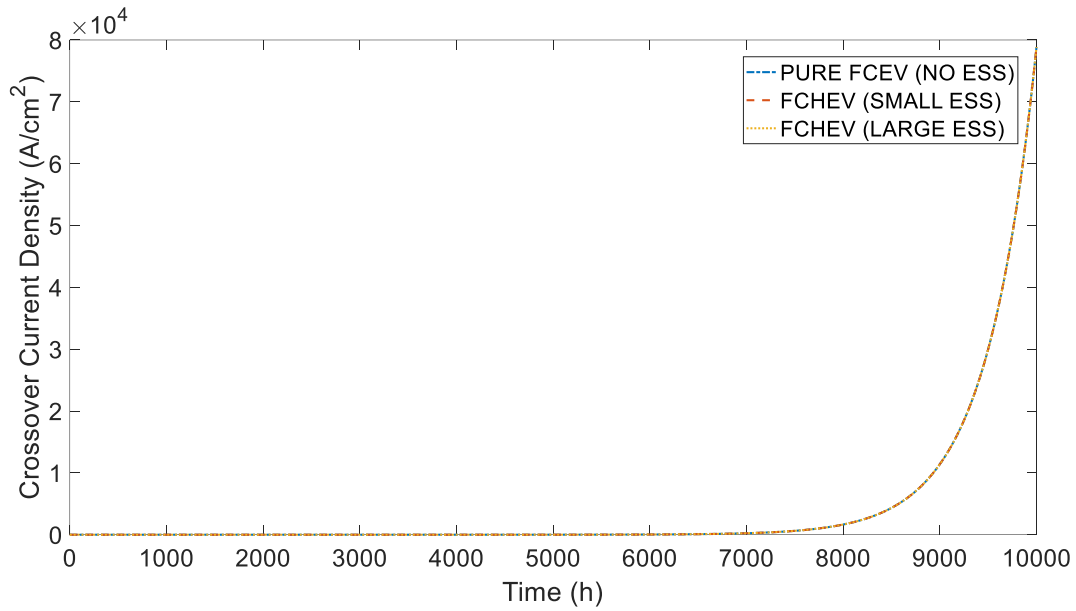


Figure 5-9. Crossover current density degradation with time

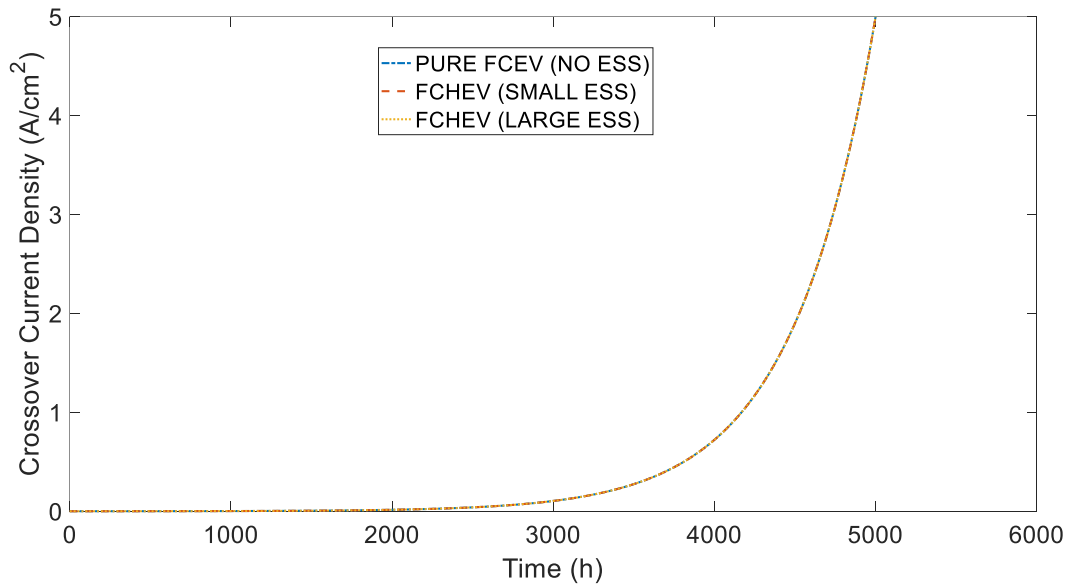


Figure 5-10. Crossover current density degradation with time closer look.

Ohmic resistance in the new model is a combination of resistance to the migration of electrons and protons through the internal and external circuits, as plotted in Figure 5-11. The variation in this term with time is around 28.6 percent of the initial value, which yields to 0.002 V degradation after 10,000 hours equals 0.16 percent of reversible voltage. Degradation of this term is higher when there is a larger ESS because the vehicle's total weight has been increased, leading to increased motor input power and PEMFC output power. Working at a higher power load causes more degradation in this term.

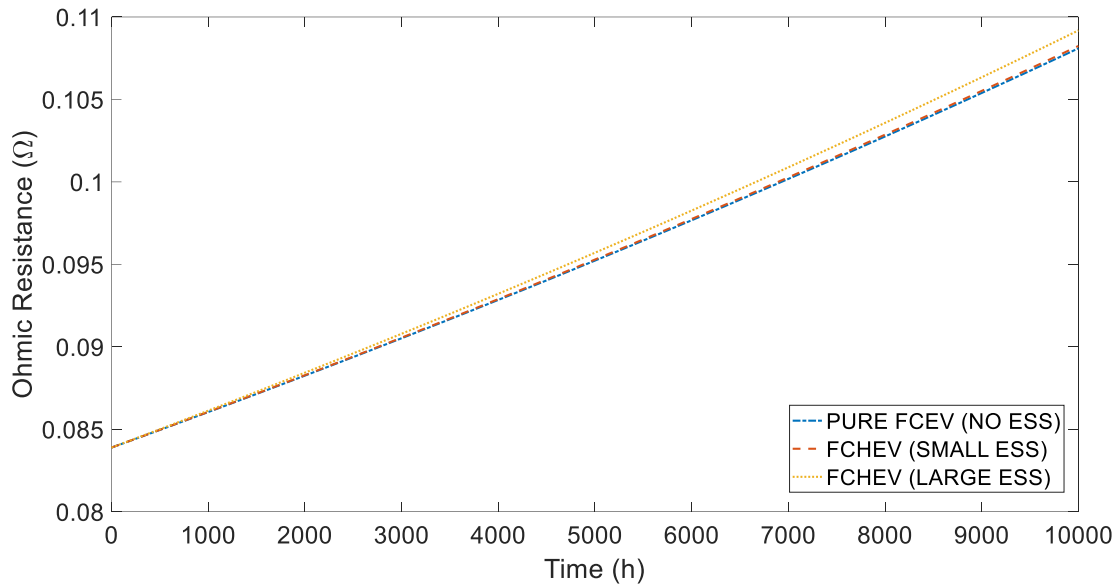


Figure 5-11. Ohmic resistance increase with time

Figure D-10 and Figure D-11 in Appendix D. demonstrate the degradation of the two terms related to the concentration loss. There is no significant change because first, the data used in forming the model is the degradation data from a PEMFC tested under a midrange dynamic load. Predictably, there is not considerable degradation in concentration loss in this simulation. The second reason is that the degradation in these terms under the high power load mode is not produced since the UDDS cycle does not lead to the high power propulsion.

The last term in the model is the active surface area (plotted in Figure 5-12), which degrades in the simulation's three different load modes. The degradation rate is much higher initially, but the rate of decrease becomes smooth after 5,000 hours. Based on the nature of the data, the same degradation parameters for the active surface area in all three different load modes are used. The degradation in this term is related to the operating time only and not the cycle number. Still, with better data, more accurate results for the active surface area are achievable.

Changes of the three main terms of the polarization curve model with the operation time are demonstrated. First-term is the activation loss, plotted in Figure 5-13. This term has five different parameters, but the exchange current density and the charge transfer are considered constant in the model based on the literature, previous simulations, and the model's simplicity. So the three remaining parameters are active surface area and crossover current density that degrades with time and load mode, and the working current density that changes with load mode only. There is a noticeable increase at the beginning, where the active surface area decreased vastly. Still, the apparent increase is after 3000 hours, where the

crossover current density begins to expand considerably. So the crossover current density is the main reason for degradation in the activation term.

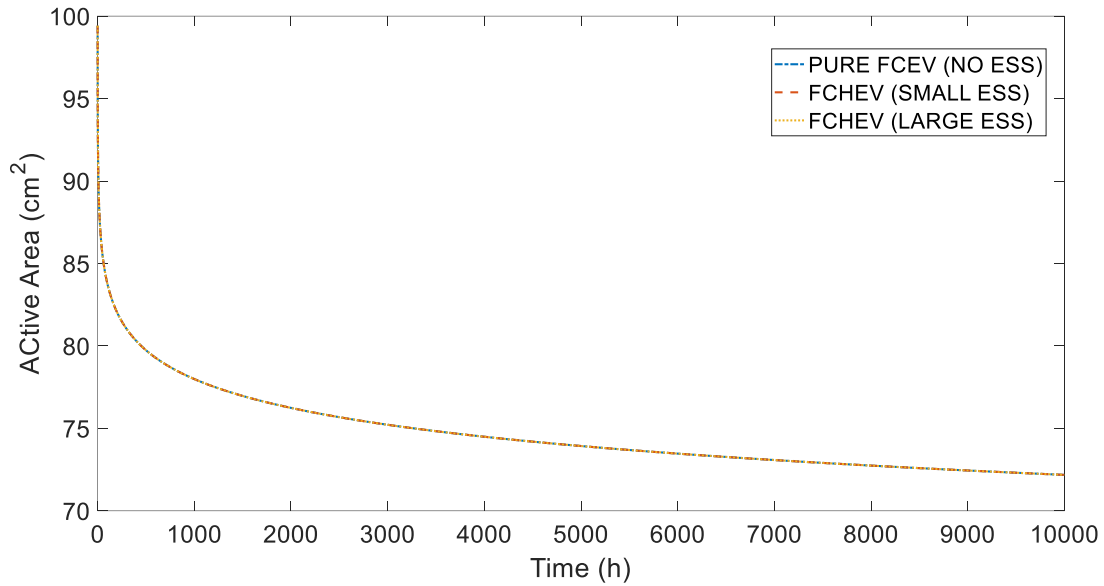


Figure 5-12. Active surface area degradation with time

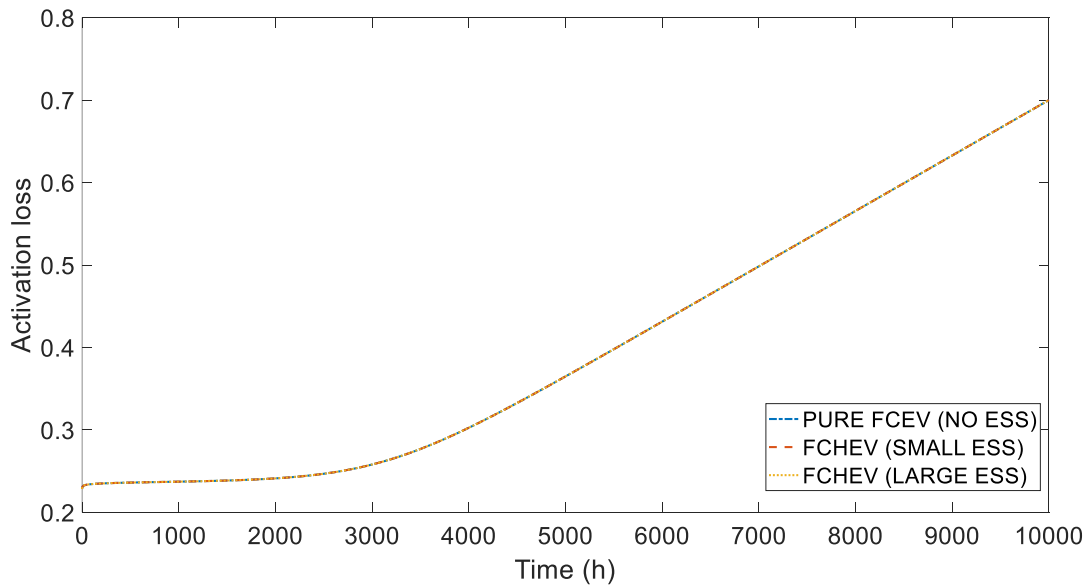


Figure 5-13. Activation loss term degradation with time

Figure 5-14 represents the degradation in the ohmic loss term. The effect of the active surface area is prominent at the initial hours. After 10,000 hours, the increase in this term is about 0.075 V, which is 95 percent of the initial value.

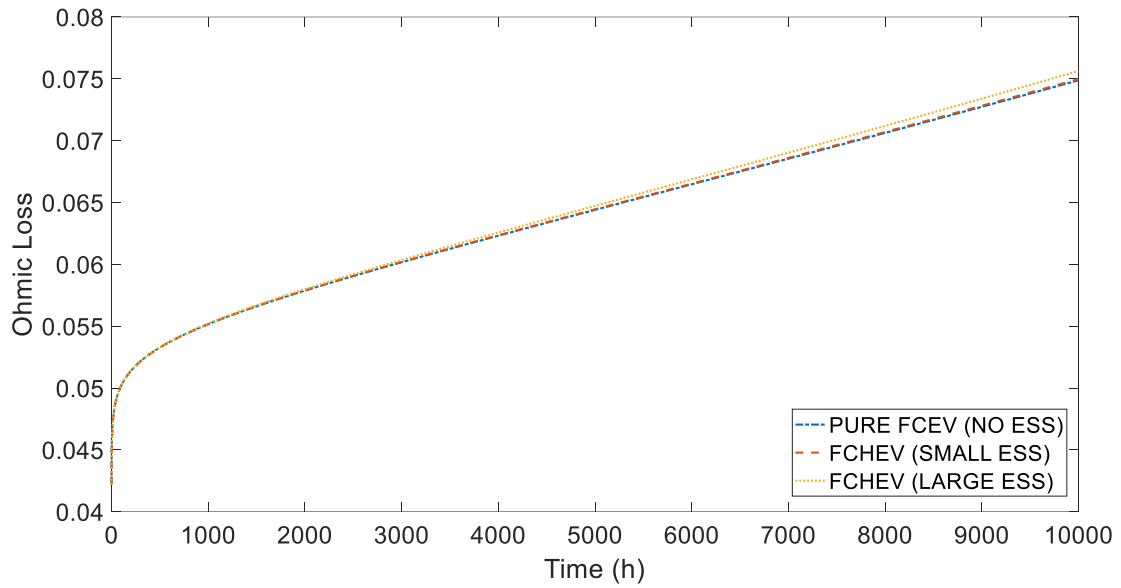


Figure 5-14. Ohmic loss term degradation with time

Figure 5-15 shows the last term of the polarization curve. As discussed in this simulation, the concentration loss parameters do not vary with time. Still, as the active surface area decreases, it affects this term and causes an increasing trend similar to the decline in the active surface area.

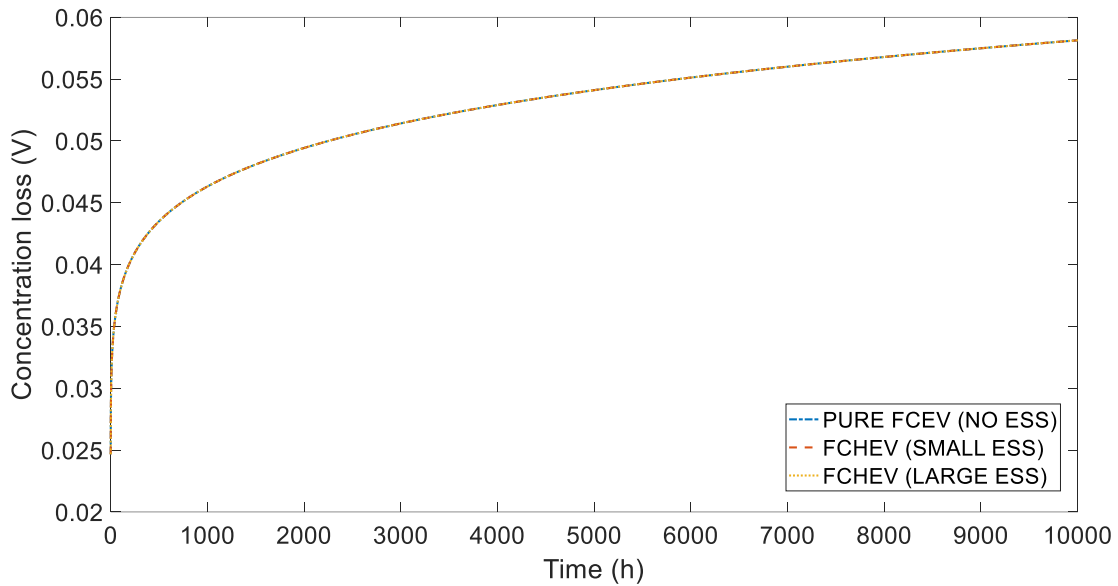


Figure 5-15. Concentration loss term degradation with time

5.4. Voltage Degradation and PEMFC Life

Voltage degradation of PEMFCs for the FCEV with a small ESS is shown in Figure 5-16, and two others cases are shown in Figure D-12 and Figure D-15 in Appendix D. with four different currents plotted. Voltage degradation slope increases approximately after 4,000 hours for all three powertrains, which indicates the end of life of this PEMFC. In Figure 5-17, one-cycle-length voltage changes at four different times are plotted. With a higher voltage, the degradation is faster, especially during initial operations. This is because the PEMFC has worked more under lower voltages in the simulation. The voltage differences between the initial time (with no degradation) and the time at 1,000, 4,000, and 10,000 hours are plotted in Figure 5-18. The voltage difference at 1,000 hours is less than 0.1V at any point of a cycle, but after 4,000 hours, a voltage difference showing over 0.3V at higher voltages and a bit less than 0.1V at low voltage in the cycle. The 0.3V decrease is around 30 percent of the initial OCV, indicating the end of life of the PEMFC. Finally, the voltage difference at 10,000 hours shows that the PEMFC is entirely dead because, by estimation, the idling voltage of the PEMFC is around 0.3V, around 30 percent of initial OCV, which is too low for a PEMFC.

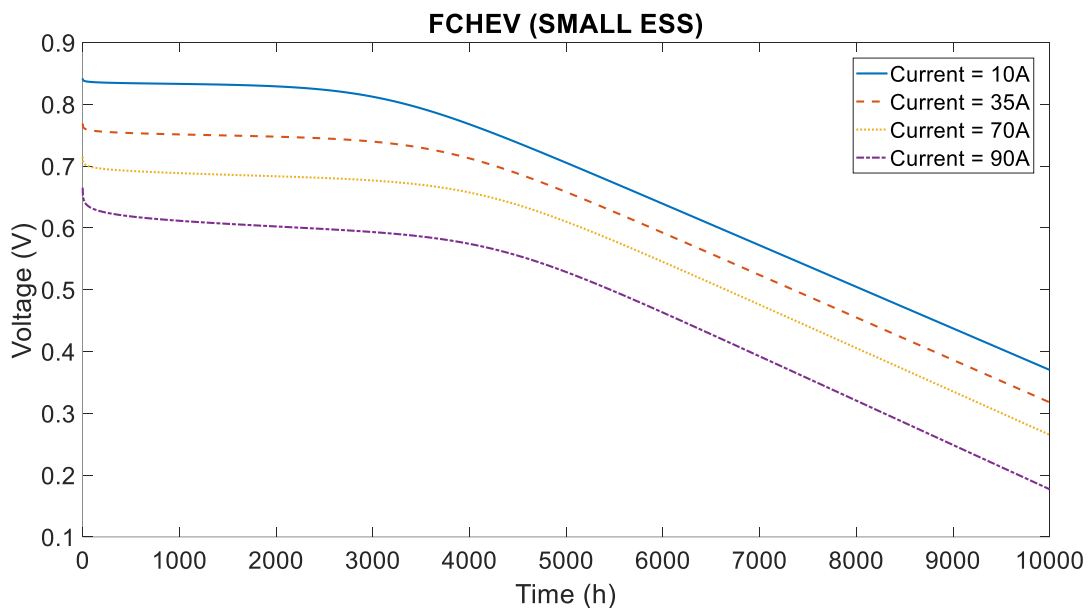


Figure 5-16. Voltage degradation with time in four different currents: 10A, 35A, 70A, and 90 A for powertrain with small ESS

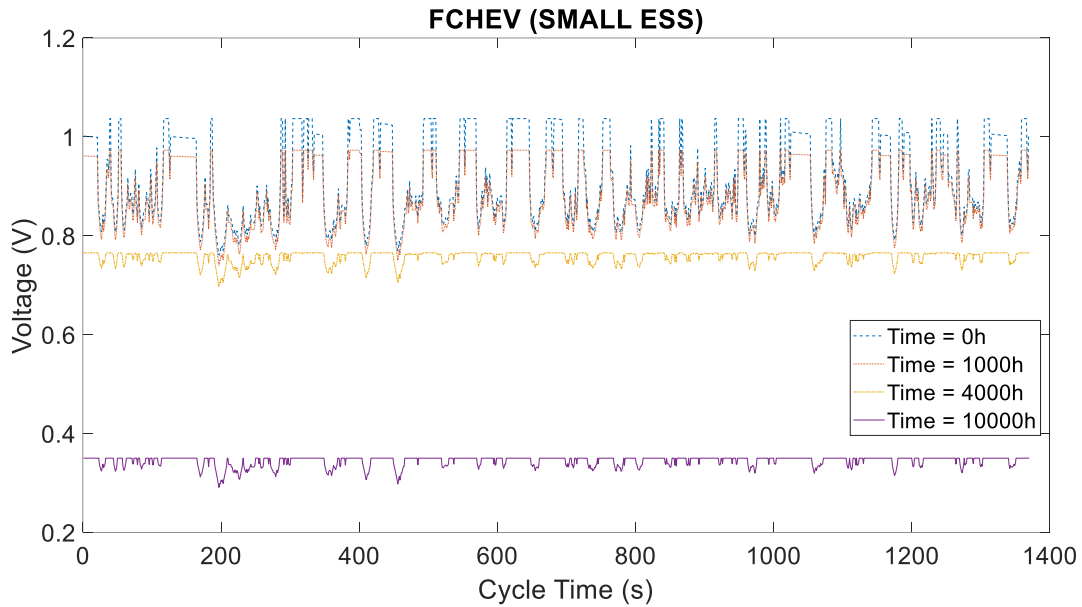


Figure 5-17. PEMFC voltage degradation in one load mode and at four different times: 0h, 1,000h, 4,000h, and 10,000h for the powertrain with small ESS

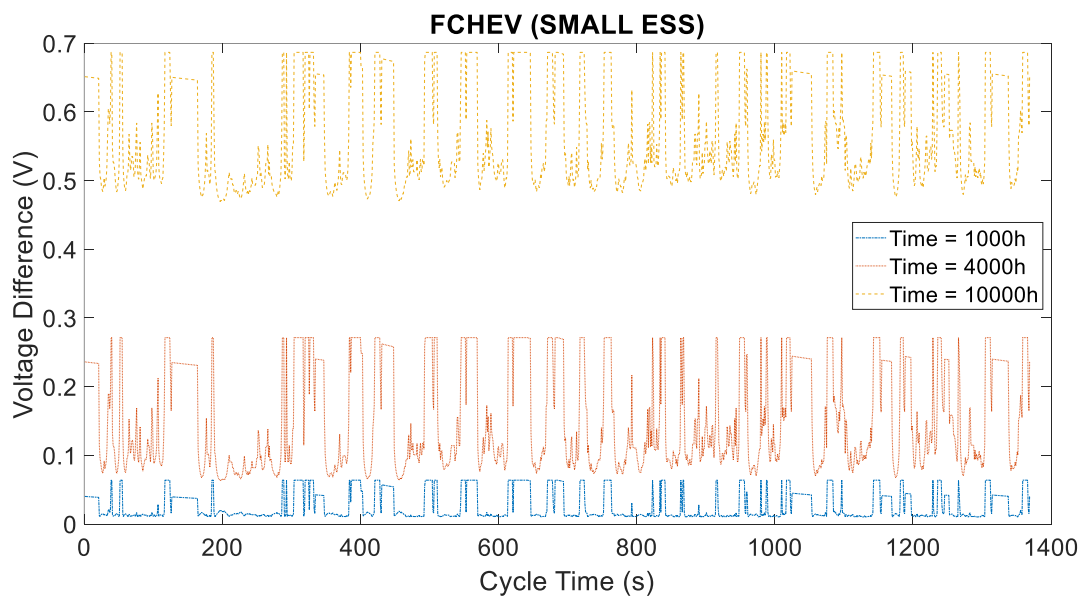


Figure 5-18. PEMFC voltage difference in one load mode and three different times: 1,000h, 4,000h, and 10,000h with time 0h for the powertrain with small ESS

Voltage degradations at different currents are plotted in Figure 5-19. The differences between the three powertrains are insignificant, but the PEMFC with large ESS shows a bit more degradation because of more power needed by the PEMFC to charge the ESS and drive the motor due to the excess weight of the ESS. Nevertheless, this difference is negligible within this range.

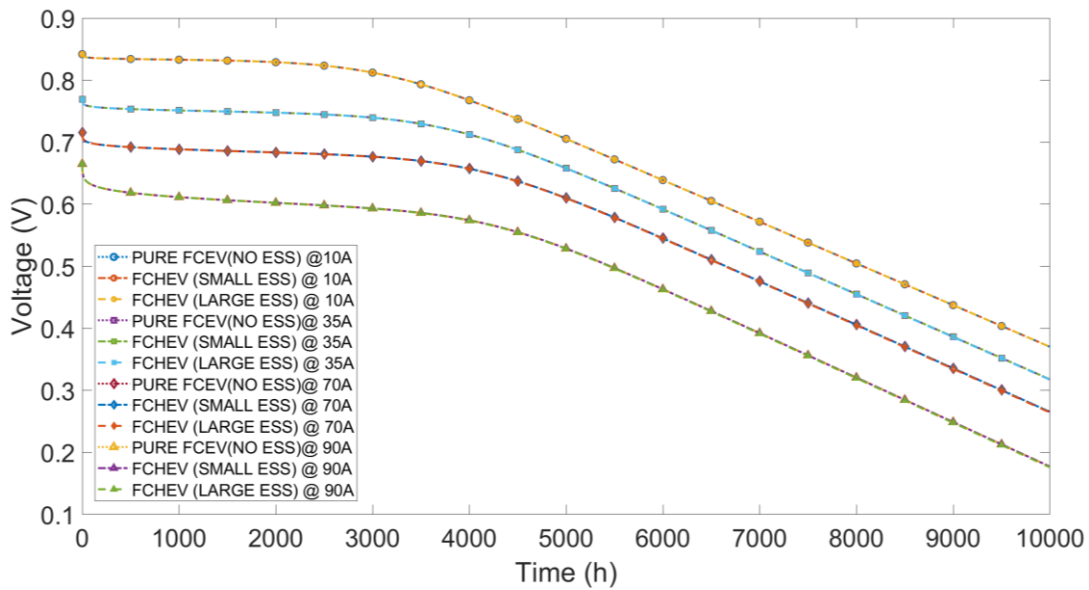


Figure 5-19. Comparison of voltage degradation in three powertrains and four different currents: 10A, 35A, 70A, and 90A

5.5. Summary

The newly introduced performance degradation models have been used based on the loading on the PEMFC system resulted from different FCEVs operating under the repeated UDDS driving cycles. The results showed that the crossover current density is the leading cause of the PEMFCs’ end of life at around 4,000 hours of operation. The simulation in this chapter demonstrates the ability of the newly introduced models to predict the PEMFC’s degradation in the FCEV/FCHEV applications. Furthermore, these models can help determine the sizes of FCEV’s powertrain components in the optimal design of the FCEV and produce the PEMFC-ESS energy management strategies in the optimal control of an FCEV.

Chapter 6. Conclusion and Research Contributions

6.1. Summary

Performance degradation of PEMFC with different load modes in the vehicular application is one of the most critical issues with the PEMFC commercialization. A reliable and easy-to-use model for predicting the performance and RUL of a PEMFC system without carrying out expensive experiments is essential for FCEVs' design and control development. This study introduces four new semi-empirical performance degradation models for FCEV applications in four main steps.

First, a new semi-empirical performance model for a PEMFC is introduced based on the learning from an extensive literature review and PEMFC experiment test data. Modifications have been made to the polarization equation, and a new term has been added that considers PtO potential. This new model achieved better accuracy compared to previously introduced performance models when tested using experimental data. The results showed that the voltage loss due to the PtO potential is significant, which is about 16 percent of reversible voltage and up to 30 percent of all losses. It has thus been added as an essential term in the performance model that has not been considered in previous PEMFC performance degradation models.

Secondly, the degradation behaviour associated with all model parameters is captured using the existing PEMFC degradation formula and fitting with available PEMFC experimental data.

Thirdly, the new semi-empirical performance degradation model for a PEMFC is defined by amending the degradation formula for each parameter of the PEMFC performance model. The new model showed improved accuracy compared to the existing models in the literature.

By removing certain terms, four specific models are defined for each PEMFC load mode found in vehicular applications, i.e., startup/shutdown, idling, dynamic, and high power load modes. Early research found that the PEMFCs in an FCEV show significantly different performance degradation trends under each of these distinct operating modes. Finally, the newly introduced PEMFC performance degradation model is customized with the four representative operation modes of an FCEV. A new semi-empirical PEMFC performance degradation model has been introduced, presenting a non-linear variation for PtO potential and active surface area and an exponential degradation with crossover current, ohmic resistance, and concentration loss.

6.2. Recommendations

The new model might be improved in three areas. First, model validation using a larger array of experimental data specific to each operating mode would be beneficial. The data used were from experiments done in the midrange voltage of a PEMFC; thus, a better prediction at low or high current densities, in which performance degradation due to concentration loss exists, could not be derived. At the same time, the model could not show significant degradation. Secondly, uniform degradation parameters for different load modes are used since only one data set related to the dynamic load mode is available. Last, the PEMFC experimental data are from seven years ago, in 2014, representing the performance degradation behaviours of the PEMFC with the older technology than the recent PEMFCs.

Because of the lack of accessible data, the degradation effects of the startup/shutdown mode were ignored. Also, the high power load mode was not in the simulation because the 80 kW fuel cell has worked with less than 50 percent of max power since the UDDS cycle does not demand high propulsion power. Future simulations can include the effect of these two load modes by using better experimental data and different driving cycles with more intense driving. Optimizing the PEMFC system and ESS sizes should be studied in the future, using the new models to guide the power control and energy management of the FCEV.

6.3. Research Contributions

The research contributions of this work can be summarized into the following areas:

- A new semi-empirical performance model that incorporates the physical PEMFC parameters, like exchange current density, loss current density, etc., was introduced. The new PEMFC performance model is fitted using experimental performance data and has superior accuracy to other semi-empirical performance models.
- The physical parameters of the new semi-empirical PEMFC performance are linked to the associated degradation formula derived from the literature and curve fitting. The parameters of these formulas are determined using curve fitting with experimental PEMFC degradation data to form a new semi-empirical PEMFC performance degradation model. The newly proposed PEMFC performance degradation model presented better prediction accuracy than existing models.
- We considered the voltage degradation because of Pt/PtO potential at the catalyst as a performance degradation parameter in the new semi-empirical model of PEMFC. PtO potential has been

discussed in some literature as a degrading parameter of PEMFC, but it has not been used in the PEMFC performance degradation models before.

- An electrochemically derived equation for activation loss, an inverse sin hyperbolic formula, is used to cover all ranges of current densities, especially very low values which are essential to have physically meaningful results. Instead of a logarithmic form of concentration loss, an improved experimental expression is used.
- The new semi-empirical performance degradation model has been modified using experimental PEMFC performance degradation data under FCHEV operation modes, including startup/shutdown, idling, dynamic, and high power. These load modes present different impacts on PEMFC performance degradation. The newly introduced model has been simplified for each mode of operation as the PEMFC works at different current densities and voltages. Each voltage loss term and degrading parameter has a different effect on the PEMFC performance degradation.
- The newly introduced performance and performance degradation models have been validated using several sets of experimental data and existing models in the literature to show the improved accuracy and capability of the new models.
- The newly introduced PEMFC performance and performance degradation models are used to model and design FCEVs as an example of model application. The example illustrated the process, function, and value of these new models in FCEV development. The new performance degradation model can predict the performance of PEMFC and projected operation life under given vehicle specifications, powertrain system design, control strategies, and a driving cycle.

References

1. Sutharssan, T., et al., *A review on prognostics and health monitoring of proton exchange membrane fuel cell*. Renewable and Sustainable Energy Reviews, 2017. **75**: p. 440-450.
2. Liu, H., et al., *Prognostics methods and degradation indexes of proton exchange membrane fuel cells: A review*. Renewable and Sustainable Energy Reviews, 2020. **123**: p. 109721.
3. Chen, H., P. Pei, and M. Song, *Lifetime prediction and the economic lifetime of proton exchange membrane fuel cells*. Applied Energy, 2015. **142**: p. 154-163.
4. Feng, Y. and Z. Dong, *Integrated design and control optimization of fuel cell hybrid mining truck with minimized lifecycle cost*. Applied Energy, 2020. **270**: p. 115164.
5. Feng, Y. and Z. Dong, *Optimal energy management strategy of fuel-cell battery hybrid electric mining truck to achieve minimum lifecycle operation costs*. International Journal of Energy Research, 2020. **44**(13): p. 10797-10808.
6. Bao-Lian, Y. and H. Ming, *Solutions for the durability of fuel cells in vehicle applications*. Journal of Automotive Safety and Energy, 2011. **2**(2): p. 91.
7. Chen, H., et al., *A review of durability test protocols of the proton exchange membrane fuel cells for vehicle*. Applied Energy, 2018. **224**: p. 289-299.
8. Zhang, T., et al., *A review of automotive proton exchange membrane fuel cell degradation under start-stop operating condition*. Applied energy, 2018. **223**: p. 249-262.
9. Perry, M.L., et al., *Operating requirements for durable polymer-electrolyte fuel cell stacks, in Polymer electrolyte fuel cell durability*. 2009, Springer. p. 399-417.
10. Yu, Y., et al., *A review on performance degradation of proton exchange membrane fuel cells during startup and shutdown processes: Causes, consequences, and mitigation strategies*. Journal of Power Sources, 2012. **205**: p. 10-23.
11. Fuller, T. and G. Gray, *Carbon corrosion induced by partial hydrogen coverage*. ECS Transactions, 2006. **1**(8): p. 345-353.
12. Tang, H., et al., *PEM fuel cell cathode carbon corrosion due to the formation of air/fuel boundary at the anode*. Journal of Power Sources, 2006. **158**(2): p. 1306-1312.
13. Reiser, C.A., et al., *A reverse-current decay mechanism for fuel cells*. Electrochemical and Solid-State Letters, 2005. **8**(6): p. A273-A276.
14. Kim, J., J. Lee, and Y. Tak, *Relationship between carbon corrosion and positive electrode potential in a proton-exchange membrane fuel cell during start/stop operation*. Journal of Power Sources, 2009. **192**(2): p. 674-678.
15. Yousfi-Steiner, N., et al., *A review on polymer electrolyte membrane fuel cell catalyst degradation and starvation issues: Causes, consequences and diagnostic for mitigation*. Journal of Power Sources, 2009. **194**(1): p. 130-145.
16. Yi, B. and M. Hou, *Solutions for the durability of fuel cells in vehicle applications*. J Automotive Safety and Energy, 2011. **2**(2): p. 91-100.
17. Pei, P., Q. Chang, and T. Tang, *A quick evaluating method for automotive fuel cell lifetime*. International Journal of Hydrogen Energy, 2008. **33**(14): p. 3829-3836.
18. Yuan, X.-Z., et al., *Degradation of a polymer exchange membrane fuel cell stack with Nafion® membranes of different thicknesses: Part I. In situ diagnosis*. Journal of Power Sources, 2010. **195**(22): p. 7594-7599.
19. Wu, J., et al., *Proton exchange membrane fuel cell degradation under close to open-circuit conditions: Part I: In situ diagnosis*. Journal of Power Sources, 2010. **195**(4): p. 1171-1176.
20. Miyazawa, A., E. Tada, and A. Nishikata, *Influence of corrosion of SS316L bipolar plate on PEFC performance*. Journal of power sources, 2013. **231**: p. 226-233.
21. Dou, M., et al., *Behaviors of proton exchange membrane fuel cells under oxidant starvation*. Journal of Power Sources, 2011. **196**(5): p. 2759-2762.

22. Taniguchi, A., et al., *Analysis of degradation in PEMFC caused by cell reversal during air starvation*. International Journal of Hydrogen Energy, 2008. **33**(9): p. 2323-2329.
23. Patterson, T.W. and R.M. Darling, *Damage to the cathode catalyst of a PEM fuel cell caused by localized fuel starvation*. Electrochemical and Solid State Letters, 2006. **9**(4): p. A183.
24. Weng, F.-B., C.-Y. Hsu, and C.-W. Li, *Experimental investigation of PEM fuel cell aging under current cycling using segmented fuel cell*. international journal of hydrogen energy, 2010. **35**(8): p. 3664-3675.
25. Chang, Y., et al., *Effect of humidity and thermal cycling on the catalyst layer structural changes in polymer electrolyte membrane fuel cells*. Energy Conversion and Management, 2019. **189**: p. 24-32.
26. Liu, M., et al., *Diagnosis of membrane electrode assembly degradation with drive cycle test technique*. International journal of hydrogen energy, 2014. **39**(26): p. 14370-14375.
27. Mukundan, R., et al., *Membrane accelerated stress test development for polymer electrolyte fuel cell durability validated using field and drive cycle testing*. Journal of The Electrochemical Society, 2018. **165**(6): p. F3085.
28. Alavijeh, A.S., et al., *Microstructural and mechanical characterization of catalyst coated membranes subjected to in situ hygrothermal fatigue*. Journal of The Electrochemical Society, 2015. **162**(14): p. F1461.
29. Venkatesan, S.V., M. Dutta, and E. Kjeang, *Mesosopic degradation effects of voltage cycled cathode catalyst layers in polymer electrolyte fuel cells*. Electrochemistry Communications, 2016. **72**: p. 15-18.
30. Wang, G., et al., *Degradation behavior of a proton exchange membrane fuel cell stack under dynamic cycles between idling and rated condition*. International Journal of Hydrogen Energy, 2018. **43**(9): p. 4471-4481.
31. Guétaz, L., S. Escribano, and O. Sicardy, *Study by electron microscopy of proton exchange membrane fuel cell membrane-electrode assembly degradation mechanisms: Influence of local conditions*. Journal of Power Sources, 2012. **212**: p. 169-178.
32. Gazdzick, P., et al., *Evaluation of reversible and irreversible degradation rates of polymer electrolyte membrane fuel cells tested in automotive conditions*. Journal of Power Sources, 2016. **327**: p. 86-95.
33. Kundu, S., et al., *Reversible and irreversible degradation in fuel cells during open circuit voltage durability testing*. Journal of Power Sources, 2008. **182**(1): p. 254-258.
34. Prasanna, M., et al., *Effects of MEA fabrication method on durability of polymer electrolyte membrane fuel cells*. Electrochimica Acta, 2008. **53**(16): p. 5434-5441.
35. Zhang, S., et al., *Effects of open-circuit operation on membrane and catalyst layer degradation in proton exchange membrane fuel cells*. Journal of Power Sources, 2010. **195**(4): p. 1142-1148.
36. Hu, Z., et al., *A semiempirical dynamic model of reversible open circuit voltage drop in a PEM fuel cell*. International Journal of Energy Research, 2019. **43**(7): p. 2550-2561.
37. Zhang, J., et al., *PEM fuel cell open circuit voltage (OCV) in the temperature range of 23 C to 120 C*. Journal of power sources, 2006. **163**(1): p. 532-537.
38. Zago, M., et al., *Experimental analysis of recoverable performance loss induced by platinum oxide formation at the polymer electrolyte membrane fuel cell cathode*. Journal of Power Sources, 2020. **455**: p. 227990.
39. Jouin, M., et al., *Degradations analysis and aging modeling for health assessment and prognostics of PEMFC*. Reliability Engineering & System Safety, 2016. **148**: p. 78-95.
40. Zhang, X., L. Guo, and H. Liu, *Recovery mechanisms in proton exchange membrane fuel cells after accelerated stress tests*. Journal of Power Sources, 2015. **296**: p. 327-334.
41. Rowe, A. and X. Li, *Mathematical modeling of proton exchange membrane fuel cells*. Journal of power sources, 2001. **102**(1-2): p. 82-96.

42. Bressel, M., et al. *Fuel cell remaining useful life prediction and uncertainty quantification under an automotive profile*. in *IECON 2016-42nd Annual Conference of the IEEE Industrial Electronics Society*. 2016. IEEE.
43. Liu, H., et al., *Prognostics of Proton Exchange Membrane Fuel Cells Using A Model-based Method*. *IFAC-PapersOnLine*, 2017. **50**(1): p. 4757-4762.
44. Mao, L., L. Jackson, and T. Jackson, *Investigation of polymer electrolyte membrane fuel cell internal behaviour during long term operation and its use in prognostics*. *Journal of Power Sources*, 2017. **362**: p. 39-49.
45. Hu, Z., et al., *A reconstructed fuel cell life-prediction model for a fuel cell hybrid city bus*. *Energy conversion and management*, 2018. **156**: p. 723-732.
46. Wishart, J., Z. Dong, and M. Secanell, *Optimization of a PEM fuel cell system based on empirical data and a generalized electrochemical semi-empirical model*. *Journal of Power Sources*, 2006. **161**(2): p. 1041-1055.
47. Sharaf, O.Z. and M.F. Orhan, *An overview of fuel cell technology: Fundamentals and applications*. *Renewable and Sustainable Energy Reviews*, 2014. **32**: p. 810-853.
48. Jouin, M., et al., *PEMFC aging modeling for prognostics and health assessment*. *IFAC-PapersOnLine*, 2015. **48**(21): p. 790-795.
49. Jouin, M., et al., *Prognostics of PEM fuel cells under a combined heat and power profile*. *IFAC-PapersOnLine*, 2015. **48**(3): p. 26-31.
50. Jha, M.S., et al., *Particle filter based hybrid prognostics of proton exchange membrane fuel cell in bond graph framework*. *Computers & Chemical Engineering*, 2016. **95**: p. 216-230.
51. Zhu, L. and J. Chen, *Prognostics of PEM fuel cells based on Gaussian process state space models*. *Energy*, 2018. **149**: p. 63-73.
52. Liu, J., et al., *Remaining useful life prediction of PEMFC based on long short-term memory recurrent neural networks*. *International Journal of Hydrogen Energy*, 2019. **44**(11): p. 5470-5480.
53. Chen, J., et al., *A novel health indicator for PEMFC state of health estimation and remaining useful life prediction*. *International Journal of Hydrogen Energy*, 2017. **42**(31): p. 20230-20238.
54. Reiser, C.A., et al., *A reverse-current decay mechanism for fuel cells*. *Electrochemical and Solid State Letters*, 2005. **8**(6): p. A273.
55. Eom, K., et al., *Effects of Pt loading in the anode on the durability of a membrane-electrode assembly for polymer electrolyte membrane fuel cells during startup/shutdown cycling*. *International journal of hydrogen energy*, 2012. **37**(23): p. 18455-18462.
56. Shen, Q., et al., *Study on the processes of start-up and shutdown in proton exchange membrane fuel cells*. *Journal of Power Sources*, 2009. **189**(2): p. 1114-1119.
57. Katayanagi, Y., et al., *Cross-sectional observation of nanostructured catalyst layer of polymer electrolyte fuel cell using FIB/SEM*. *Journal of Power Sources*, 2015. **280**: p. 210-216.
58. Dhanushkodi, S., et al., *Use of mechanistic carbon corrosion model to predict performance loss in Polymer Electrolyte Membrane fuel cells*. *Journal of Power Sources*, 2014. **267**: p. 171-181.
59. Roen, L., C. Paik, and T. Jarvi, *Electrocatalytic corrosion of carbon support in PEMFC cathodes*. *Electrochemical and Solid State Letters*, 2003. **7**(1): p. A19.
60. Ishigami, Y., et al., *Corrosion of carbon supports at cathode during hydrogen/air replacement at anode studied by visualization of oxygen partial pressures in a PEFC—Start-up/shut-down simulation*. *Journal of Power Sources*, 2011. **196**(6): p. 3003-3008.
61. Lin, R., et al., *Investigating the effect of start-up and shut-down cycles on the performance of the proton exchange membrane fuel cell by segmented cell technology*. *International Journal of Hydrogen Energy*, 2015. **40**(43): p. 14952-14962.
62. Lamibrac, A., et al., *Local degradations resulting from repeated start-ups and shut-downs in proton exchange membrane fuel cell (PEMFC)*. *Energy Procedia*, 2012. **29**: p. 318-324.
63. Durst, J., et al., *Degradation heterogeneities induced by repetitive start/stop events in proton exchange membrane fuel cell: Inlet vs. outlet and channel vs. land*. *Applied Catalysis B: Environmental*, 2013. **138**: p. 416-426.

64. Kreitmeier, S., A. Wokaun, and F.N. Büchi, *Local catalyst support degradation during polymer electrolyte fuel cell start-up and shutdown*. Journal of the Electrochemical Society, 2012. **159**(11): p. F787.
65. Franck-Lacaze, L., et al., *Ageing of PEMFC's due to operation at low current density: Investigation of oxidative degradation*. international journal of hydrogen energy, 2010. **35**(19): p. 10472-10481.
66. Han, M., et al., *Accelerated testing of polymer electrolyte membranes under open-circuit voltage conditions for durable proton exchange membrane fuel cells*. International Journal of Hydrogen Energy, 2017. **42**(52): p. 30787-30791.
67. Gaumont, T., et al., *Measurement of protonic resistance of catalyst layers as a tool for degradation monitoring*. International Journal of Hydrogen Energy, 2017. **42**(3): p. 1800-1812.
68. Gummalla, M., et al., *Degradation of polymer-electrolyte membranes in fuel cells: II. Theoretical model*. Journal of The Electrochemical Society, 2010. **157**(11): p. B1542.
69. Kundu, S., et al., *Open circuit voltage durability study and model of catalyst coated membranes at different humidification levels*. Journal of Power Sources, 2010. **195**(21): p. 7323-7331.
70. Ghassemzadeh, L., et al., *Chemical degradation of Nafion membranes under mimic fuel cell conditions as investigated by solid-state NMR spectroscopy*. The Journal of Physical Chemistry C, 2010. **114**(34): p. 14635-14645.
71. Ferreira, P., et al., *Instability of Pt/C electrocatalysts in proton exchange membrane fuel cells: a mechanistic investigation*. Journal of the Electrochemical Society, 2005. **152**(11): p. A2256.
72. Akita, T., et al., *Analytical TEM study of Pt particle deposition in the proton-exchange membrane of a membrane-electrode-assembly*. Journal of Power Sources, 2006. **159**(1): p. 461-467.
73. Guilminot, E., et al., *Detection of Pt²⁺ ions and Pt nanoparticles inside the membrane of a used PEMFC*. Journal of The Electrochemical Society, 2006. **154**(1): p. B96.
74. Wang, X., R. Kumar, and D.J. Myers, *Effect of voltage on platinum dissolution: relevance to polymer electrolyte fuel cells*. Electrochemical and Solid State Letters, 2006. **9**(5): p. A225.
75. Guilminot, E., et al., *Membrane and active layer degradation upon PEMFC steady-state operation: I. platinum dissolution and redistribution within the MEA*. Journal of The Electrochemical Society, 2007. **154**(11): p. B1106.
76. Zhang, J., et al., *Effect of hydrogen and oxygen partial pressure on Pt precipitation within the membrane of PEMFCs*. Journal of the electrochemical society, 2007. **154**(10): p. B1006.
77. Narimani, M., J. DeVaal, and F. Golnaraghi, *Hydrogen emission characterization for proton exchange membrane fuel cell during oxygen starvation—Part 1: Low oxygen concentration*. International Journal of Hydrogen Energy, 2016. **41**(8): p. 4843-4853.
78. Narimani, M., J. DeVaal, and F. Golnaraghi, *Hydrogen emission characterization for proton exchange membrane fuel cell during oxygen starvation—Part 2: Effect of hydrogen transfer leak*. International Journal of Hydrogen Energy, 2016. **41**(41): p. 18641-18653.
79. Zhao, J., et al., *Experimental observations of microstructure changes in the catalyst layers of proton exchange membrane fuel cells under wet-dry cycles*. Journal of The Electrochemical Society, 2018. **165**(6): p. F3337.
80. Zhang, X., et al., *Load profile based empirical model for the lifetime prediction of an automotive PEM fuel cell*. International Journal of Hydrogen Energy, 2017. **42**(16): p. 11868-11878.
81. Lu, L., et al., *A semi-empirical voltage degradation model for a low-pressure proton exchange membrane fuel cell stack under bus city driving cycles*. Journal of power sources, 2007. **164**(1): p. 306-314.
82. Frano, B., *PEM fuel cells: theory and practice*. Academic, Burlington, 2005.
83. Noren, D. and M. Hoffman, *Clarifying the Butler–Volmer equation and related approximations for calculating activation losses in solid oxide fuel cell models*. Journal of Power Sources, 2005. **152**: p. 175-181.
84. Owejan, J.P., *Transport resistance in polymer electrolyte fuel cells*. PHD dissertation, University of Tennessee, Knoxville, 2014.

85. Hao, D., et al., *An improved empirical fuel cell polarization curve model based on review analysis*. International Journal of Chemical Engineering, 2016. (volume 2016) p.10
86. F.Research. *IEEEPHMdatachallenge2014*. 2014; Available from: <http://eng.fclab.fr/ieeephm-2014-data-challenge/>.
87. Pizzutilo, E., et al., *On the need of improved accelerated degradation protocols (ADPs): examination of platinum dissolution and carbon corrosion in half-cell tests*. Journal of the electrochemical society, 2016. **163**(14): p. F1510.
88. Yu, Y., et al., *Comparison of degradation behaviors for open-ended and closed proton exchange membrane fuel cells during startup and shutdown cycles*. Journal of Power Sources, 2011. **196**(11): p. 5077-5083.
89. Shao-Horn, Y., et al., *Instability of supported platinum nanoparticles in low-temperature fuel cells*. Topics in Catalysis, 2007. **46**(3-4): p. 285-305.
90. Sharma, R., et al., *Evolution of the degradation mechanisms with the number of stress cycles during an accelerated stress test of carbon supported platinum nanoparticles*. Journal of Electroanalytical Chemistry, 2019. **838**: p. 82-88.
91. Gribov, E., et al., *Analysis of the corrosion kinetic of Pt/C catalysts prepared on different carbon supports under the "Start-Stop" cycling*. Electrocatalysis, 2016. **7**(2): p. 159-173.
92. Borup, R.L., et al., *PEM fuel cell electrocatalyst durability measurements*. Journal of Power Sources, 2006. **163**(1): p. 76-81.
93. Jao, T.-C., et al., *Degradation mechanism study of PTFE/Nafion membrane in MEA utilizing an accelerated degradation technique*. International journal of hydrogen energy, 2012. **37**(18): p. 13623-13630.
94. Tang, H., et al., *A degradation study of Nafion proton exchange membrane of PEM fuel cells*. Journal of Power Sources, 2007. **170**(1): p. 85-92.
95. Collier, A., et al., *Degradation of polymer electrolyte membranes*. International Journal of Hydrogen Energy, 2006. **31**(13): p. 1838-1854.
96. Inaba, M., et al., *Gas crossover and membrane degradation in polymer electrolyte fuel cells*. Electrochimica Acta, 2006. **51**(26): p. 5746-5753.
97. Madden, T., et al., *Proton exchange membrane fuel cell degradation: mechanisms and recent progress*. Handbook of Fuel Cells, 2010.
98. Merlo, L., et al., *Resistance to peroxide degradation of Hyflon® Ion membranes*. Journal of Power Sources, 2007. **171**(1): p. 140-147.
99. Wu, B., et al., *The degradation study of Nafion/PTFE composite membrane in PEM fuel cell under accelerated stress tests*. International journal of hydrogen energy, 2014. **39**(26): p. 14381-14390.
100. Ren, P., et al., *Degradation mechanisms of proton exchange membrane fuel cell under typical automotive operating conditions*. Progress in Energy and Combustion Science, 2020. **80**: p. 100859.
101. Lin, R., et al., *Investigation of dynamic driving cycle effect on performance degradation and micro-structure change of PEM fuel cell*. International Journal of Hydrogen Energy, 2009. **34**(5): p. 2369-2376.
102. Vengatesan, S., et al., *Diagnosis of MEA degradation under accelerated relative humidity cycling*. Journal of Power Sources, 2011. **196**(11): p. 5045-5052.
103. Panha, K., et al., *Accelerated durability testing via reactants relative humidity cycling on PEM fuel cells*. Applied Energy, 2012. **93**: p. 90-97.
104. *Toyota Mirai*. 2021; Available from: <https://www.toyota-europe.com/world-of-toyota/feel/environment/better-air/fuel-cell-vehicle>.
105. Park, J., et al., *A review of the gas diffusion layer in proton exchange membrane fuel cells: durability and degradation*. Applied Energy, 2015. **155**: p. 866-880.
106. Wu, J., et al., *A review of PEM fuel cell durability: Degradation mechanisms and mitigation strategies*. Journal of Power Sources, 2008. **184**(1): p. 104-119.

107. Liu, D. and S. Case, *Durability study of proton exchange membrane fuel cells under dynamic testing conditions with cyclic current profile*. Journal of Power Sources, 2006. **162**(1): p. 521-531.
108. de BFA, D.V. and G. Janssen, *Review: durability and degradation issues of PEM fuel cell components*. Fuel Cells, 2008. **8**: p. 3-22.
109. Schmittinger, W. and A. Vahidi, *A review of the main parameters influencing long-term performance and durability of PEM fuel cells*. Journal of power sources, 2008. **180**(1): p. 1-14.
110. Kocha, S.S., *Electrochemical degradation: electrocatalyst and support durability*, in *Polymer electrolyte fuel cell degradation*. 2012, Academic Press Oxford. p. 89-214.
111. Zhou, Z.-M., et al., *Durability study of Pt-Pd/C as PEMFC cathode catalyst*. international journal of hydrogen energy, 2010. **35**(4): p. 1719-1726.
112. Tawfik, H., Y. Hung, and D. Mahajan, *Bipolar plate durability and challenges*, in *Polymer Electrolyte Fuel Cell Degradation*. 2012, Academic Press. p. 249-291.
113. Latorrata, S., et al., *Novel superhydrophobic gas diffusion media for PEM fuel cells: Evaluation of performance and durability*. Chem. Eng, 2014. **41**: p. 241-245.
114. Chun, J.H., et al., *Improvement of the mechanical durability of micro porous layer in a proton exchange membrane fuel cell by elimination of surface cracks*. Renewable energy, 2012. **48**: p. 35-41.
115. Schulze, M., et al., *Degradation of sealings for PEFC test cells during fuel cell operation*. Journal of Power Sources, 2004. **127**(1-2): p. 222-229.
116. Ahn, S.-Y., et al., *Performance and lifetime analysis of the kW-class PEMFC stack*. Journal of Power Sources, 2002. **106**(1-2): p. 295-303.
117. Cleghorn, S., et al., *A polymer electrolyte fuel cell life test: 3 years of continuous operation*. Journal of Power Sources, 2006. **158**(1): p. 446-454.
118. St-Pierre, J. and N. Jia, *Successful demonstration of ballard PEMFCs for space shuttle applications*. Journal of New Materials for Electrochemical Systems, 2002. **5**(4): p. 263-272.
119. Xu, H., et al., *Effect of relative humidity on membrane degradation rate and mechanism in PEM fuel cells*. Ecs Transactions, 2007. **6**(13): p. 51.
120. Lim, C., et al., *Membrane degradation during combined chemical and mechanical accelerated stress testing of polymer electrolyte fuel cells*. Journal of Power Sources, 2014. **257**: p. 102-110.
121. Mittal, V.O., H.R. Kunz, and J.M. Fenton, *Effect of catalyst properties on membrane degradation rate and the underlying degradation mechanism in PEMFCs*. Journal of the Electrochemical Society, 2006. **153**(9): p. A1755.
122. Mittal, V.O., H.R. Kunz, and J.M. Fenton, *Membrane degradation mechanisms in PEMFCs*. Journal of The Electrochemical Society, 2007. **154**(7): p. B652.
123. Sompalli, B., et al., *Membrane degradation at catalyst layer edges in PEMFC MEAs*. Journal of The Electrochemical Society, 2007. **154**(12): p. B1349.
124. Yuan, X.-Z., et al., *Degradation of a PEM fuel cell stack with Nafion® membranes of different thicknesses. Part II: Ex situ diagnosis*. Journal of Power Sources, 2012. **205**: p. 324-334.
125. Chandesris, M., et al., *Membrane degradation in PEM fuel cells: From experimental results to semi-empirical degradation laws*. International Journal of Hydrogen Energy, 2017. **42**(12): p. 8139-8149.
126. Urchaga, P., et al., *Catalyst degradation in fuel cell electrodes: Accelerated stress tests and model-based analysis*. Electrochimica Acta, 2015. **176**: p. 1500-1510.
127. Kneer, A., et al., *Correlation of changes in electrochemical and structural parameters due to voltage cycling induced degradation in PEM fuel cells*. Journal of The Electrochemical Society, 2018. **165**(6): p. F3241.
128. Kneer, A. and N. Wagner, *A semi-empirical catalyst degradation model based on voltage cycling under automotive operating conditions in PEM fuel cells*. Journal of The Electrochemical Society, 2019. **166**(2): p. F120.
129. Kneer, A., et al., *Effect of dwell time and scan rate during voltage cycling on catalyst degradation in PEM fuel cells*. Journal of The Electrochemical Society, 2018. **165**(10): p. F805.

130. Sharma, R. and S.M. Andersen, *Quantification on degradation mechanisms of polymer electrolyte membrane fuel cell catalyst layers during an accelerated stress test*. *Acs Catalysis*, 2018. **8**(4): p. 3424-3434.
131. White, R.T., et al., *4D in situ visualization of electrode morphology changes during accelerated degradation in fuel cells by X-ray computed tomography*. *Journal of Power Sources*, 2017. **350**: p. 94-102.
132. White, R.T., et al., *Four-dimensional joint visualization of electrode degradation and liquid water distribution inside operating polymer electrolyte fuel cells*. *Scientific reports*, 2019. **9**(1): p. 1-12.
133. Speder, J., et al., *Comparative degradation study of carbon supported proton exchange membrane fuel cell electrocatalysts—The influence of the platinum to carbon ratio on the degradation rate*. *Journal of Power Sources*, 2014. **261**: p. 14-22.
134. Hitchcock, A.P., et al., *Carbon corrosion of proton exchange membrane fuel cell catalyst layers studied by scanning transmission X-ray microscopy*. *Journal of Power Sources*, 2014. **266**: p. 66-78.
135. Pauchet, J., et al., *Performance loss of proton exchange membrane fuel cell due to hydrophobicity loss in gas diffusion layer: Analysis by multiscale approach combining pore network and performance modelling*. *international journal of hydrogen energy*, 2012. **37**(2): p. 1628-1641.
136. Liu, H., et al., *Accelerated degradation of polymer electrolyte membrane fuel cell gas diffusion layers*. *Journal of The Electrochemical Society*, 2017. **164**(7): p. F695.
137. George, M.G., et al., *Accelerated degradation of polymer electrolyte membrane fuel cell gas diffusion layers*. *Journal of The Electrochemical Society*, 2017. **164**(7): p. F714.
138. Cui, T., Y. Chao, and J. Van Zee, *Sealing force prediction of elastomeric seal material for PEM fuel cell under temperature cycling*. *International journal of hydrogen energy*, 2014. **39**(3): p. 1430-1438.

Appendix A. Related Vehicle Technical Specifications

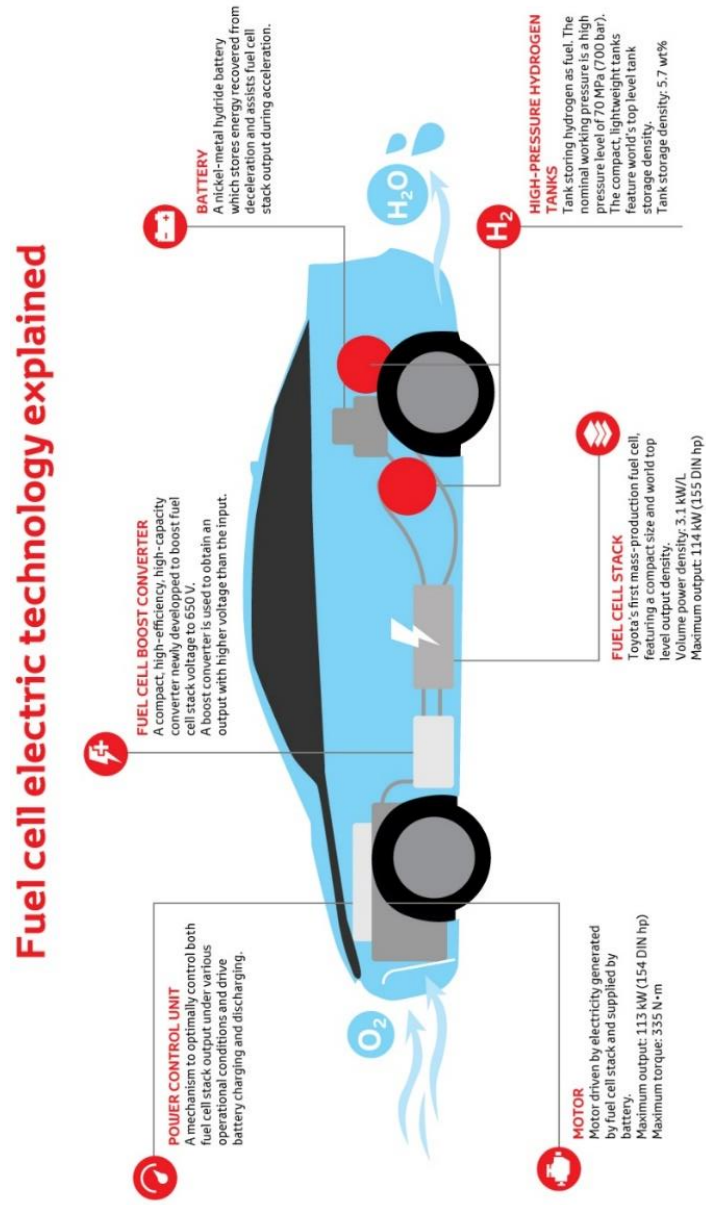


Figure A-1. FCHEV architecture (Toyota Mirai) [104]

Toyota Prius Technical specification

TOYOTA PRIUS TECHNICAL SPECIFICATIONS

HYBRID SYNERGY DRIVE		
Type	Series/parallel, full hybrid	
System output (bhp/kW)	134/100	
ENGINE		
Engine type	2ZR-FXE (Atkinson cycle)	
No. of cylinders	Four in-line	
Valve mechanism	16-valve DOHC with VVT-i	
Bore x stroke (mm)	80.5 x 88.3	
Displacement (cc)	1,798	
Compression ratio	13.0:1	
Fuel system	EFI	
Octane No.	95 or greater	
Max. power (bhp/kW @ rpm)	98/73 @ 5,200	
Max. torque (Nm @ rpm)	142 @ 4,000	
Emissions level	Euro 5	
ELECTRIC MOTOR		
Motor type	Permanent magnet, synchronous	
Max. voltage (CD V)	650	
Max. power (bhp)	80	
Max. torque (Nm)	207	
HIGH-VOLTAGE BATTERY		
Battery type	Nickel-metal hydride	
Nominal voltage (SC V)	201.6 (168 x 1.2V cells)	
No. of battery modules	28	
Battery capacity (Ah)	6.5	
System voltage (V)	650	
TRANSMISSION		
Transmission type	Electric CVT	
Gear ratios	Forward	2.683
	Reverse	2.683
Differential gear ratio	3.267	
PERFORMANCE		
Max. speed (mph)	112	
Full system power (bhp/kW)	134/100	
0-62mph acceleration (sec)	10.4	
FUEL CONSUMPTION		
	15in wheel	17in wheel
Combined	72.4	70.6
Extra urban (mpg)	76.4	74.3
Urban (mpg)	72.4	70.6
Fuel tank capacity (l)	45	

Figure A-2. Toyota Prius technical specification

Nissan Leaf Technical specification

features + specifications: Nissan LEAF™



- zero tailpipe emissions/Zero Emissions Vehicle (ZEV)
- 100% electric - no gas required
- high response 80kW AC synchronous electric motor
- range –100 miles/charge based upon US EPA LA4 City cycle¹
- speeds up to 90 mph
- 5 passengers, 5 doors
- Nissan Connection powered by CARWINGS™²

mechanical

motor + battery

80 kW AC synchronous motor	24 kWh lithium-ion battery	3.3 kW onboard charger	120V portable trickle charging cable ³
-------------------------------	-------------------------------	---------------------------	--

- battery heater

SL version includes SV features plus:

- Quick Charge Port (standard on SL)

brakes

- 4-wheel power-assisted vented disc brakes
- regenerative brakes
- 4-wheel Anti-lock Braking System (ABS)
- Electronic Brake force Distribution (EBD)
- Brake Assist (BA)
- electronic parking brake

suspension and steering

- independent strut front suspension with stabilizer bar
- torsion bar rear axle with integrated stabilizer bar
- vehicle-speed-sensitive electric power steering

Figure A-3. Nissan Leaf technical specification

Toyota Mirai Technical specification

TOYOTA MIRAI TECHNICAL SPECIFICATIONS	
FUEL CELL STACK	
Model code	FCA110
Type	Polymer electrolyte
Number of cells	370
Connection method	Series
Max. output bhp/kW	153/114
BATTERY	
Type	Nickel-metal hydride
Number of cells	34
Nominal voltage	244
Capacity (Ah)	6.5
Connection method	Series
ELECTRIC MOTOR/GENERATOR	
Motor model code	4JM
Type	Permanent magnet, synchronous
Max. power (bhp/kW)	152/113
Max. torque (Nm)	335
DRIVETRAIN	
Layout	Front-wheel drive
Transmission gear ratio	1.000:1
Reduction gear ratio/final drive	3.478:1
SUSPENSION	
Front suspension	MacPherson strut with anti-roll bar
Rear suspension	Torsion beam
STEERING	
Type	Rack and pinion., electric power steering
Ratio	14.8:1
Turns lock-to-lock	2.81
Min. turning circle – body (m)	11.4
BRAKES	
Type - front	Ventilated disc

Figure A-4. Toyota Mirai technical specification

Appendix B. PEMFC Performance Degradation due to Degrading Components

There are five main components in a PEMFC: the sealing gasket, bipolar plate, gas diffusion layer, catalyst layer, and membrane. Each one has its degradation process. To minimize the cost and time of experimental tests and have good results, it would be better to focus first on the parts with a higher level of degradation. Therefore, scientists classify PEMFC components based on their impact on the reduction of PEMFC life. Jouin, Gouriveau [48], classified the components according to their contribution to the degradation of a PEMFC stack in three classes:

- Class A: membrane and electrodes.
- Class B: GDL and bipolar plates.
- Class C: sealing gaskets.

Class A refers to the components that are subject to most degradation processes and contribute to the performance degradation of PEMFC. By comparison, class C are components that have the most negligible effect on the performance degradation of PEMFC. Membrane and electrodes (Catalyst layers) play an essential role in PEMFC degradation, as most of the degradation phenomenon occurs or affects these parts of PEMFC. In the next section, an overview of degradation causes and effects on these components is presented.

Proton Exchange Membrane (PEM)

A PEMFC stack comprises several cells, and each cell has a membrane-electrode assembly (MEA). Because the cells are connected in series, failure in one MEA will cause the failure of the stack.

The membrane needs to be hydrated to facilitate hydrogen cations to pass through; however, excess water in a membrane may cause flooding, decreasing performance, and increasing degradation [105]. The most common material for membranes is polymers of perfluorosulfonic acid (PFSA), such as the Nafion. Improving its conductivity needs sufficient water [95]. The importance of membrane in PEMFC degradation comes from its role as a proton conductor and a separator between cathode and anode. Therefore, the membrane should have high proton conductivity, thermal and chemical stability, good mechanical resistance, flexibility, low gas permeability, and low water drag [39]. Jouin, Gouriveau [39] proposed three different categories for membrane degradation: chemical, mechanical degradation, and crossover, explained in more detail below, also summarized in Figure B-1. The degradation mechanism in the membrane can be divided into three different categories Jouin, Gouriveau [39], [105]:

Chemical degradation:

It is caused by contamination and radicals produced in the cathode and anode during chemical reactions or corrosion of the stack components, impurities from gases, or humidifier tanks[1, 39]. Three types of radicals have been introduced since now as hydroxide (HO^-) [98, 106], carbon monoxide (CO) [1] and hydroperoxide (HOO^-) [106]. It causes a reduction in membrane thickness which leads to gas crossovers and mechanical weakness. It can be measured by monitoring the hydrogen crossover [39].

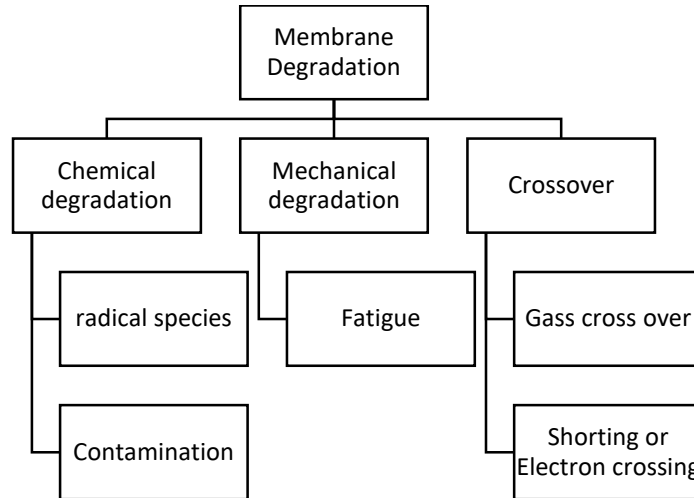


Figure B-1. Membrane degradation processes

Mechanical degradation:

Several mechanical degradation causes such as thermal stresses [24], mechanical stress, thermal and humidity cycling [1], excessive or non-uniform pressure have been reported [106]. Gas crossover can take place due to the current inversion [39]. In critical cases due to manufacturing flaws, the PEMFC may break down in a shorter time than usual [106]

Shorting:

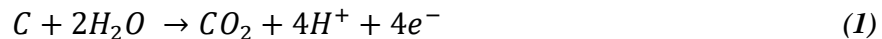
Shorting is the phenomenon of crossing electrons through membrane instead of common electrons path, results in performance decrease and local heat generation at a membrane, leading to membrane degradation. So far, General Motors researchers have found two types of shorting in PEMFC: soft shorting is caused by external electron conductive penetration to the membrane, and critical shorting has more severity and causes failure and Ohmic resistance increase [39]. The gas crossover phenomenon is like shorting but much more severe and occurs when both Hydrogen and Oxygen cross the membrane directly, however Oxygen crossover has not been reported in many research papers and seems less important. A significant

consequence of gas crossover is the reaction of O₂ and H₂ directly as combustion, which produces heat of combustion that leads to the death of Cell and stack [39].

Several researchers have studied crossover, which resulted in an exponential increase in gas crossover during the degradation of PEMFC [93, 99, 107]. de BFA and Janssen [108] proposed that a crossover current of 10 mA/cm² could be encountered as PEMFC end of life.

Electrodes (Anode and Cathode Catalysts)

Electrodes are made up of the first catalyst layer, generally made of platinum (Pt) nanoparticles on the surface of carbon particles surrounded by ionomers. Second, the carbon support allows electrons, water, and gasses to move quickly. According to Schmittinger and Vahidi [109] degradation phenomenon in cathode and anode electrodes of a PEMFC is different. So these two parts are responsible for degradation in electrodes, leading to loss of active surface area and consequently loss of electrochemical activity. Carbon is generally oxidized under the influence of three different conditions, namely: high temperature, high oxygen concentration, and the high potential environment with the reaction bellow [8]:



Degradation caused by carbon corrosion is much higher than the dissolution of Pt since carbon acts as platinum support, and any degradation may severely degrade the electrode structure, leading to the limitation of mass transfer [8]. The degradation of PEMFC electrodes is highly dependent on load cycling. Results of Kocha et al. [110] showed the impact of three different load cycles on the durability of PEMFC electrodes:

Table B-1. PEMFC electrode degradation caused by different load cycling

load mode	Degradation participation percentage
Idling	28%
Startup/Shutdown	28%
Dynamic Load	44%

According to Tang et al. [12], electrode thickness decreased after several startup/shutdown up to one-third because of carbon corrosion [8]. Working in an idling load is a favorable condition to increase platinum degradation [39]. Anode electrode seems to experience any degradation caused by dissolution, oxidation, and agglomeration of Platinum, regardless of operating conditions, while the cathode is not [39]. Almost all the mitigation methods to reduce startup/shutdown degradation effects are divided into “finding key material for catalyst” and “system control strategies” [8].

Table B-2. Electrode degradation phenomenon and consequences

Cause(phenomenon)	result	Reference
Sudden increases in current	reduction of the catalyst area	Weng, Hsu [24]
reverse current during start-up	catalyst corrosion	Reiser, Bregoli [13]
fuel starvation	carbon catalyst corrosion	Zhou, Shao [111]
hydrogen-air interface	carbon catalyst corrosion	Zhou, Shao [111]
carbon corrosion	Electrode thickness decreased	Tang, Qi [12]

Bipolar

The bipolar plates have several roles: current-conducting, gas channel flow field, water and thermal management, and a separator between cells [106, 112]. In addition, bipolar plates have three degradation mechanisms [39] shown in Figure B-2. The ageing of bipolar plates has less importance than other components of PEMFC for researchers, and there is less degradation modeling. However, tests related to corrosion can be done using potentiodynamic polarization curves of the materials [112].

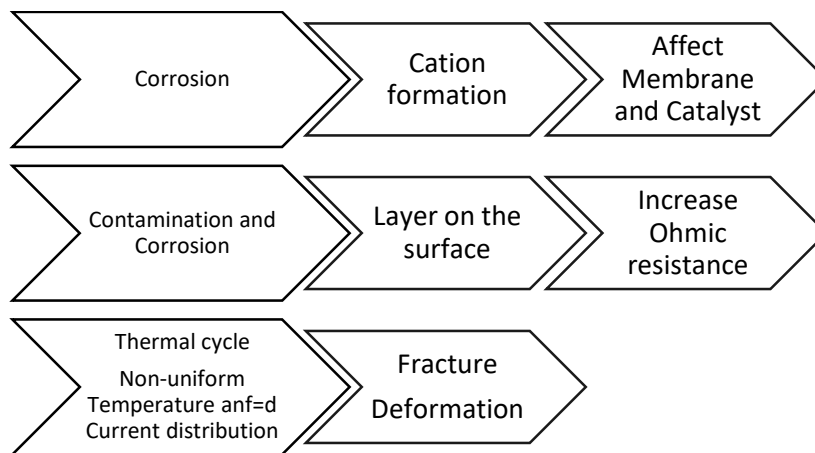


Figure B-2. Degradation in bipolar plates of PEMFC

GDL

GDL has some significant roles listed below [39] a) diffusing inlet gasses at the cathode and anode to reach equal to the reaction sites, b) removing liquid water produced as a result of reaction c) helping water management in the membrane and electrodes d) transferring electrons between electrodes and bipolar plates. However, GDL materials experience three major degradation processes: loss of hydrophobicity, carbon corrosion, and loss of porosity. Jouin, Gouriveau [39] developed ASTs showed that GDL degradation is primarily due to mechanical stresses that increase mass transfer resistance.

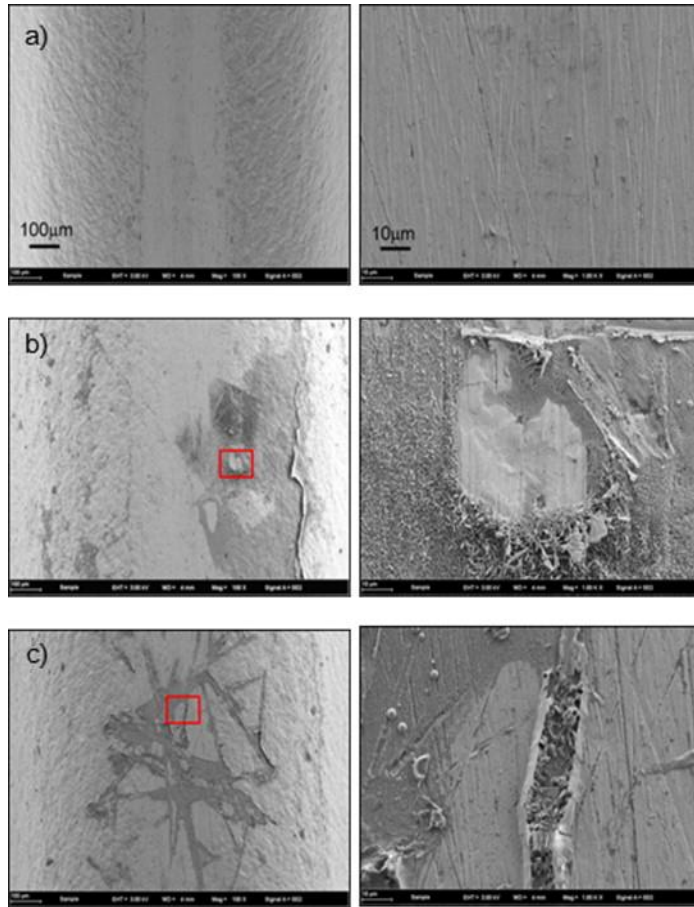


Figure B-3. Bipolar plate SEM images: a) starting time, b) and c) after 300 h degradation test [20]

Results showed a reduction in contact angle and GDL weight, carbon erosion, and an increase in mass transfer and ohmic resistance [113]. The degradation in GDL can be classified into Mechanical and Chemical [105].

A) Mechanical degradation in GDL

Four categories are available in the mechanical degradation of GDL:

Effect of compression force: Increasing compression force and pressure positively and negatively impact PEMFC performance [105].

GDL degradation in freezing/thawing condition: Freezing of remained water in PEMFC after shutting down or because of the cold start in the subfreezing temperatures causes mechanical stresses in GDL, membranes, and electrode as a consequence of volume expansion [105].

Dissolution effect on GDL: The existence of water due to the reaction production or humidified air or fuel may cause hydration of GDL by dissolving GDL carbon material [105].

Erosion of GDL by continuous gas flow: Erosion of GDL can be a primary effect of gasses flowing through it, primarily because of the removal of water in gasses that stick to the GDL surface's cracks [114]. According to Ha [105], carbon felt-type GDL shows stronger resistance to gas erosion than carbon paper-type GDL. A test performed by Latorrata et al. [113] showed a decrease in contact angle and GDL weight, carbon erosion, and an increase in mass transfer and ohmic resistance.

B) Chemical degradation in GDL

Chemical degradation of GDL is mainly because of carbon corrosion. Air may exist at anode and cathode during startup/shutdown, shut down, and local hydrogen starvation due to the leakage or membrane crossover. Thus, the hydrogen/air interface causes a potential difference in carbon corrosion and oxygen evolution [105].

Sealing gasket

The sealing gasket is responsible for preventing any leakage or mixing of air and fuel, so an appropriate packaging pressure is needed for this. The standard material used in the sealing gasket is silicone [115]. Several researchers have worked on the degradation of sealing gasket, and they observed sealing material remained in other parts of PEMFC, which cause performance degradation[115-118]. However, gasket degradation does not directly impact PEMFC performance [39]; it may have various further outcomes such as membrane contamination and electrodes [106]. Loss of its holding force thus decreases compression force, external leakage of cooling, or appearance of shorting [39].

PEMFC components degradation in literature

Membrane degradation

Xu, Boroup [119] studied the effect of relative humidity (RH) on membrane degradation. They conducted two different tests. The first one showed that at OCV potential degradation rate in 60 percent RH is more than 20 percent and 100 percent RH after 100 hours. They explained that increasing RH increases hydrogen and oxygen gas permeability; however, it decreases the “rate constant for oxygen radical formation.” In the other test, the degradation rate increased when RH decreased to 20 percent after 500 hours of working at 0.6 V and 100 percent RH. Higher RH causes lower hydrogen crossover, shown during an H₂/N₂ test; however, its degradation in an H₂/O₂ test remained almost constant in 100 percent and 3 percent RH but in 20 percent and 60 percent test increased surprisingly. Lim, Ghassemzadeh [120] carried out a cyclic OCV test to simultaneously study mechanical/chemical degradation of the membrane in PEMFC.

The constant potential at OCV was considered as chemical and cyclic RH as mechanical degradation. The formation of pinholes and membrane thinning resulted from chemical degradation, and as a result of the mechanical degradation, the membrane became stiffer and more brittle. Mittal et al. [121, 122] studied the effect of the catalyst layer on membrane degradation. The unwanted and direct reaction between O_2 and H_2 because of crossover is the primary source of membrane chemical degradation. Sompalli, Litterer [123] experimented with a model to research membrane degradation in contact with the catalyst layer. Their results prove that high potential at the cathode is a significant reason for membrane degradation. They also showed that RH has an insignificant effect on membrane degradation at all points of the membrane. Yuan et al. [18, 124] tested four cells PEMFC with different Nafion membranes: N117, N115, NR212, and NR211 of various thicknesses for 1000 hours. According to their results, a thinner membrane has more hydrogen crossover. Hydrogen crossover causes pinholes (as a result of direct reaction with O_2 , which produces heat), leading to membrane degradation. So a thinner membrane has more degradation rate in hydrogen crossover, leading to membrane thinning and pinholes formation. This chain ends up with a drastic increase in membrane degradation in a shorter time.

Chandesris, Vincent [125] studied the effect of pressure, humidity, and cell potential on membrane degradation experimentally in different operating conditions. Using a semi-empirical model, they concluded that lowering RH causes membrane thinning, pinhole formation, and OCV reduction. However, increasing RH will prevent pinhole formation and improve PEMFC life. Test results showed that cathode oxygen partial pressure has a linear effect on membrane degradation. Wu, Zhao [99] performed an AST for 100 hours and studied the impact of RH cycling and load cycling on the Nafion/PTFE composite membrane in a PEMFC. In this test, the chemical degradation of the membrane, membrane thinning, Pt particles agglomeration in membrane/catalyst interface, and cathode ionomer loss were degradation effects of RH/potential cycling in the membrane. They confirmed that hydrogen crossover or OCV under H_2/N_2 inlet gas shows membrane failure. Tang, Peikang [94] studied the effect of different mechanical, chemical, and potential conditions on the degradation of a Nafion NR111 membrane PEMFC. The high degradation rate at OCV potential is mainly due to the H_2O_2 attack due to H_2/O_2 crossover and reaction in the membrane. Inaba, Kinumoto [96] studied the effect of startup/shutdown on membrane degradation, focusing on hydrogen crossover. Hydrogen crossover increased with cell temperature, humidity, and hydrogen pressure. Liu and Case [107] concluded that after 500 hours of cyclic current loading, the most significant degradation source was increasing in hydrogen crossover because pinhole formation while in constant current test remains almost unchanged. Mass transport limitations were the primary source of degradation in the later test, which was not a completely irreversible degradation process and resolved after decreasing current. The whole test was 1000 hours which was the end of life for their tested PEMFC. They also established a semi-

empirical model which proved the need for a “standard PEMFC durability test protocol” and “membrane pinhole reduction study”.

Electrodes degradation

Urchaga, Kadyk [126] analyzed degradation data and resulted that higher upper potential in square-wave form potential cycling and increasing cell temperature increase degradation of PEMFC. Kneer, Jankovic [127] studied the effect of potential cycling on electrode degradation of a PEMFC and concluded that Electro Chemical Surface Area (ECSA or active surface area) loss is a primary effect that leads to an increased oxygen transport resistance reaction sites. Pt dissolution was observed, but as 92 percent of the initial Pt mass was still in the electrode, Pt particle agglomeration is the leading cause of ECSA loss during potential cycling. They showed that higher RH, temperature, and the possible upper limit have more ECSA loss [128]. ECSA loss rate was more at a longer cycle, proving that the number of cycles is as vital as their duration. They showed that oxide layer formation has an essential effect on Pt particle redistribution [129]. Sharma and Andersen [130] carried out a potential cycling test between 0.4 and 1.6 V for 7000 cycles. The results showed a significant reduction in ECSA as high as 64 percent loss due to the Pt dissolution (6%), ionomer corrosion (19%), Pt agglomeration (30%), and carbon corrosion (45%).

White, Wu [131] studied electrode degradation during potential cycling using a four-dimensional approach, carbon corrosion, catalyst thinning, and crack; they observed propagation. They also showed that the delamination of the cathode catalyst layer leading to separation from GDL is another degradation effect in the electrode [132]. Speder, Zana [133] concluded that the Pt/c loading ratio does not significantly affect ECSA degradation at load cycling potential. However, in the startup/shutdown test, the ECSA degradation rate increased with rising Pt loading, and the very high Pt loading catalyst layer experienced a decrease in ECSA degradation rate. Hitchcock, Berejnov [134] observed Pt agglomeration and migration, carbon support corrosion, catalyst thinning, Pt particles in the membrane as degradation effects in the catalyst layer.

GDL degradation

Hydrophobicity loss is an essential effect of degradation in the gas diffusion layer based on a study by Pauchet, Prat [135], causing an increase in flooding and performance loss. According to Liu, George [136], carbon corrosion is a significant degradation effect in GDL that causes a decrease in contact angle, thus hydrophobicity loss. George, Liu [137] found that the degradation of GDL triggers a reduction in limiting current density and an increase in oxygen mass transport resistance.

Gasket degradation

Cui, Chao [138] showed that temperature cycling is a prominent cause of mechanical degradation in sealing gaskets in PEMFC. Experiment results revealed an increase in material stiffness at higher temperatures.

Appendix C. Sources PEMFC Performance Degradation Data

IEEE PHM 2014 Data

FC stack

The PEMFC stacks are 5-cell stacks with 100 cm² of the active surface area assembled at FCLAB. The test nominal current density is 0.7 A/cm² with a maximum current density of 1 A/cm². A 1 kW test bench is used for the experiments [86].

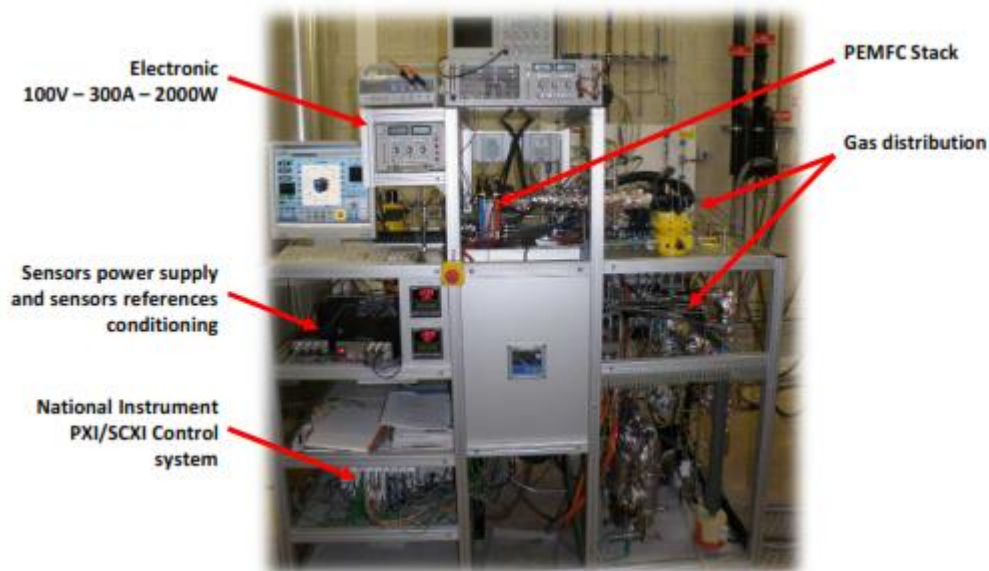


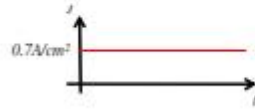
Figure C-1. 1 KW fuel cell test bench [86]

Two sets of tests:

Two stacks were tested separately. The first one was tested with the constant current, and the second one was tested with the rippled current. The average nominal current density at both was 0.7 A/cm². So the FC1 tested in stationary conditions, and the FC2 tested in dynamic loads. The oscillation was 10 percent with a frequency of 5 kHz. For each of them, characterization tests were carried on every one week approximately.

FC1 - Long-term test without current ripples

Ageing @ - $I_{nom} = 70 \text{ A}$ ($j = 0.7 \text{ A/cm}^2$)



FC2 - Long-term test with high frequencies current ripples

Ageing @ - $I_{nom} = 70 \text{ A}$ ($j = 0.7 \text{ A/cm}^2$)

- Triangular current ripples: $\pm 10\%$ of I_{nom} @ 5 kHz

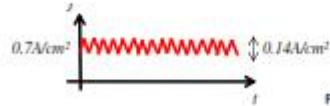


Figure C-2. Two tests have been done for the experiment[86]

The results were given through two excel sheets for each test. No. 1 is the polarization curve data reported each week, and No. 2 is the voltage degradation data with other operating parameters for each hour.

Table C-1. Results excel sheet No. 1 description

Column	Description	Unit
1-5	cells voltages	V
6	stack voltage	V
7	current	A
8	current density	A/cm ²

Table C-2. Results excel sheet No. 2 descriptions

Column	Description	Unit
1	time	h
2-6	cells voltages	V
7	stack voltage	V
8	current density	A/cm ²
9	current	A
10-11	inlet/outlet temp. of H2	C
12-13	inlet/outlet temp. of Air	C
14-15	inlet/outlet temp. of cooling water	C
16-17	inlet/outlet pressure of Air	mbar
18-19	outlet/inlet pressure of H2	mbar
20-21	inlet/outlet flow rate of H2	l/min
22-23	inlet/outlet flow rate of Air	l/min
24	flow rate of cooling water	l/min
25	inlet hygrometry of Air	%

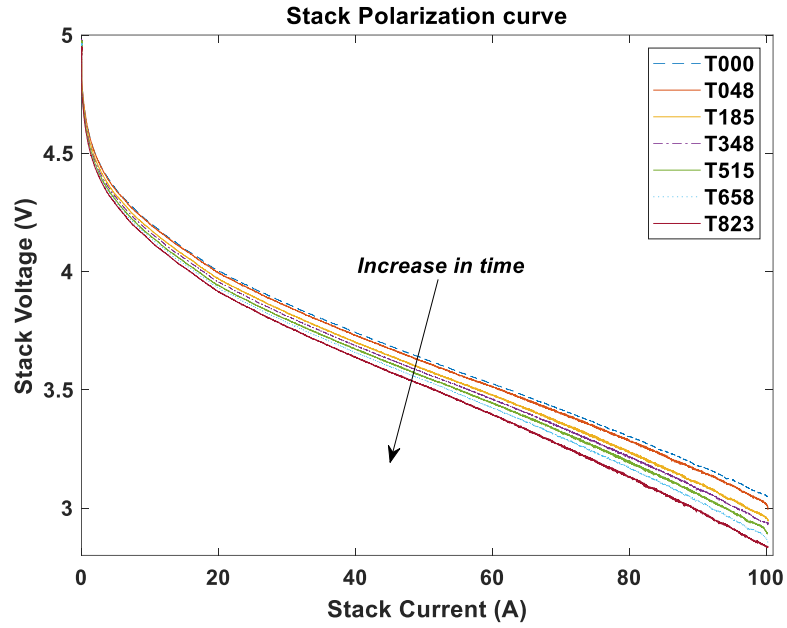


Figure C-3. Polarization curve test data with a constant current for the different times during degradation

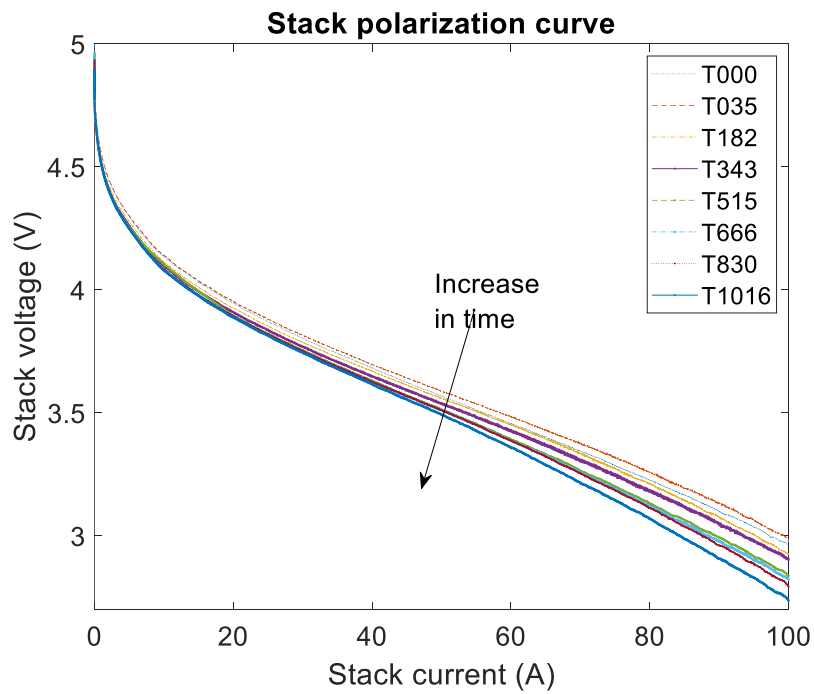


Figure C-4. Polarization curve test data with a rippled current for the different times during degradation

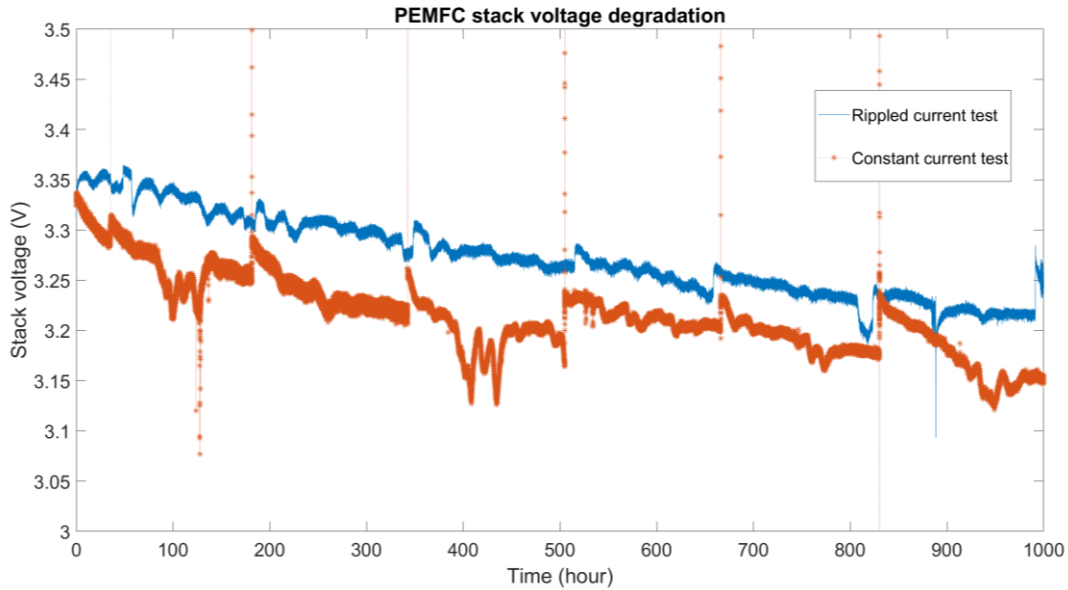


Figure C-5. PEMFC stack voltage degradation data for both tests with rippled current and the test with a constant current

Experimental data from Lin et al. [101]

A single cell with an active surface area of 50 cm² and 40 percent Pt/C was made in their lab. The test duration was 370 hours, and the load mode was a dynamic load shown in Figure C-6. Cold starting, idling, dynamic load, high power load was considered in the test load mode, and each cycle was 20 minutes.

Polarization curves at different times and the voltage degradation curve at different currents were reported as test results shown in Figure C-7.

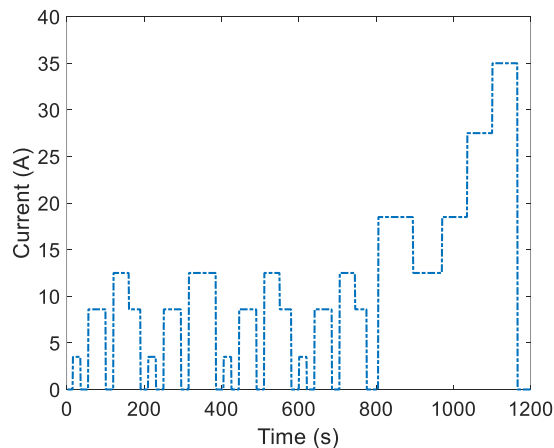
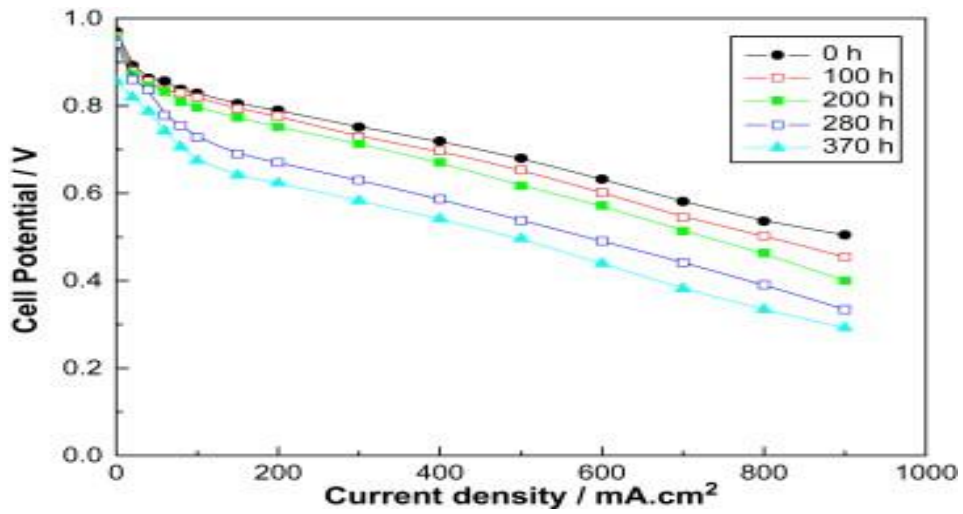
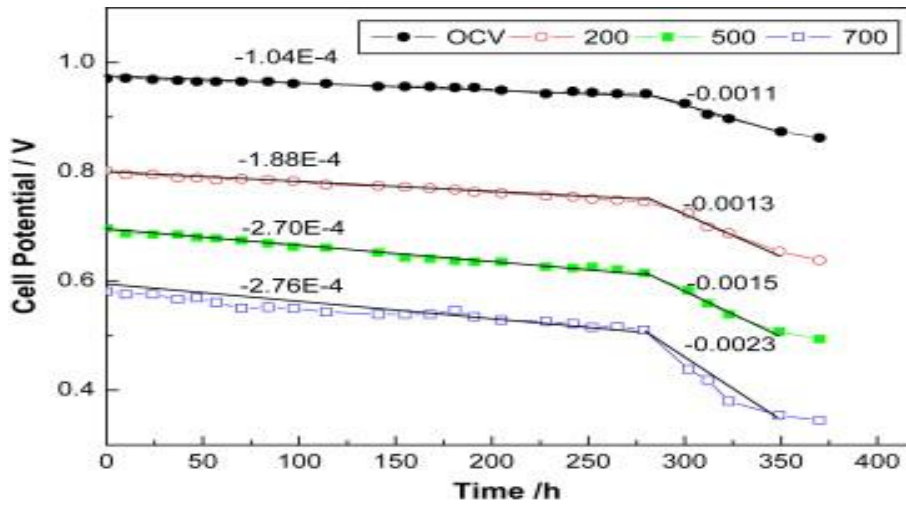


Figure C-6. load mode used in the experiment



(a) Polarization curves after different operation time



(b) voltage degradation at different current densities

Figure C-7. Experimental data [101]

Appendix D. Additional Results of FCEV Simulation

Model Fitting Results

Figure D-1 is plotted using the new performance degradation model fitted with only the polarization curve at the beginning and the voltage degradation data. Then it has been expanded over a broader range of current from 0 to 100 A, and polarization curve data are plotted to compare at different times. The model parameters are estimated using degradation data at midrange current density; thus, the new performance degradation model using these parameters has better prediction when PEMFC works at the same range of current densities. By fitting the new performance degradation model using polarization curve data at different times plus voltage degradation data at $i = 0.7 \text{ A/cm}^2$ the results are more precise, and Figure D-2 shows that the new performance degradation can predict the performance of PEMFC in very low current densities very well. These results prove that the new model gives us a perfect prediction by having degradation data at various voltages. However, to get the best results with these accessible data, the model parameters should be made using the mentioned experimental data.

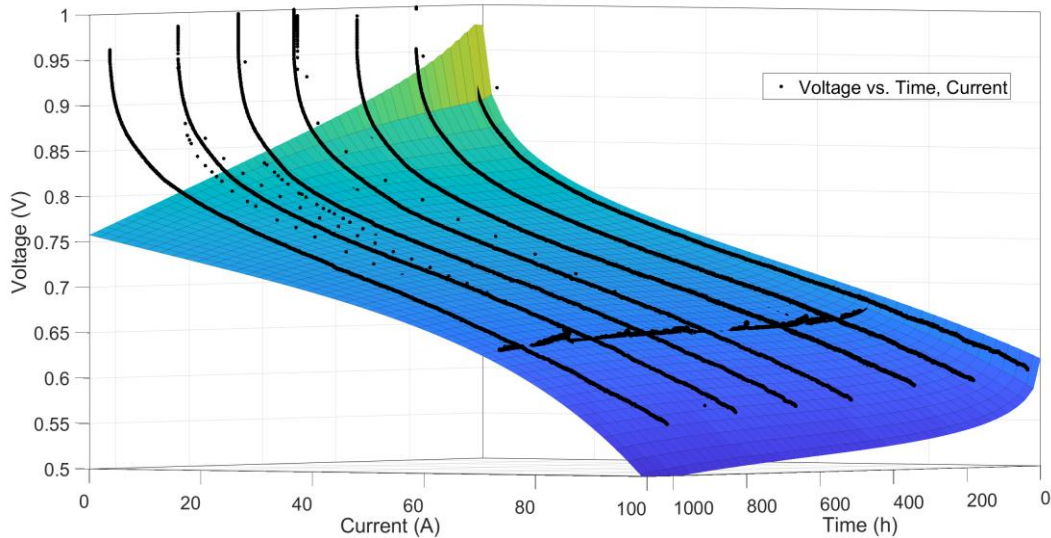


Figure D-1. Performance degradation model prediction expanded at the time for the model fitted with test2

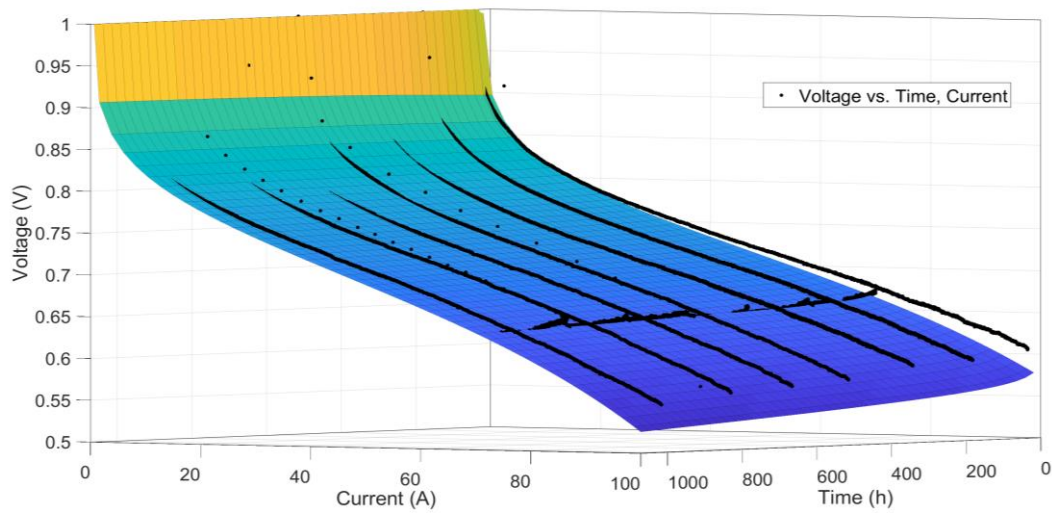


Figure D-2. Performance degradation model plot fitted with polarization curves at different times and voltage degradation at $I = 0.7 \text{ A/cm}^2$ for test2

ADVISOR simulation results

The results of the FCEV simulation in ADVISOR are plotted in Figure D-3 and Figure D-4 as fuel cell and ESS output power and motor input power.

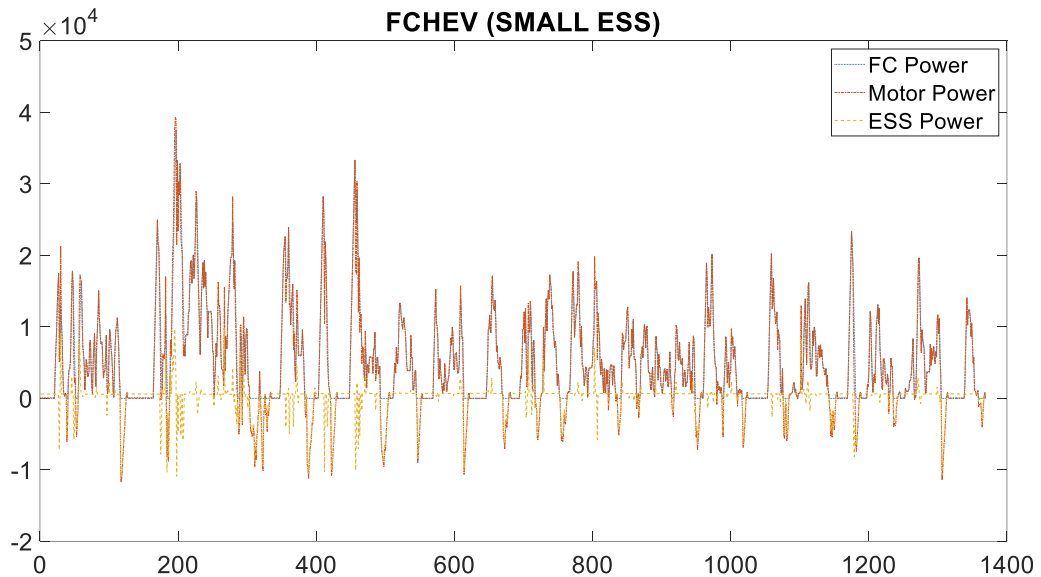


Figure D-3. ADVISOR simulation power results for the FCHEV with small ESS

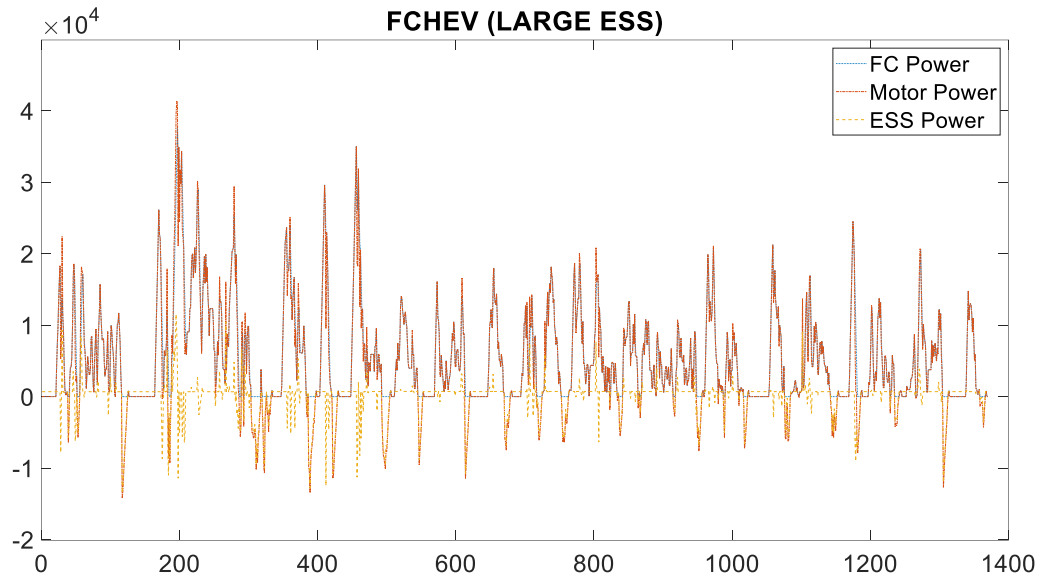


Figure D-4. ADVISOR simulation power results for the FCHEV with large ESS

Simulation results plots related to the other two powertrains with no ESS and large ESS are shown here as they were similar to the powertrain with small ESS. Besides that, Figure D-5 demonstrates a comparison between the output load of PEMFC in a pure PEMFC vehicle with no ESS and two others that show that the PEMFC attached to the larger ess needs to have more power output.

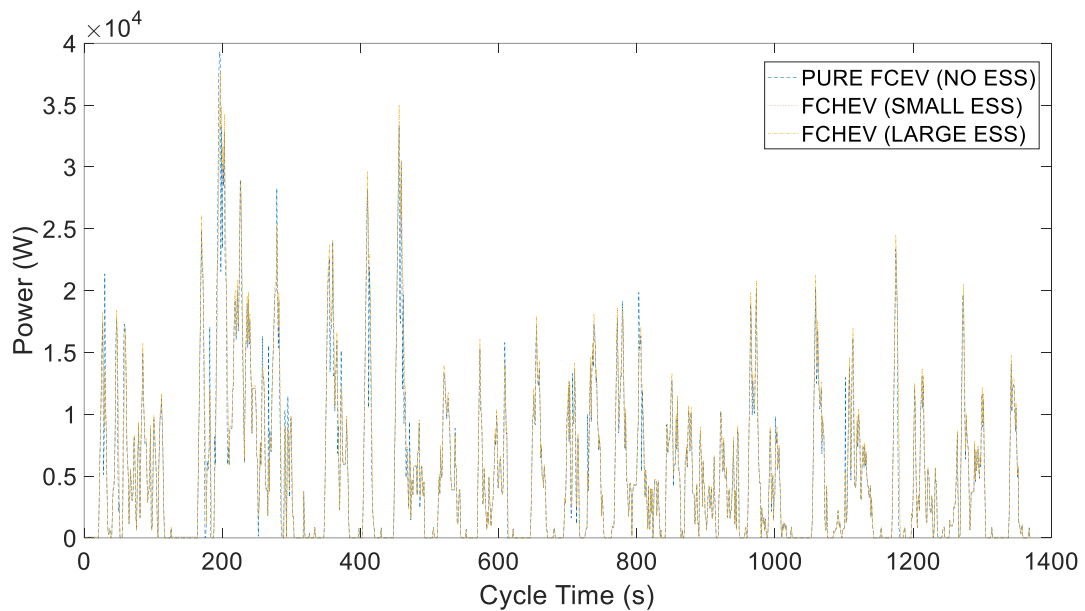


Figure D-5. PEMFC's output load power comparison between three powertrains

Figure D-6 and Figure D-7 show the voltage difference between FCHEV with a small ESS and large ESS and an FCEV with now ESS. Thus, using an ESS does not necessarily mean decrease in fuel cell output power at all the time.

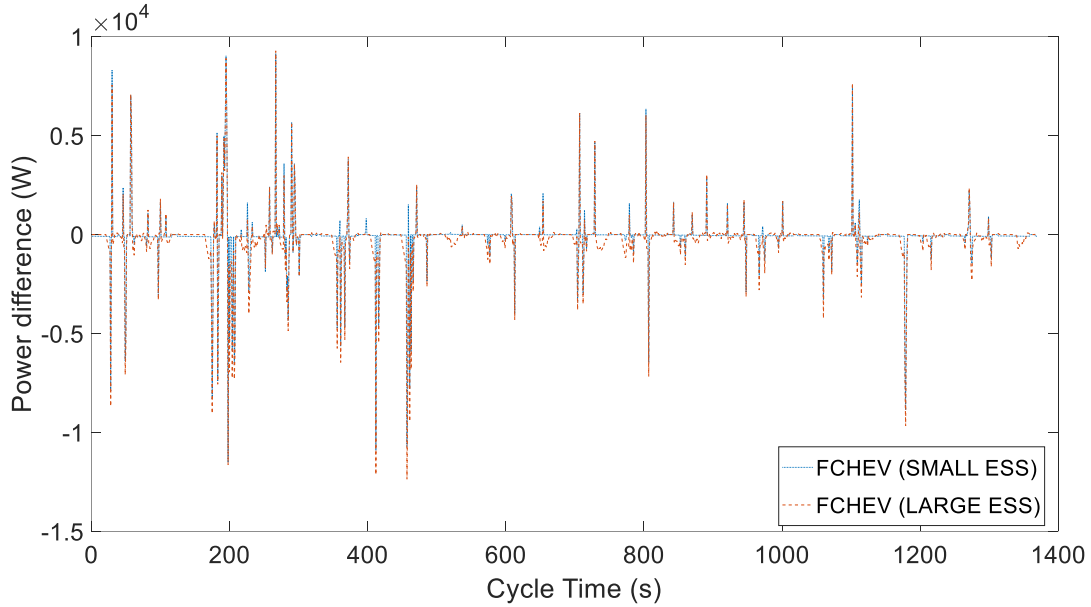


Figure D-6. The power difference between the powertrain with no ESS and two others

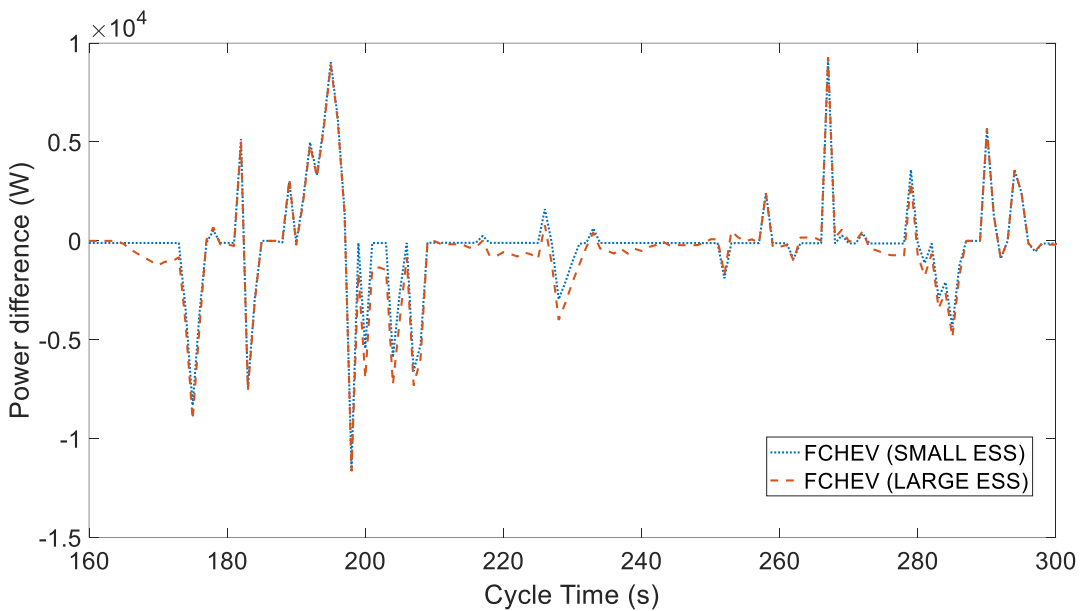


Figure D-7. Propulsion power of an FCEV with no ESS and a large ESS

Model simulation results

Figure D-8 and Figure D-9 show the voltage and current in one cycle for the fuel cell in an FCEV with no ESS and a large ESS used in the performance degradation simulation of PEMFC for the related powertrain.

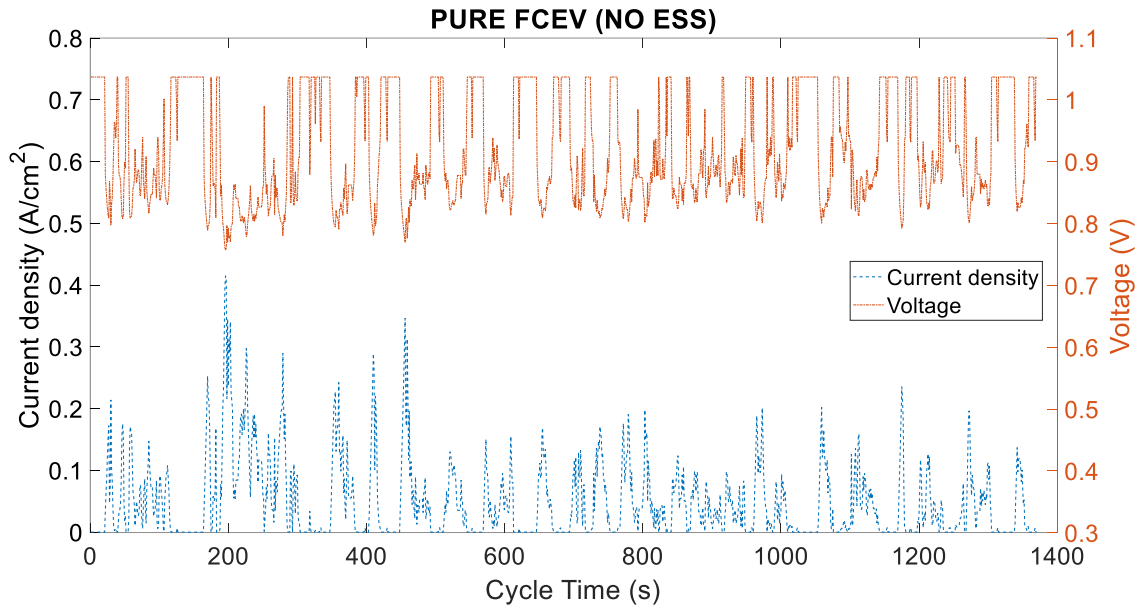


Figure D-8. Voltage and Current density of PEMFC in one cycle for simulation with no ESS

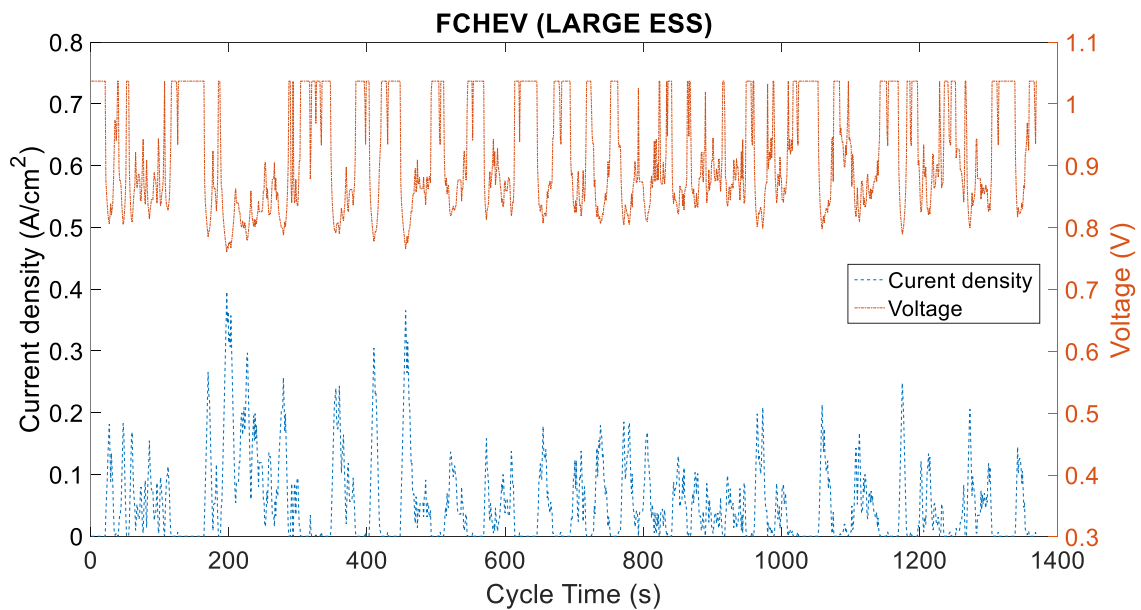


Figure D-9. Voltage and Current of PEMFC in one cycle for simulation with large ESS

Figure D-10 and Figure D-11 show the degradation in m and n , two parameters related to the concentration loss. However, they did not show any significant degradation because of the nature of data that are explained before.

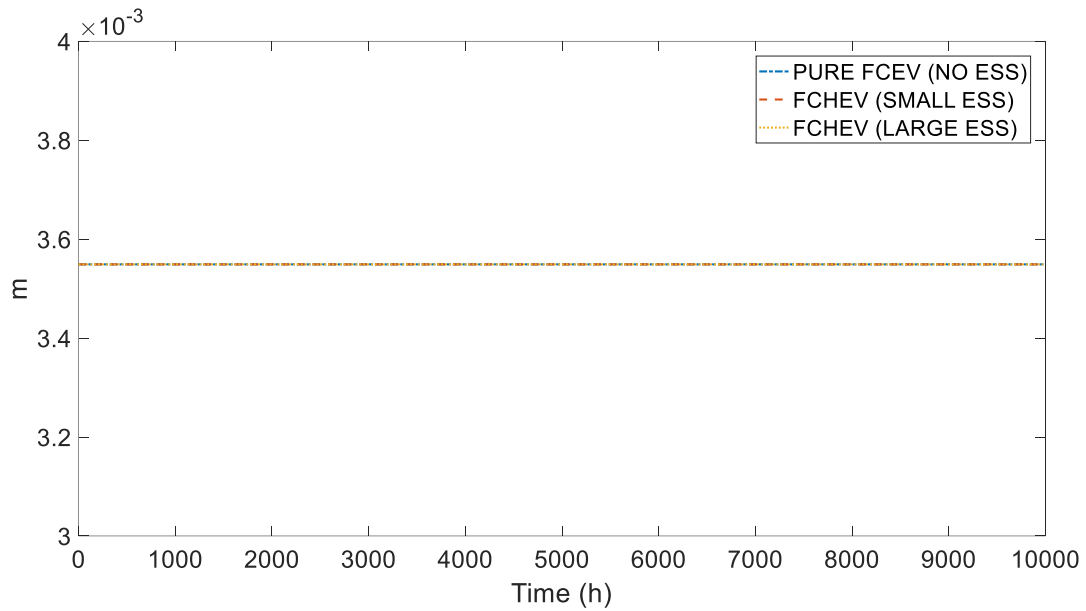


Figure D-10. Concentration loss parameter (m) changing with time

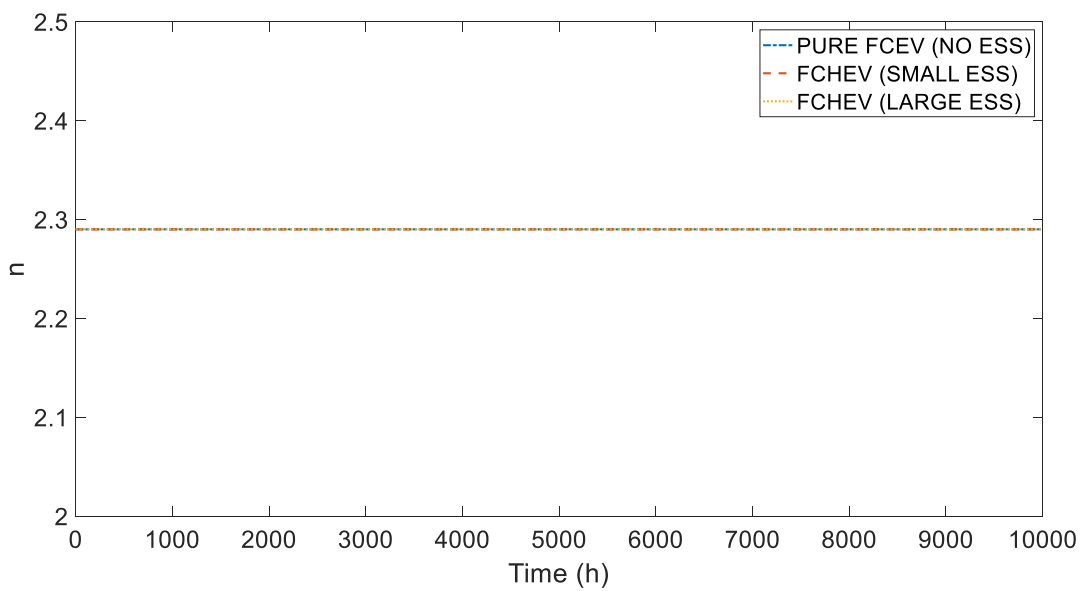


Figure D-11. Concentration loss parameter (n) changing with time

Figure D-12 to Figure D-17 are for the vehicle with no ESS and a large ESS with the same explanation as in chapter 5 for the PEMFC in an FCEV with a small ESS.

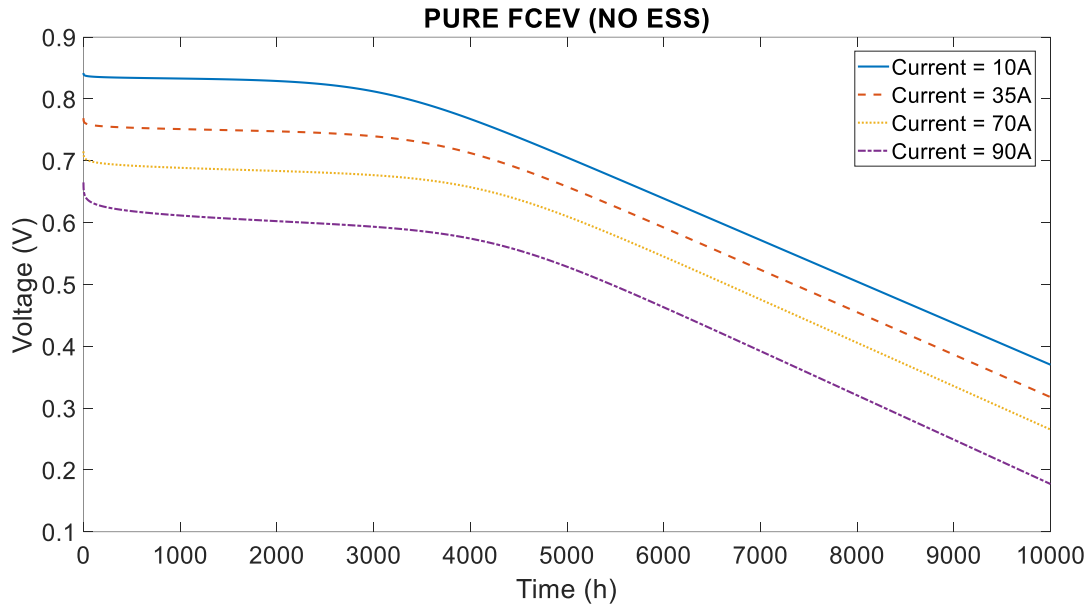


Figure D-12. Voltage degradation with time in four different currents: 10A, 35A, 70A, and 90 A for powertrain with no ESS

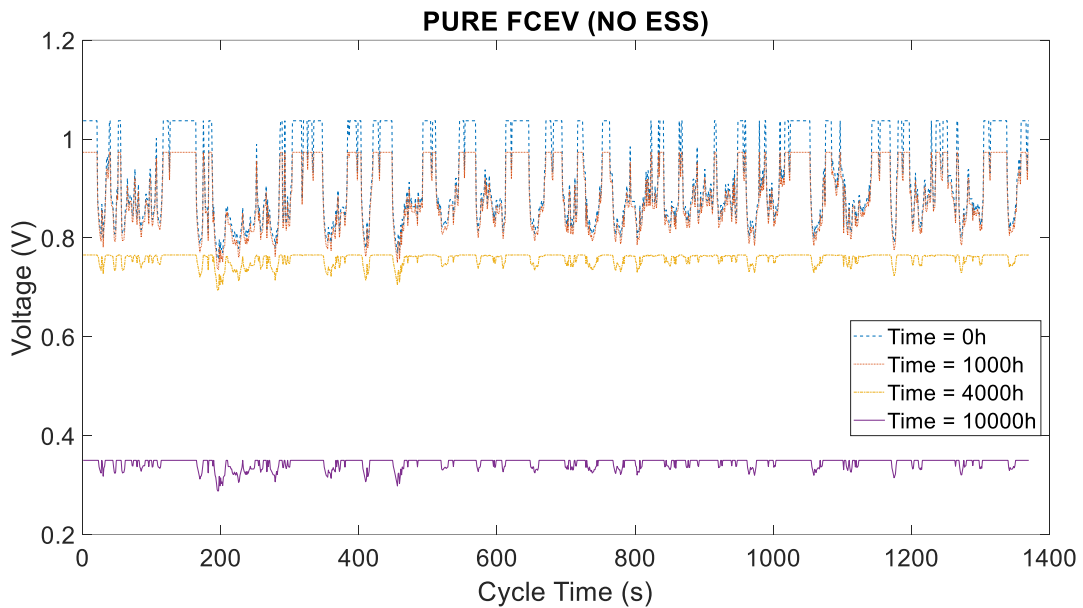


Figure D-13. PEMFC voltage degradation in one load mode and four different times: 0h, 1,000h, 4,000h, and 10,000h for the powertrain with no ESS

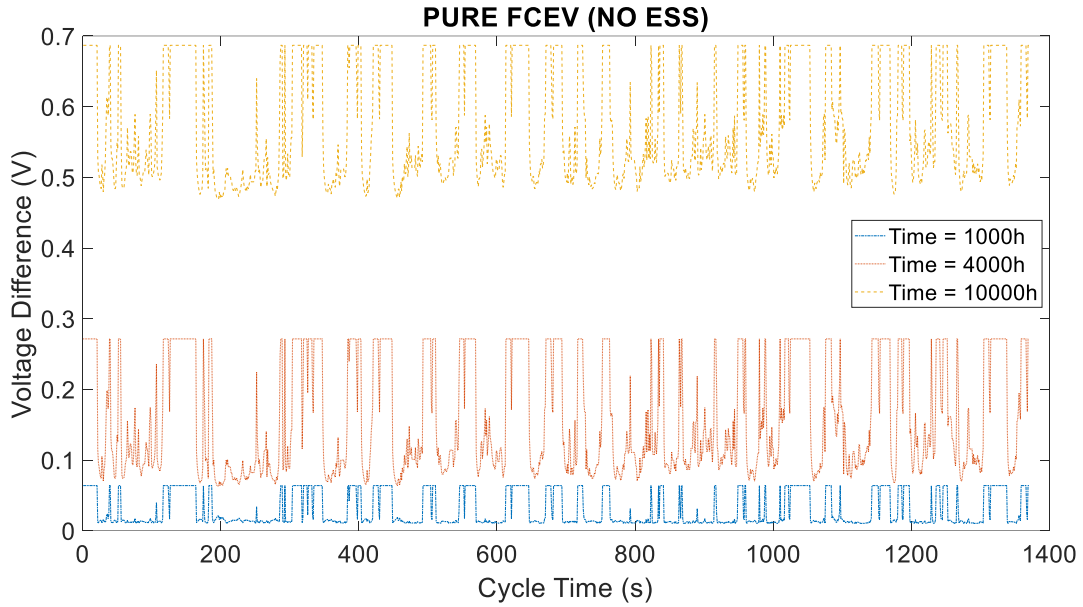


Figure D-14. PEMFC voltage difference in one load mode and three different times: 1,000h, 4,000h, and 10,000h with time 0h for powertrain with no ESS

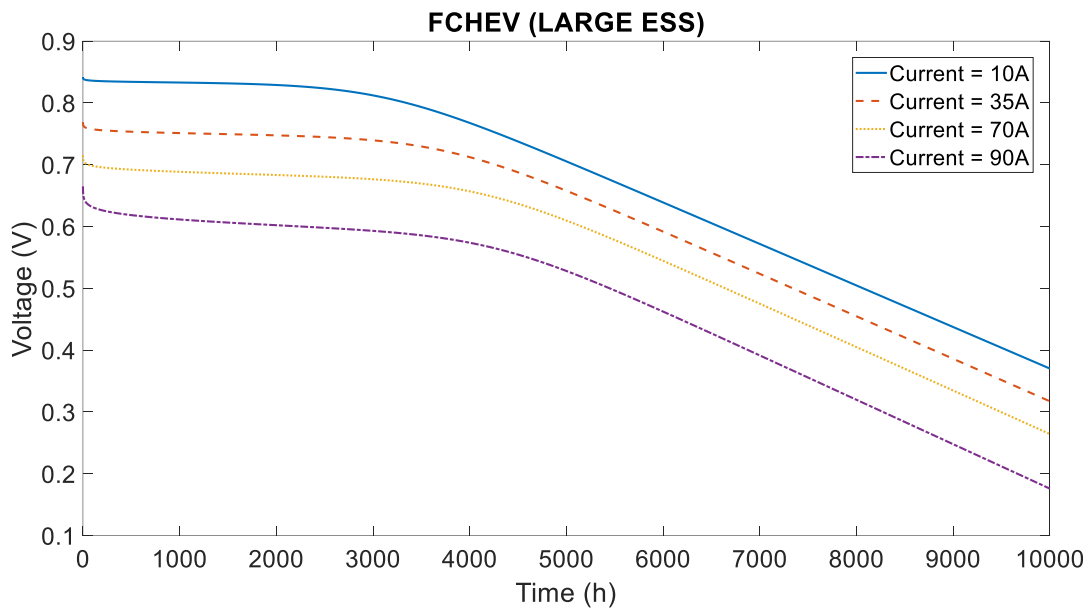


Figure D-15. Voltage degradation with time in four different currents: 10A, 35A, 70A, and 90 A for powertrain with large ESS

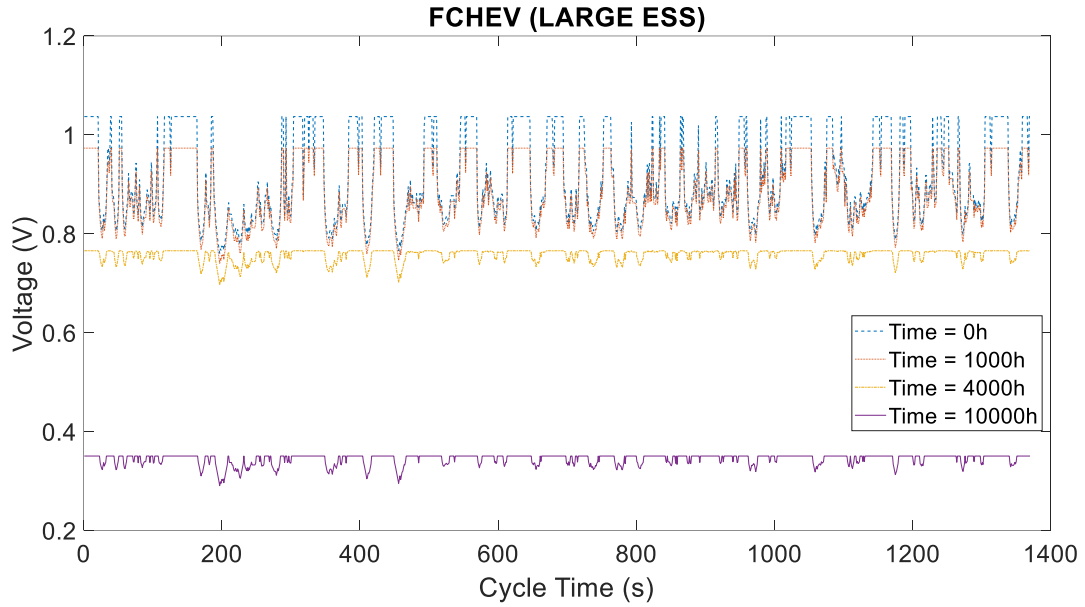


Figure D-16. PEMFC voltage degradation in one load mode and four different times: 0h, 1,000h, 4,000h, and 10,000h for the powertrain with large ESS

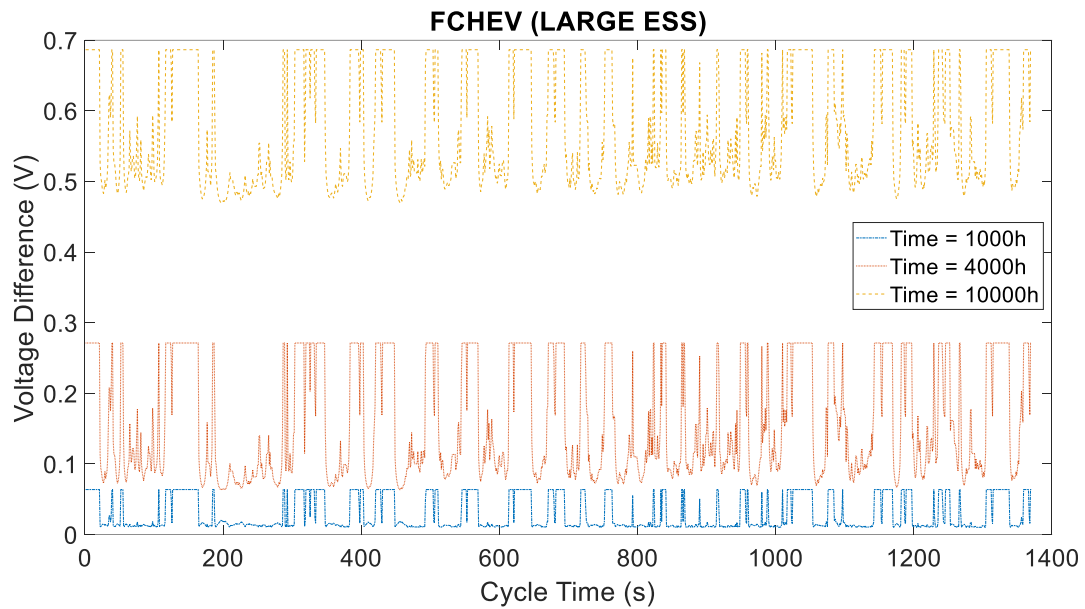


Figure D-17. PEMFC voltage difference in one load mode and three different times: 1,000h, 4,000h, and 10,000h with time 0h for powertrain with large ESS

Appendix E. MATLAB Codes of Performance Degradation Simulations

Example MATLAB code for finding RUL using PEMFC performance degradation model

```
clear;
clc;
filename = xlsread('Result.xlsx');
Pwr(1:1370,1:3) = filename(1:1370,1:3);
tic
for i = 1371:36000000
    Pwr(i,:) = Pwr(i-1370,:);
end
toc
a = 99.42;
a1 = 0.1597;
a2 = 0.03476;
a3 = 0.0003151;
a4 = 0.0002829;
a5 = 0.08389;
a6 = 0.003549;
a7 = 2.29;
Volg = 1.23-a1-a2*asinh(((x/a)+a3)/a4)-(x/a)*a5-a6*(exp((x/a)*a7)-1);
Powr = (x)*Volg;
Volg_I = 1.23-a1-a2*asinh(((x/a)+a3)/a4);
Powr_I = (x)*Volg_I;
Volg_D = 1.23-a1-a2*asinh(((x/a)+a3)/a4)-(x/a)*a5;
Powr_D = (x)*Volg_D;
for j = 1:3
    tic
    disp('Start part one')
    for i = 1:1370
        P = Pwr(i,j);
        if P <= 7500
            C = vpasolve(Powr_I-P/1250,x);
            Curr(i,j) = C;
            Vltg_B(i,j) = 1.23-a1-a2*asinh(((C/a)+a3)/a4);
        elseif P > 67500
            C = vpasolve(Powr-P/1250,x);
            Curr(i,j) = C;
            Vltg_B(i,j) = 1.23-a1-a2*asinh(((C/a)+a3)/a4)-(C/a)*a5-a6*(exp((C/a)*a7)-1);
        else
            C = vpasolve(Powr_D-P/1250,x);
            Curr(i,j) = C;
            Vltg_B(i,j) = 1.23-a1-a2*asinh(((C/a)+a3)/a4)-(C/a)*a5;
        end
    end
end
disp('End part one')
toc
tic
for i = 1371:36000000
    Curr(i,j) = Curr(i-1370,j);
    Vltg_B(i,j) = Vltg_B(i-1370,j);
```

```

end
toc
disp('End part one')
end
tic
toc
disp('Start part two')
for j = 1:3
tic
a = 99.42;
a1 = 0.1597;
a2 = 0.03476;
a21 = 2.779e-06;
a23 = 0.001934;
a25 = 9.141e-05;
a26 = 0.0001618;
a27 = 2.337e-14;
a3 = 0.0003151;
a4 = 0.0002829;
a5 = 0.08389;
a6 = 0.003549;
a7 = 2.29;
aa = 2.524;
ab = 4.864;
for i = 1:36000000
time(i,j) = i;
m = Pwr(i,j);
t = 1/3600;
a = 99.42-aa*log(ab*t*i+1);
if m <= 7500
a1 = a1+a21*t;
a3 = a3*exp(a23*t);
C = Curr(i,j);
Vltg(i,j) = 1.23-a1-a2*asinh(((C/a)+a3)/a4);
elseif m > 67500
a5 = a5*exp(a25*t);
a6 = a6*exp(a26*t);
a7 = a7*exp(a27*t);
C = Curr(i,j);
Vltg(i,j) = 1.23-a1-a2*asinh(((C/a)+a3)/a4)-(C/a)*a5-a6*(exp((C/a)*a7)-1);
else
a3 = a3*exp(a23*t);
a5 = a5*exp(a25*t);
C = Curr(i,j);
Vltg(i,j) = 1.23-a1-a2*asinh(((C/a)+a3)/a4)-(C/a)*a5;
end
a_a(i,j) = a;
a_1(i,j) = a1;
a_3(i,j) = a3;
a_5(i,j) = a5;
a_6(i,j) = a6;
a_7(i,j) = a7;
end
toc
end
disp('End part two')

```